# FINAL REPORT
# SPACE SHUTTLE SRM INTERIM CONTRACT
# PART II

28 June 1974



Thiokol / WASATCH DIVISION
A DIVISION OF THIOKOL CORPORATION


Publications No. 74334

TWR-10075

# FINAL REPORT
# SPACE SHUTTLE SRM INTERIM CONTRACT

28 June 1974

By

THIOKOL/WASATCH DIVISION
A Division of Thiokol Corporation
P.O. Box 524, Brigham City, Utah 84302

Prepared For

NATIONAL AERONAUTICS AND SPACE ADMINISTRATION

George C. Marshall Space Flight Center

Contract NAS8-30754

CONTENTS

CONTENTS (Cont)

## ILLUSTRATIONS

ILLUSTRATIONS (Cont)

ILLUSTRATIONS (Cont)

ILLUSTRATIONS (Cont)

## TABLES

TABLES (Cont)

## 3.4 PROPELLANT

The SRM propellant formulation has remained basically unchanged throughout the interim contract, i.e., same aluminum level and solid loading. Design ramifications have created different web thicknesses and motor operating pressures which have necessitated small changes in the required propellant burning rate at 1,000 psia. However, the SRM burning rate remains well within the range demonstrated in the Poseidon and Minuteman first stage motors. Any change in propellant burning rate can be accomplished readily by a slight modification in the oxidizer particle size distribution. The ballistic and mechanical properties of the propellant remain unchanged from the baseline (Configuration 0).

### 3.4.1 Grain Design

Early in the interim contract the propellant grain configuration was subjected to minor alterations as required to reflect changes in propellant weight. A departure point was reached when the performance requirements shown in figure 3-47 were replaced by a residual force requirement (see Section 2, figure 2-4). The definition of residual force is "that force delivered by the SRM to the ET" (drag losses are included). The total SRM thrust is thus the sum of the residual force plus the product of the SRB mass times vehicle acceleration. Vehicle payload capability is relatively sensitive to the SRM thrust-time performance. Therefore, using this performance requirement approach ties SRM performance much more directly to vehicle performance than was previously realized.

A subroutine has been incorporated into Thiokol's Automated Design Program (ADP) which calculates the vacuum thrust time performance required to yield the residual thrust-time history requested. Basic inputs are the residual force-time, acceleration time, ambient pressure time histories, and SRB inert weight.

This routine also calculates the required burnrate and burning surface area versus web history. It accounts for pressure drop due to mass addition, throat erosion, a burnrate that varies as a function of web distance burned, and a pressure dependant C*. Figure 3-48 presents the target surface area-web history required

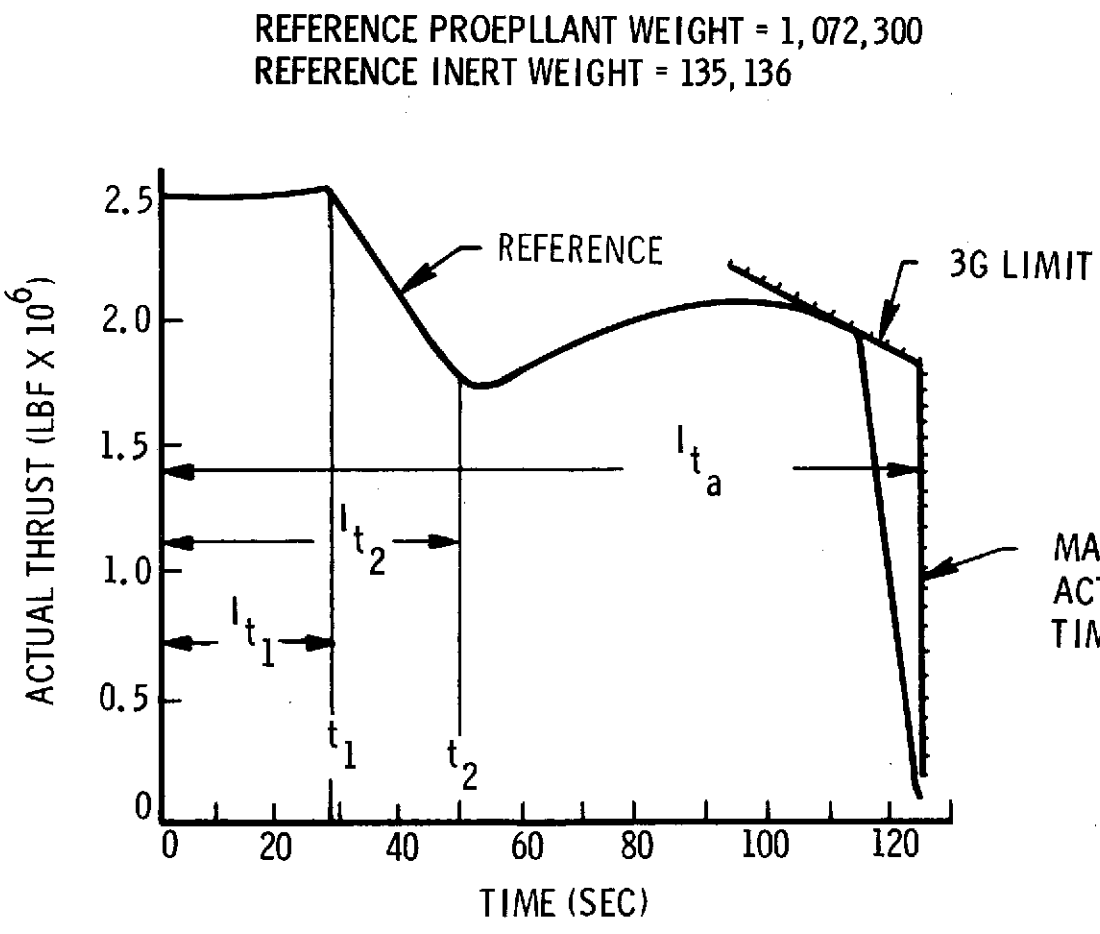


SL THRUST $(0 \leq t_F \leq t_1)$

$F_{SL} = 2.626\ [1 + \Delta W_P/W_P] \pm 2\%$ MLBF

IMPULSE, LBF-SEC

$I_{t_1} = 0.275\ (I_{t_a}) \pm 1/2\%$

$I_{t_2} = 0.460\ (I_{t_a}) \pm 1/2\%$

$I_{t_a} = 267.6 \times 10^6 \quad (1 + \Delta W_P/W_P)$

TIME, SEC

$t_1 = 28$

$t_2 = 50$

$t_{a\ MAX} = 124.6$

Figure 3-47. SRM Requirements - Performance

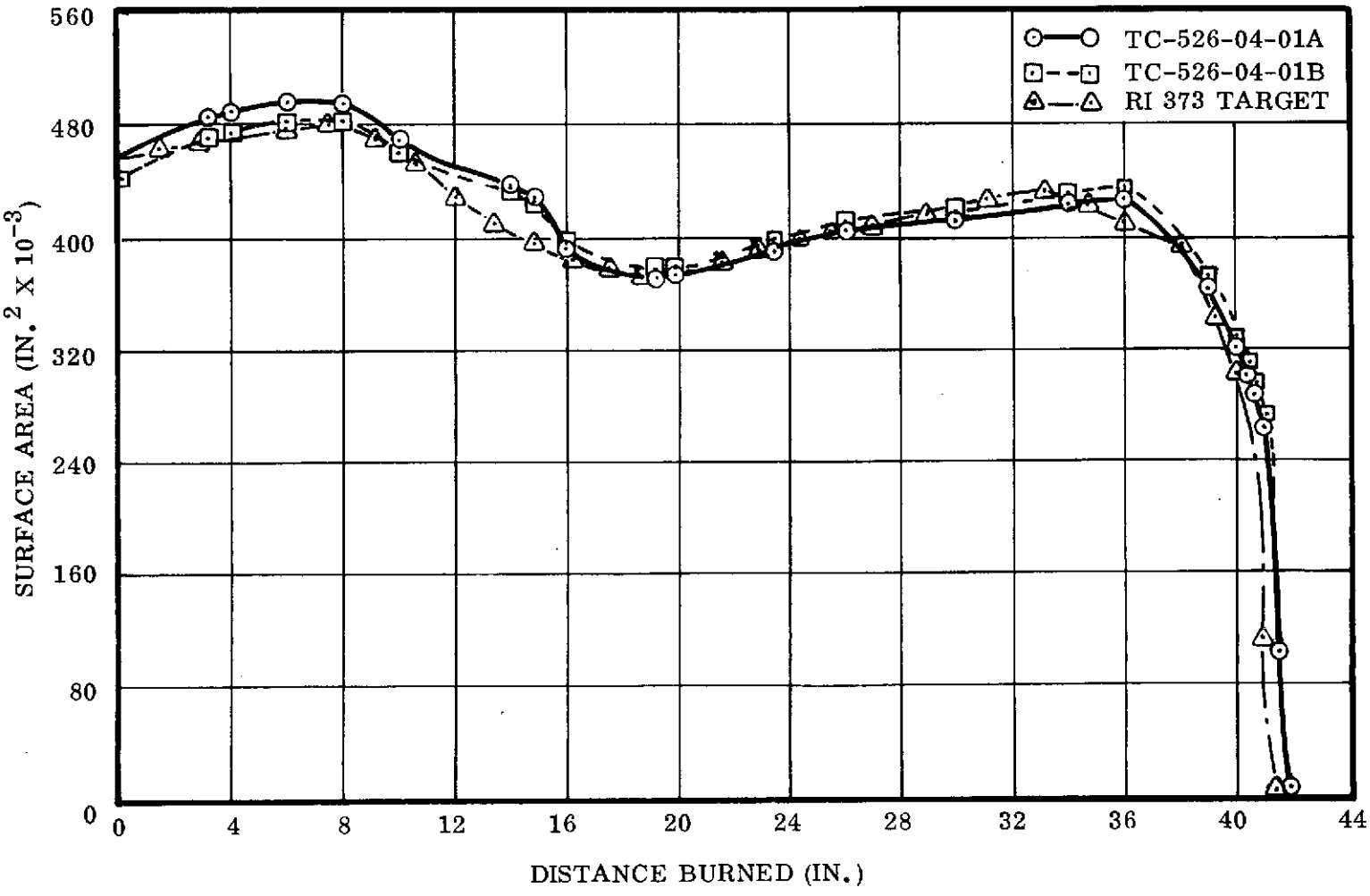


Figure 3-48. Comparison of Surface-Web Histories

to satisfy the RI case 373 residual thrust history. The surface-web history for two potential design solutions (TC-526-04-01A and TC-526-04-01B) are also shown.

Five potential design thrust-time histories were generated in a limited time and none perfectly matched the desired surface web requirements generated by the ADP from RI residual force data (Case RI, No. 373).

Figure 3-49 presents the five thrust-time histories and the basic features of each are outlined below.

| Identification No. | Design Features |
|---|---|
| TC-526-04-01A | Based upon an actual grain design. Has 456,100 $in.^2$ of initial surface area and 1,102,000 lb of propellant. |
| TC-526-04-01B | Basically the same design as configuration A except that the star was shortened (and the forward segment CP section length correspondingly increased) to reduce the initial surface area to 440,000 $in.^2$. |
| TC-526-04-01C | Not based on an actual grain design. The propellant weight was assumed to be 1,095,000 lb and the surface areas were reduced by the ratio 1,095,000/1,102,000. The web thickness was assumed to be the same as configuration A's. |
| TC-526-04-01D | The grain geometry was assumed to be that of configuration A. A burning rate correction factor was applied to the nominal rate of A. This factor rose linearly from 0.94 at 0% web to 1.04 at 50% web back to 0.96 at 100% web. |
| TC-526-04-01E | Modified -01A performance by assuming 1/2 the progressivity of A up to 20 seconds. The impulse at 20 sec was made equal to that of A. The remainder of the curve was the same as that of A. |

Figures 3-50 and 3-51, respectively, depict the grain design of configurations A and B. A single SRM motor hardware design was provided for all five of these ballistic performances.

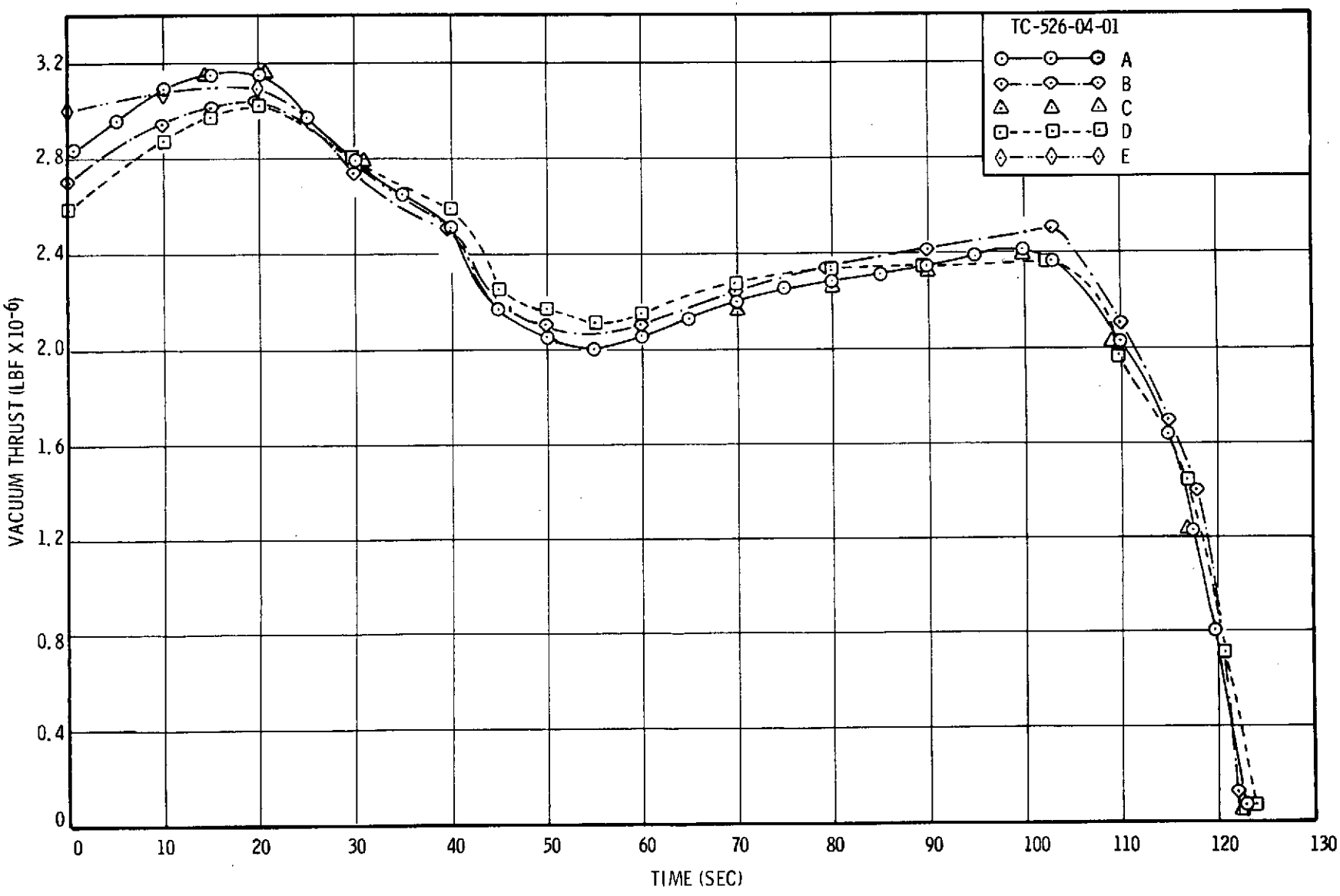


Figure 3-49. Vacuum Thrust Versus Time

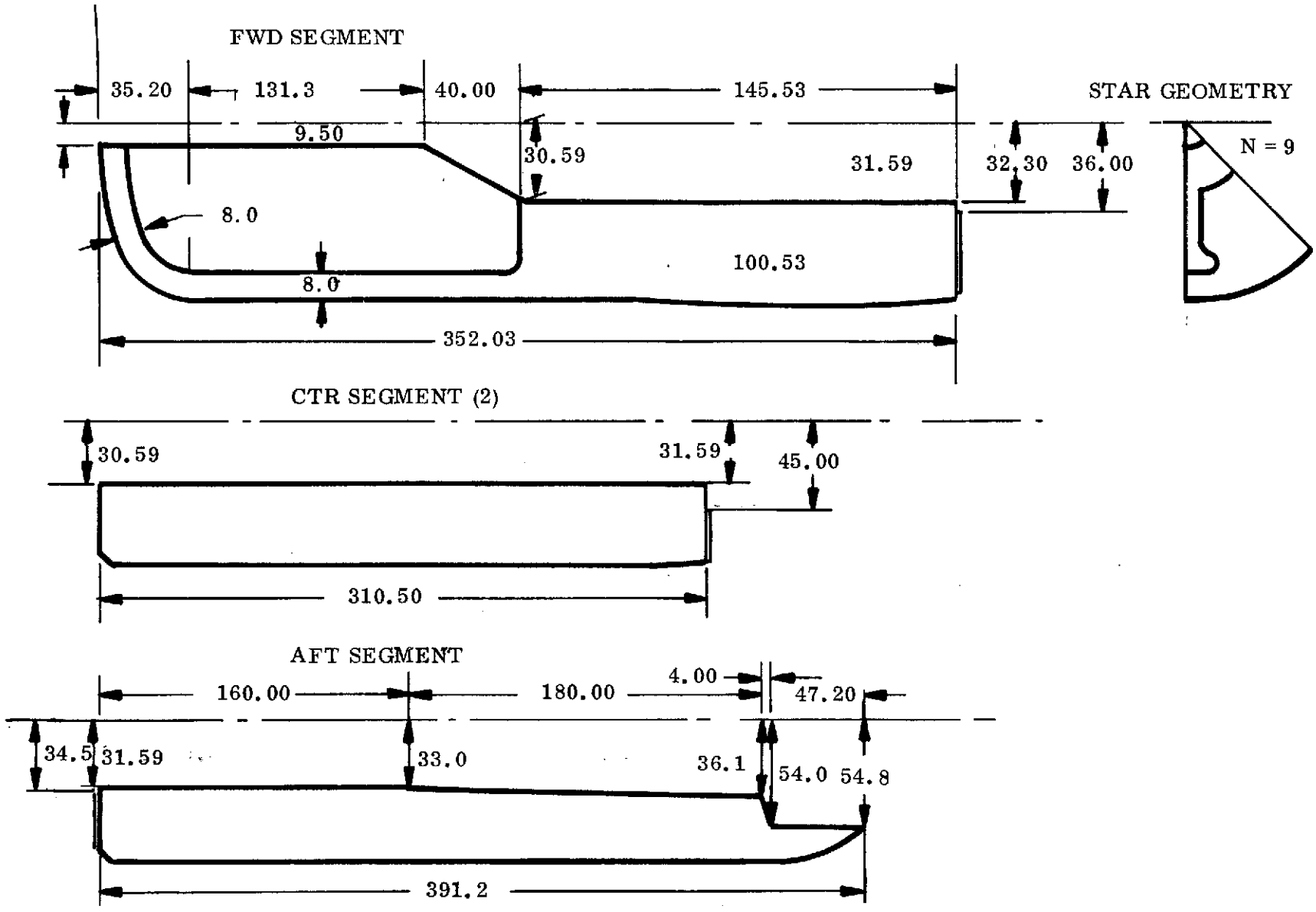


Figure 3-50. Grain Configuration (TC-526-04-01A)

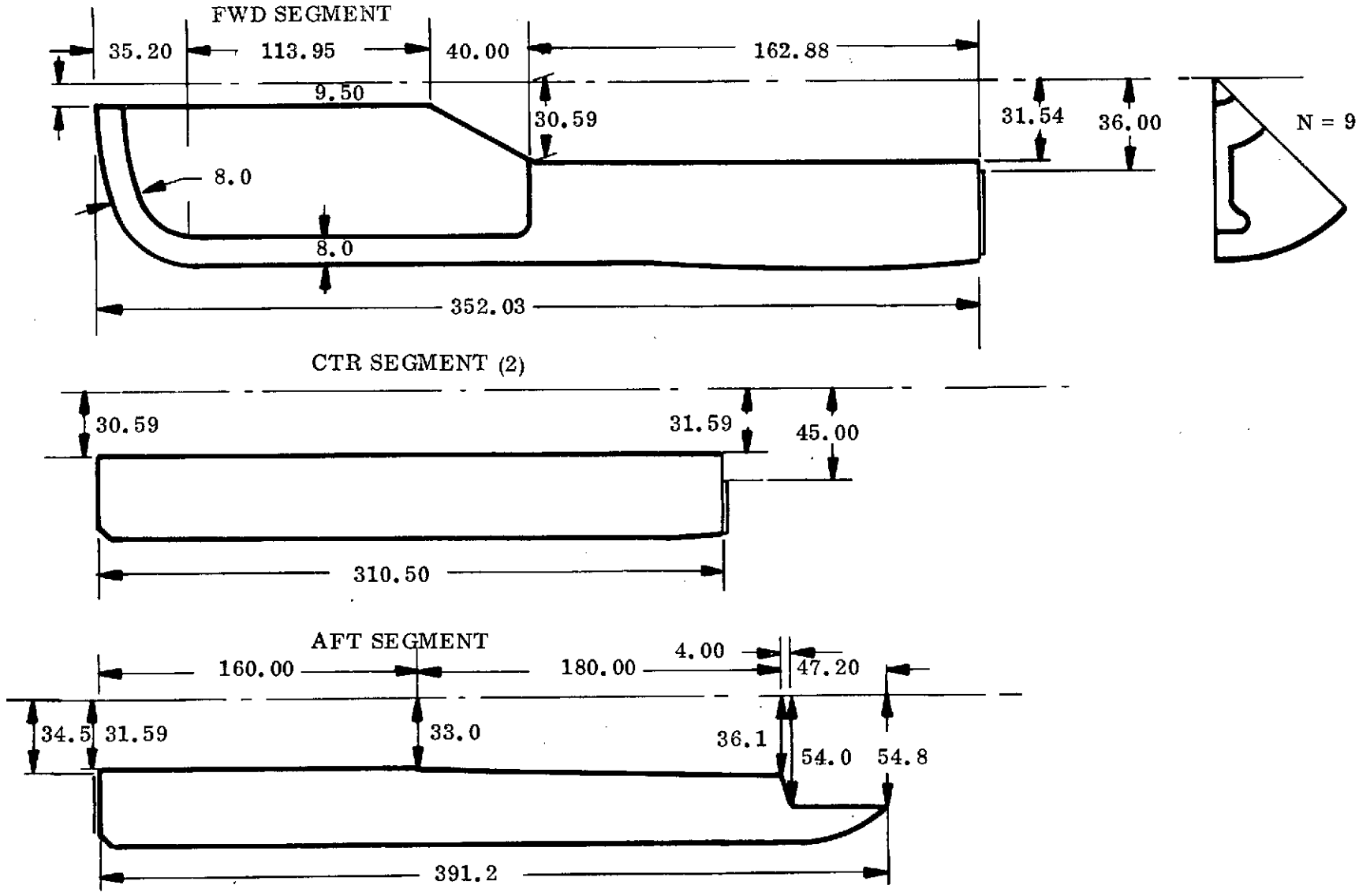


Figure 3-51. Grain Configuration (TC-526-04-01B)

RI conducted flight analysis for motors containing each of these grain configurations. By comparing the respective payload margins, a thrust shaping assessment can be made (i.e., by comparing A and E margins, the initial progressivity impact can be ascertained). These results show that payload gains can be achieved by proper thrust shaping initially and near web burnout. Table XXI lists the payload margin for each of these designs. All designs violated either maximum allowable dynamic pressure or acceleration. Results of this analysis are more fully detailed in the motor performance section of this report.

Additional work was conducted on grain design refinement. This work consisted of investigating the feasibility of replacing the 9-point dogbone star cross sectional configuration used in both A and B with an 11-point constant star thickness design. Figure 3-52 shows the basic cross sectional configuration of this design. It was determined that this design would yield a performance that is equal or superior to the 9-point dogbone. It also possesses superior manufacturing characteristics. Figure 3-53 compares the vacuum thrust performances of A with a motor containing the 11-point star.

The results of the limited study effort indicate the 11-point star will provide the desired performance with more desirable processing characteristics. Therefore, the 11-point star design will be further refined to provide the desired burning surface area versus web thickness relationship using RI case 373 as a design goal.

### 3.4.2 Motor Specific Impulse

Optimization studies conducted during the interim contract period have altered the SRM configuration in areas which affect motor performance such as nozzle geometry. Improvements in the analytical techniques have been continuous since the baseline design effort, resulting in changes in predicted nozzle losses. The baseline design SRM nozzle is compared to Configuration 1-1 in Table XXII. As is evident, the nozzle geometry is similar. The change in predicted vacuum specific impulse between the baseline design and Configuration 1 (as shown at the bottom of Table XXII) is due to the improved analytical method of evaluating the various loss mechanisms and a more efficient (although longer) nozzle on Configuration 1-1.

TABLE XXI

RESULTS FROM RI ANALYSIS OF SRM DESIGNS

| TC Design No. | Max Q (psf) | Max G | F/W | Total Margin* (lbm) |
|---|---|---|---|---|
| TC-526-04-01A | 675 | 2.91 | 1.45 | 7,200 (4,200) |
| TC-526-04-01B | 657 | 3.02 | 1.39 | 6,280 (3,280) |
| TC-526-04-01C | 670 | 2.90 | 1.45 | 6,440 (3,400) |
| TC-526-04-01D | 685 | 2.89 | 1.34 | 5,650 (2,650) |
| TC-526-04-01E | 670 | 2.91 | 1.53 | 7,290 (4,290) |
| Required Value | 650 | 3.0 | 1.5 | 7,000 (4,000) |

*Parenthetical numbers denote margin provided by the SRM

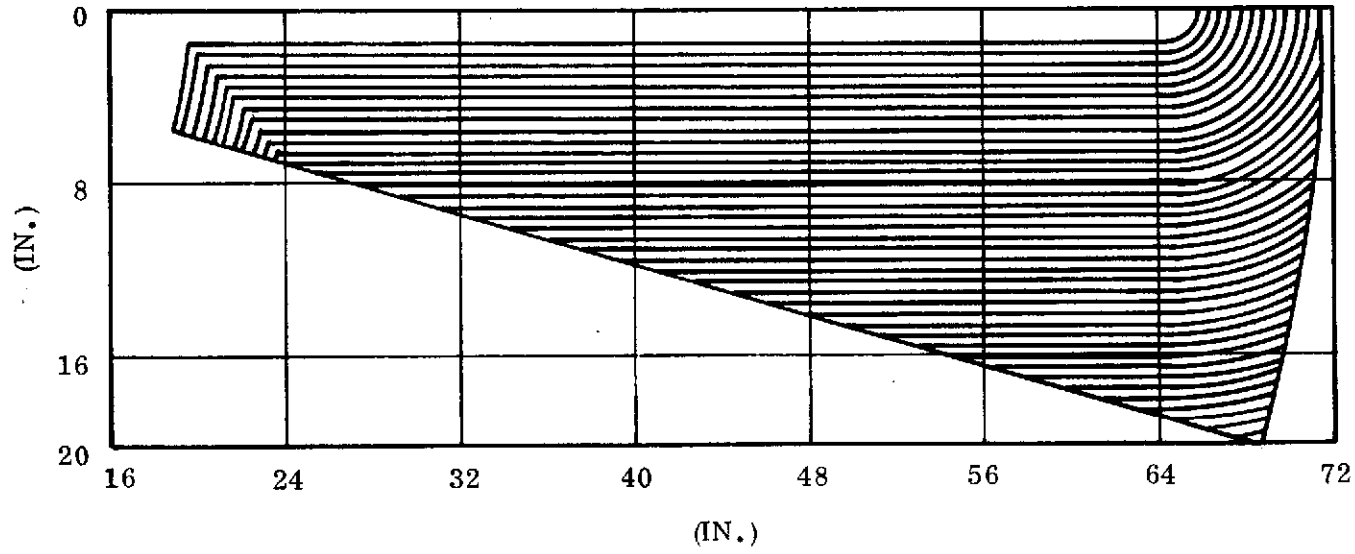


Figure 3-52. 11-Point Star Geometry

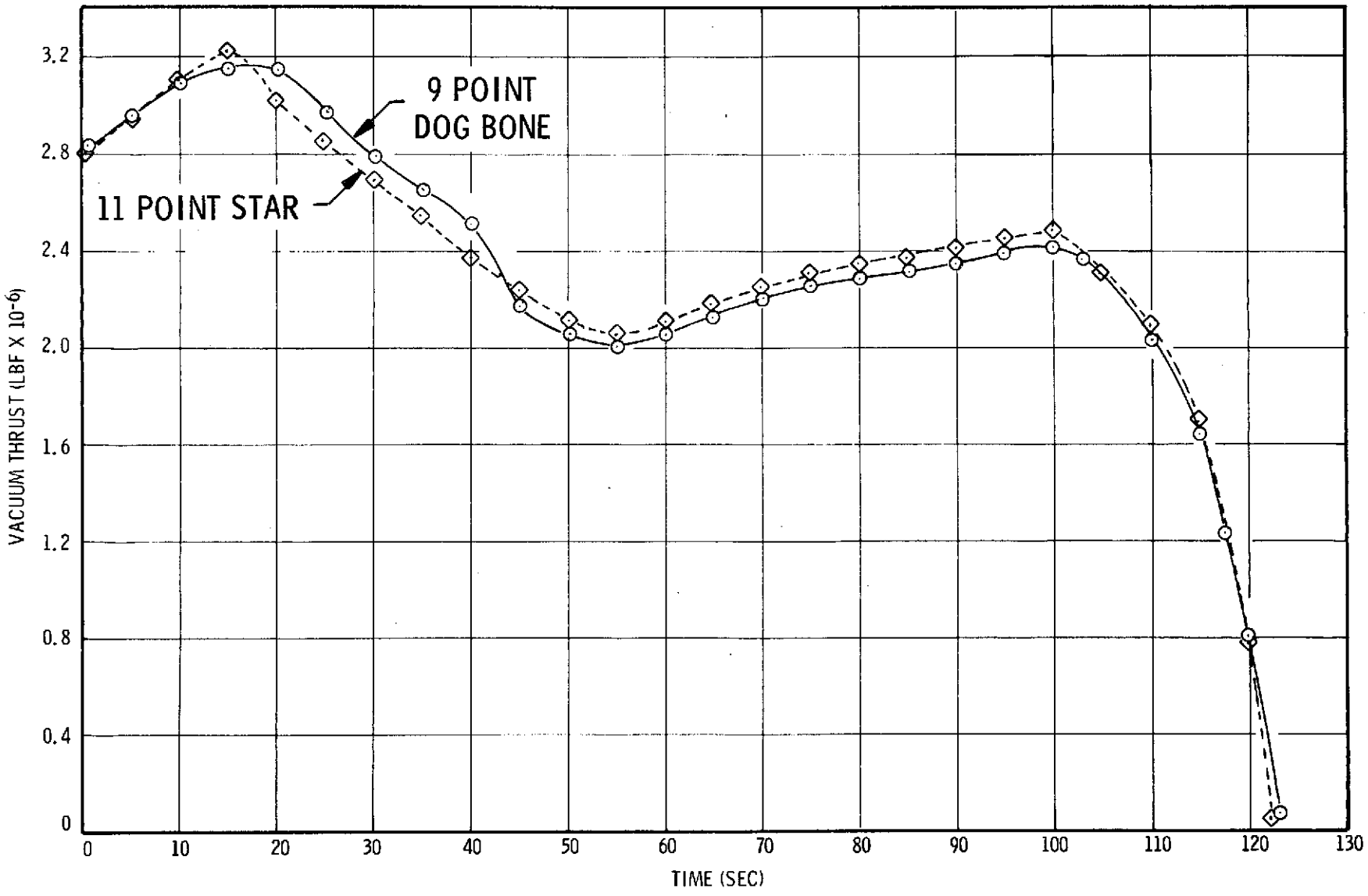


Figure 3-53. Comparison of Vacuum Thrust-Time Performance

TABLE XXII

SPECIFIC IMPULSE LOSSES

| | CONFIGURATION NO. 0 | CONFIGURATION NO. 1-1 |
|---|---|---|
| NOZZLE PARAMETERS | | |
| INITIAL EXPANSION RATIO | 6.0 | 6.0 |
| INITIAL ANGLE, DEGREE | 23.6 | 23.6 |
| TURNBACK ANGLE | 11.23 | 9.7 |
| INITIAL LENGTH-TO-THROAT RADIUS RATIO | 4.475 | 5.0 |
| LOSS CONTRIBUTORS | | |
| DIVERGENCE LOSS | 2.6 | 2.9 |
| TWO-PHASE LOSSES | 3.7 | 4.2 |
| KINETIC LOSS | 0.8 | 1.4 |
| FRICTION AND HEAT LOSSES | 2.3 | 2.6 |
| TOTAL LOSSES | 9.4 | 11.1 |
| PREDICTED AVERAGE VACUUM SPECIFIC IMPULSE | 260.5 | 258.9 |

The motor optimization program evaluates motor performance for various nozzle parameters, i.e., initial turning angle ($\theta_i$), turnback angle ($\Delta\theta$), and nozzle length-to-throat radius ratios. Since the performance loss contributors are influenced by the nozzle design, a method of analyzing the losses for a given nozzle design was required for the optimization studies. TC found a convenient method of relating total losses (or delivered specific impulse) for various nozzle configurations as shown in figure 3-54. These curves were fit by a series of equations which have been implemented into the automated design program and are used in motor optimization studies. (The specific impulse and nozzle geometry parameters given in Table XXII are a combination of initial and average values. Thus, a comparative specific impulse obtained from figure 3-54 is not possible.)

### 3.4.3 Minimum Specific Impulse

Specific impulse predictability and reproducibility have been evaluated to establish the minimum expected motor specific impulse. Motor predictability accuracy involved evaluation of historical data for analytical and empirical relationships for specific impulse prediction. The analytical analysis evaluates the various loss mechanism including two-phase losses, divergence loss, heat and friction losses, and kinetic losses. TC has conducted efficiency analyses for in excess of 50 motors which have been static tested. Comparison between predicted and measured specific impulse for these motors results in a mean of 0.11 points (i.e., predicts 0.11 points higher than measured) and a standard deviation of 1.58. The analytically predicted motor specific impulse for the baseline design was 261.5 lb-sec/lb.

An empirical evaluation of motor specific impulse using the TC-developed motor efficiency versus propellant flow rate curve yields a motor specific impulse of 260.5 lb-sec/lb. By performing a curve fit of the measured motor data and establishing limits about this curve, the predictability limits can be determined statistically. The results of such an analysis indicate that the probability is 90 percent that at least 95 percent of the distribution will be greater than:

$$\left[(I_{sp\ vac})\right]_{nom} - 1.33\% \text{ or } \left[I_{sp\ vac}\right]_{nom} - 1.33\% = \left[I_{sp\ vac}\right]_{min}$$

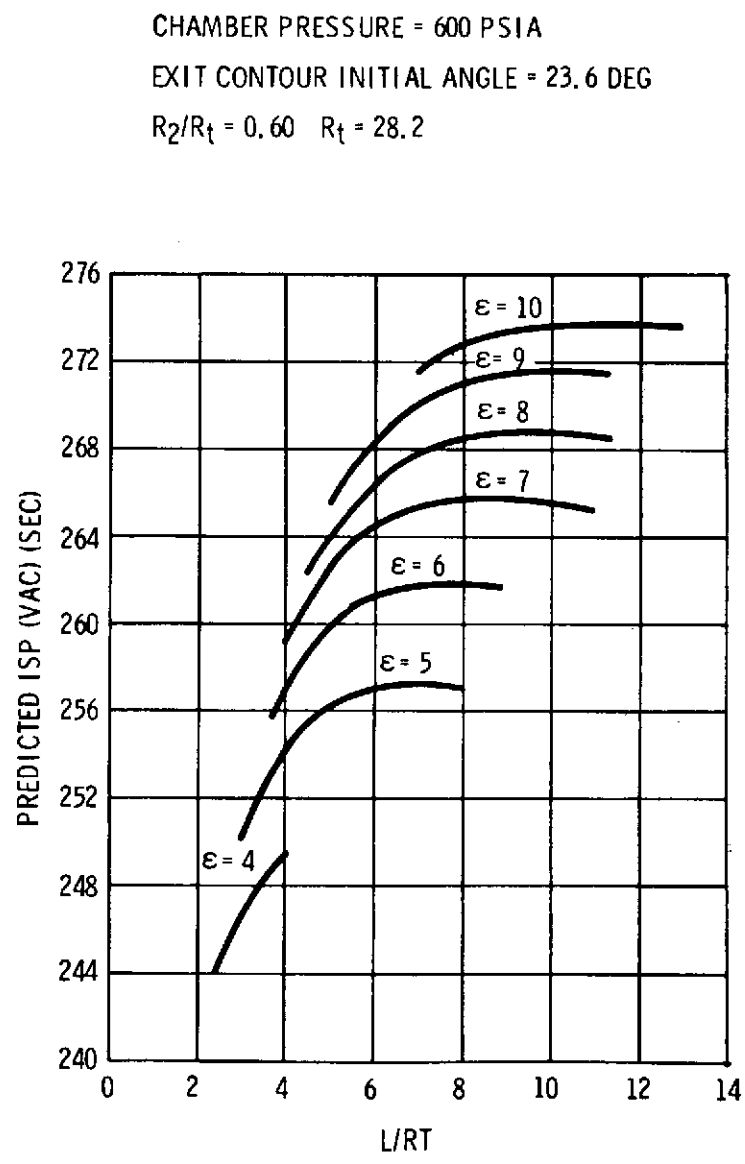


Figure 3-54. Delivered Specific Impulse Versus Nozzle Length-to-Throat Radius Ratio

(Similar statistical treatment of the analytically evaluated specific impulse results in 1.23 percent versus the 1.33 percent.) This represents the expected maximum limits on predictability for motor specific impulse. Table XXIII summarizes the predictability study.

Once the motor design has been established and performance data becomes available, the motor will have reproducibility limits the same as demonstrated on previous programs, i.e., Minuteman and Poseidon. Hisotrical data have established specific impulse limits as 0.20 % for one standard deviation. Combining the reproducibility and predictability error, the following statement is applicable:

The probability is 90 percent that at least 95 percent of the distribution will be greater than

$$\left(I_{sp\ vac}\right)_{nom} - 1.446\% \text{ or } \left(I_{sp\ vac}\right)_{min} = \left(I_{sp\ vac}\right)_{nom} - 1.446\%$$

3.4.4 Maximum G*

The effects of erosive burning are not always reproducible or predictable and, thus, can create problems particularly at or following web burnout. The effects of erosive burning are amplified at burnout, and the performance difference between two motors could be most pronounced during tailoff operation. Minimization of this tailoff variation can be assured if erosive burning is eliminated. Using the Saderholm erosive burning model and evaluating all large motor data available, the most severe erosive environment was experienced by the Titan III M, seven segment motor. This motor had a maximum mass flow rate per unit port area (G*) of 3.1 lb/sec-in.$^2$ and no erosive burning was experienced. Therefore, it was concluded that the SRM will not experience erosive burning if a G* of 3.1 is not exceeded. A maximum G* limit of 3.1 lb/sec-in.$^2$ was thus added to SRM internal ballistic design criteria. The port-to-throat area ratio of 1.3 was maintained while motor length to diameter values were allowed to vary until the G* limit was reached.

TABLE XXIII

PERFORMANCE INTERCHANGE SUMMARY

- MOTOR SPECIFIC IMPULSE EFFICIENCY
  - THEORETICAL EVALUATION OF VARIOUS LOSS MECHANISMS
  - EMPIRICAL EVALUATION OF TEST DATA
  - MOTOR EFFICIENCY DETERMINATION

    THEORETICAL CALCULATION OF LOSSES-- $\eta_{nom} = 0.975$

    EMPIRICAL EVALUATION--$\eta_{nom} = 0.972$

    PROBABILITY IS 90% THAT AT LEAST 95% OF THE DISTRIBUTION WILL BE GREATER THAN:

    $\eta_{nom} - 1.33\% = \eta_{min} = 0.959$

## 3.5 INSULATION AND LINER

The primary chamber insulation is an asbestos-silica-filled nitrile butadine rubber (NBR), and the liner is an asbestos-filled HC polymer. No insulation or liner material or process changes have resulted due to the interim study contract. However, two areas have undergone studies to evaluate conditions which could either modify the insulation design or have significant effect on other aspects of the SRM. These two areas of study are: (1) evaluation of internal case insulation temperature at water impact and the probability of generating sufficient steam within the case to result in the case sinking after the steam has condensed and, (2) the cost and schedule impact associated with increasing the case aft dome insulation thickness for the first two demonstration motor (DM) tests.

### 3.5.1 Case Internal Insulation Temperature Study

This study was expanded to include the case, nozzle, and internal case insulation heat content at splashdown. The thermal analysis considered the heating during motor operation, aerodynamic heating, and the added heat content due to reignition of the internal insulation as the spent case re-enters the atmosphere. The case insulation was divided into several areas of differing material thickness and exposure time. Each area was thermally analyzed and temperature-thickness plots were prepared. Figure 3-55 presents a typical temperature profile. The area under the curve times, the material density, and specific heat gives the heat content per inch. The heat content for each area was then determined by multiplying the heat content per linear inch by the length. The same process was applied to the nozzle materials to determine their heat contents. The results of the thermal analysis indicate a maximum internal insulation temperature of approximately 300° F and a maximum nozzle material temperature of 1600° F at splashdown.

The total internal case heat available is 771,543 Btu above a 212° F reference temperature.

A conservative SRM vertical velocity of 80 feet per second was used to determine the depth of SRM submergence and the flow rate of water entering the

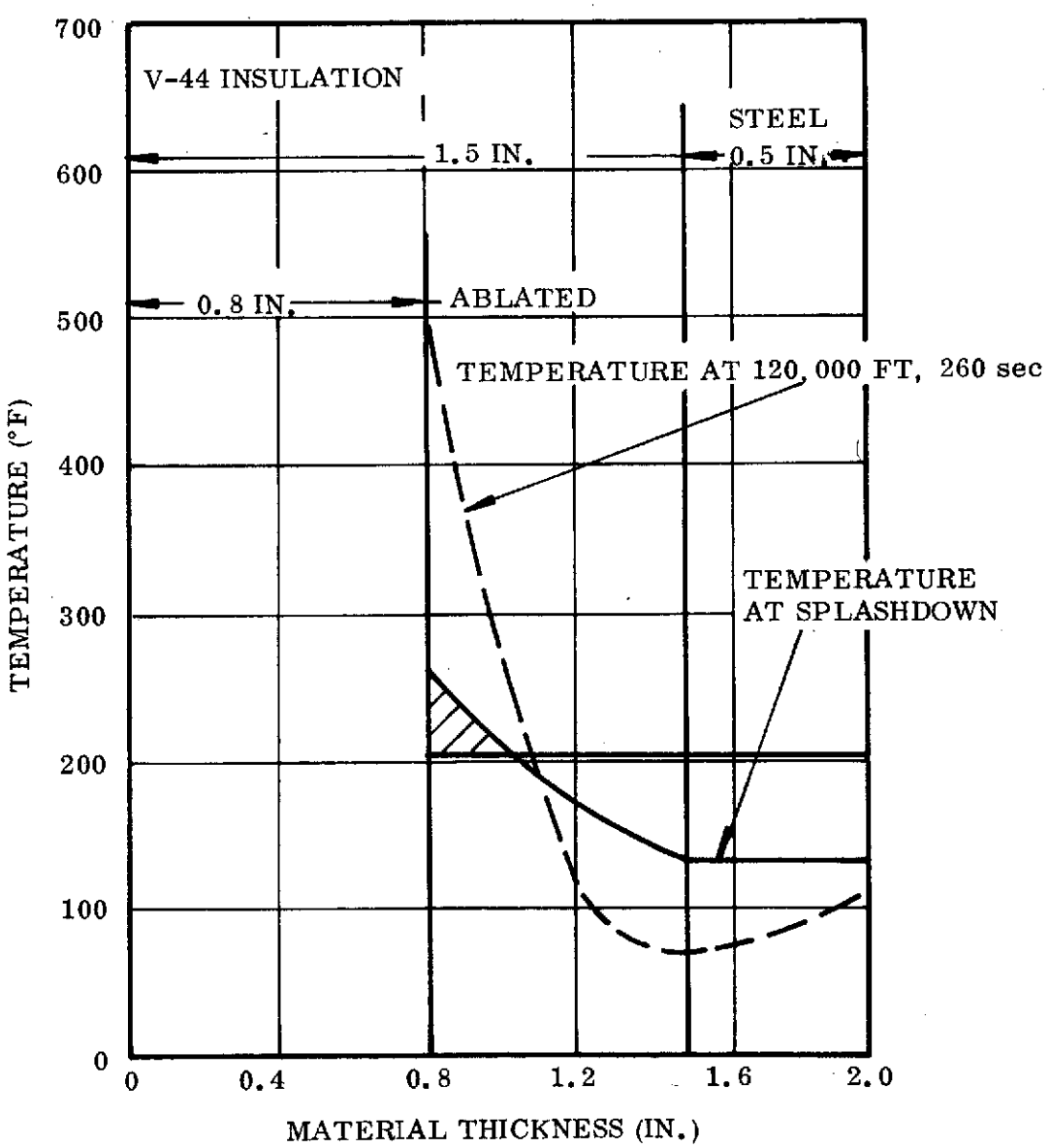


Figure 3-55. SRM Water Entry at Splashdown
(Case Insulation 1.5 In. Thick - Exposed 80 Seconds)

spent case as a function of time. (A vertical velocity greater than 80 feet per second increases the quantity of water which enters the case for a given time interval.) Water will enter the case at a rate of 115,600 lb/sec for the first second. As the water passes over the hot nozzle and into the case these components will be cooled with very little or no steam being generated. The only location which may not be cooled by this deluge of water is the forward closure insulation area. The residual heat in the forward closure could cause a minimal amount of steam generation. However, it is felt that the quantity of steam generated will not adversely effect the case buoyancy unless the nozzle end clears the water for an excessive time prior to the steam condensing, thus allowing the air-steam mixture to be exhausted.

Many factors remain unresolved such as the amount of steam which will be generated, submergence depth and time, height which entering water covers internal case, and case internal air temperature at splashdown. Also, review of the 120-inch case drop films reveals the tendency of a cool case to exhaust air. The exhasuting process appears to be generated by the wave action within the case.

Water entering the case with sufficient velocity will cover all the internal case surface and very rapidly cool these surfaces. Steam which may be generated will be trapped and will not escape until the nozzle again clears the water at which time the steam may be condensed. The time the spent case remains submerged coupled with the entry velocity will determine the amount of steam, if any, and the temperature of the trapped gases. If sufficient time and quantity of water for cooling are provided prior to the nozzle end of the case coming out of the water, the case will behave like the cool 120-inch drop test cases. The temperature of the internal case insulation will have any effect on the case buoyancy. To fully analyze this complex problem, additional heated drop tests with considerable internal instrumentation will be required. Based on the analytical studies conducted by TC, it is concluded the booster will not contain sufficient water to sink.

### 3.5.2 Aft Case Insulation Thickness

Concern about the insulation thickness requirement analysis for the aft dome has been expressed by MSFC. Alleviation of this concern can be accomplished by increasing the insulation material thickness in the first two DM tests. The remaining DMs will incorporate a design modified as a result of analyzing these full scale test data.

The resulting modified aft dome insulation for the first two DMs represents consideration of a constantly vectored nozzle duty cycle, material thickness consistent with the greater thermal environment which would exist if the vortex flow field did not occur aft of the nozzle nose (condition much more severe than anticipated), and a safety factor of 2. The resulting increase in insulation thickness has a corresponding weight increase of approximately 2,000 pounds.

## 3.6 SRM DESIGN STUDY

During the interim contract period many SRM designs were generated by Thiokol's Automated Design Program (ADP) for the purpose of evaluating the effect of varying selected design parameters on motor performance, length, inert weight, and SRM program cost. The design requirements used in this study are listed below for reference purposes. The requirements were held constant for all the designs except where special constraints were applied to investigate the effect of selected design parameters on SRM weight and cost. The results of this design study were reported at the SRM Project Design Review on 9 April 1974 (Reference TWR-10046). The aspects of this study that are related to motor performance are summarized in this section.

The design requirements for all the SRM designs were those specified in the RFP except as modified by direction or coordination with MSFC.

The requirements that varied from those in the RFP are listed below:

1. 100 ft/sec Vertical Velocity at Water Impact
2. 0-45 ft/sec Horizontal Velocity at Water Impact
3. $0 \pm 5$ deg Water Entry Angle
4. SRM/ET Attach Loads/Interface Changes
5. 2 percent Inert Weight Added
6. G* Constraint in Addition to $A_p/A_t$
7. Nozzle Exit Cone Jettisoned Prior to Water Impact
8. SRM Total Allowable Length Increased ($X_B$ 1,951 in. to 1,989.6 in.)
9. SRM OD = 146 in.
10. 1.25 Factor of Safety Using Nominal Dimensions for Water Impact Loads

In addition to the above requirement changes, other criteria were established by MSFC which differed from those used to design the baseline (Configuration 0).

These additional changes are as follows:

1. Grit Blast Allowance for 20 Uses
2. MSFC Nozzle Safety Factor Interpretation
3. Nozzle Configuration Based on Low-Cost Materials
4. Nozzle Weight Based on High-Cost Nozzle Materials
5. SRM Size and Delta Cost Based on High-Cost Nozzle Materials
6. Ring Weight for SRM/ET Aft Attach Not To Be Included in SRM Inert Weight

The approach used in the SRM design and optimization program was to couple the SRM Automated Design Program with a comprehensive SRM project cost model. The principal constraints imposed on the SRM designs were as follows:

1. Water Impact Constraints and Weight Increases Due to Local Wall Thickness Increase and Stiffeners
2. G* Upper Limit of 3.1 lb/in.$^2$-sec at 90° F
3. Nozzle Expansion Ratio Lower Limit at 5.5:1
4. 0.010 In. Delta Case Thickness Provided for Grit Blast Losses
5. 2 Percent Inert Weight Included
6. SRM Performance and Configuration Based on High-Cost Nozzle Material Weight
7. Optimized for Minimum SRM Project Cost Using Low-Cost Nozzle Materials
8. Costs Adjusted for High-Cost Nozzle Materials

The flow logic for the Automated Design Program (ADP) is presented in figure 3-56 showing the optimization loops incorporated to develop minimum cost motor designs for selected constraints in the motor evaluation block.

The required total impulse ($I_{total}$) is calculated using the SRB inert weight partials specified in the RFP. The steps in the routine are as follows:

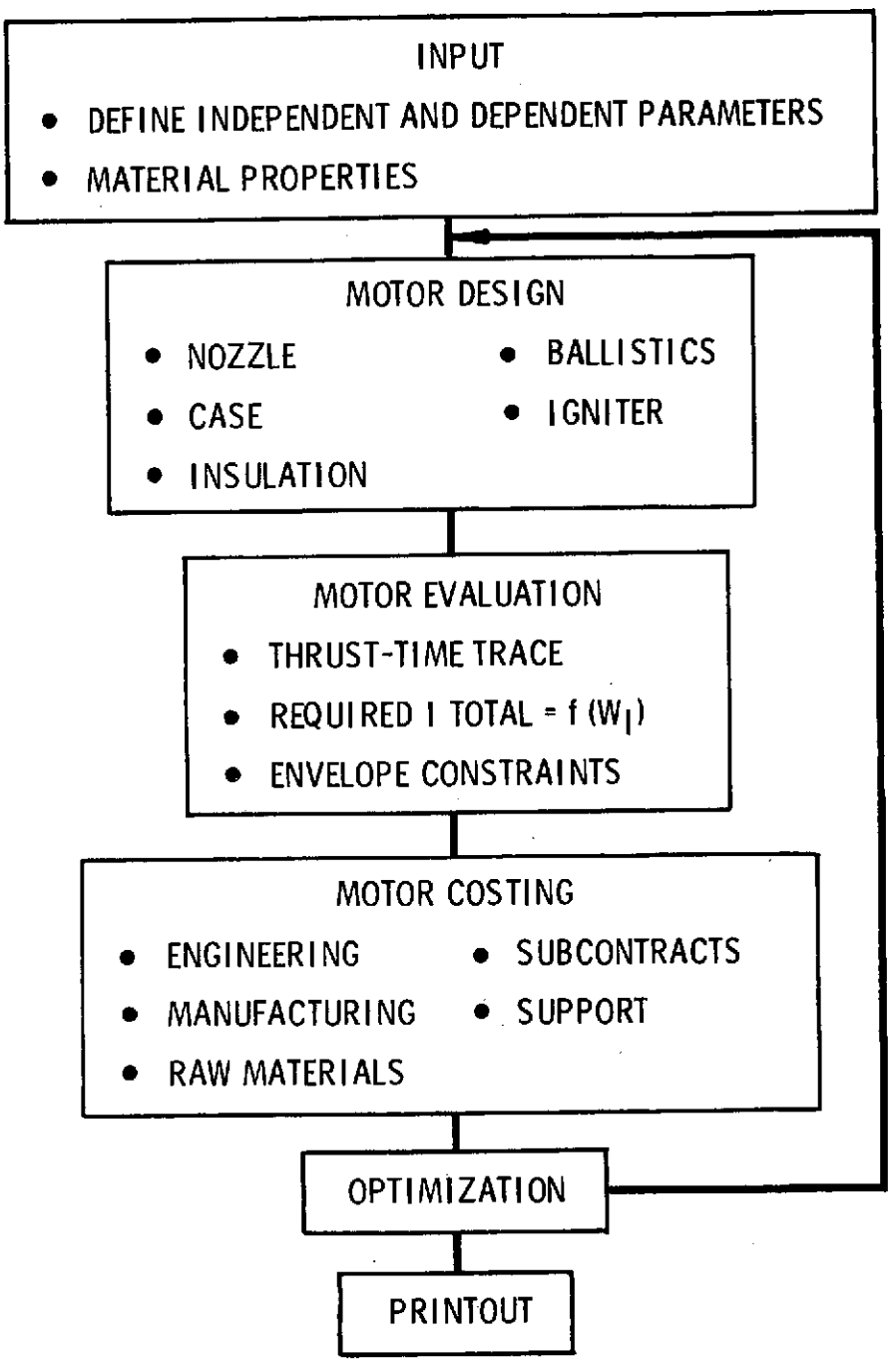


Figure 3-56. Design and Optimization Program

RFP Partials

$$\Delta W_{SRBE_1} = 16 \times (D_E - 141.3)$$

$$\Delta W_{SRBE_2} = 0.07 \times (W_{SRM_1} - 115,430)$$

$$W_P = 1.82 \times \left[(\Delta W_{SRBE_1} + \Delta W_{SRBE_2}) + (W_{SRM_1} - 115,430)\right]$$

$$\text{Required } I_{total_{(del)}} = 257.02 \times 10^6 \left(1 + \frac{\Delta W_P}{W_P}\right)$$

$$\text{Required } I_{total_{(vac)}} = I_{total_{(del)}} + \int P_A \, d_T *$$

$$W_P = I_{total_{(vac)}} / I_{sp_{(vac)}}$$

*677.13 lb-sec/in.$^2$

where

$D_e$ = exit diameter, in.

$W_{SRM}$ = SRM inert weight, lbm

$\Delta W_{SRBE_1}$ = change in SRB inert weight due to exit diameter, lbm

$\Delta W_{SRBE_2}$ = change in SRB inert weight due to SRM, lbm

$\Delta W_P$ = change in propellant weight, lbm

The major features of the model used for motor costing are as follows:

1. Component cost broken down as follows:
   a. Case (By Segment)
   b. Nozzle (By Component)
   c. Insulation (By Segment)
   d. Propellant (By Mix)
   e. Igniter
2. Labor cost by work breakdown element and Thiokol cost center

3. Refurbishment included for case, nozzle and igniter
4. RFP partials for DDT&E and operational flights used to determine added cost to SRB due to SRM design parameters

$$\Delta \$SRBE = (14,300 + 100,500)\ (D_e = 141.3)$$

$$\Delta \$SRBE = (260 + 770)\ (W_{SRM_1} = 115,430)$$

The general and specific ground rules for optimizing the SRM design reported as Configurations 1 and 2 were as following (See table XIX):

General Ground Rules

1. Concept Changes From Configuration 0
   a. New Water Impact Requirements
   b. NASA Safety Factor Interpretation on Nozzle Materials
   c. Weight Increase Applied to Nozzle to Account for High-Cost Nozzle Materials
   d. Add 2 Percent Inert Weight for Contingency

Specific Ground Rules

1. Configuration 1 - Minimize Cost of SRM (including SRB Effects)
2. Configuration 2 - Maximize Performance Within Increased Envelope

The independent parameters varied during the optimization were the following:

1. Chamber Pressure
2. Nozzle Expansion Ratio
3. Propellant Weight
4. Nozzle Contour ($\theta_i$ and $\Delta_\theta$)
5. Nozzle Submergence

The principal performance parameters for Configurations 1 and 2 are compared with Configuration 0 in Table XXIV.

TABLE XXIV

SUMMARY

| | CONFIGURATION 0 | CONFIGURATION 1 | CONFIGURATION 2 |
|---|---|---|---|
| • DIAMETER (IN.) | 146 | 146 | 146 |
| • OVERALL LENGTH (IN.) | 1,438 | 1,454 | 1,496 |
| • TOTAL DELIVERED IMPULSE (LB-SEC X $10^6$) | 259.9 | 265.8 | 276.4 |
| • PROPELLANT WEIGHT (LB) | 1,035,860 | 1,072,300 | 1,128,700 |
| • TOTAL INERT WEIGHT (LB) | 121,188 | 134,300 | 145,630 |
| • MEOP (PSIA) | 839 | 865 | 890 |
| • EXPANSION RATIO | 6:1 | 5.5:1 | 5.5:1 |
| • SPECIFIC IMPULSE $\left(\frac{\text{LBF-SEC}}{\text{LBM}}\right)$ | 260.5 | 256.6 | 253.4 |
| • MASS FRACTION | 0.895 | 0.889 | 0.886 |
| • DELTA COST ($ MILLIONS) | 0 | +77.5 | +100.4 |

The impact on cost of design changes introduced since the proposal design are tabulated as cost deltas from Configuration 0 on Table XXV.

The weight and cost partials with respect to small changes in propellant weight are presented for both Configurations 0 and 1 are presented below.

| | Configuration 0 | Configuration 1 (SRM Baseline 18 April) |
|---|---|---|
| $\frac{\Delta \text{SRM Weight}}{\Delta \text{Propellant Weight}}$, lbm / lbm | 1.170 | 1.197 |
| $\frac{\Delta \text{SRM Program Cost}}{\Delta \text{Propellant Weight}}$, $ / lbm | 385 | 397 |

Both the weight and cost partials are lower for Configuration 0 than for Configuration 1. (The Configuration 1 referred to here is the SRM Baseline (18 April) discussed in Section 3.1.) This occurs because Configuration 0 has a thinner case wall thickness and lower G* than Configuration 1, resulting in a lower increase in inert weight per unit increase in propellant weight.

The mass properties for Configurations 0, 1, and 2 are presented for comparison on Table XXVI. The reasons for the difference between the case weights for Configurations 0 and 1 are detailed on Table XXVII to expalin the increase of about 8,000 lbm.

The case segment arrangements for Configurations 0, 1, and 2 are illustrated for comparison on figure 3-57. The case and casting segment lengths for all three configurations are the same, forward of the attach segment. Configurations 1 and 2 both have an additional case segment in the aft casting segment because of the shorter attach segment caused by incorporation of dual flanges to react SRM/ET attach loads.

The fabrication constraints for 146-inch diameter cases are illustrated in figure 3-58. The maximum pin-to-pin length for a cylindrical segment with thicknesses up to 0.581 inch and no upsets for flanges is 156 inches. The length of a case segment with an upset for ET attachment depends upon the distance of the double flange from the joint. If the double upset is 6 inches from the joint, the segment can be up to 135 inches long; however, if the double upset is 36 inches from the joint, the maximum segment length is only 100 inches.

TABLE XXV

IMPACT OF DESIGN CHANGES FROM CONFIGURATION 0 TO 1

| | Δ COST $M |
|---|---|
| 2% INERT WEIGHT CONTINGENCY | 2.31* |
| REVISED F.S. FOR NOZZLE PLASTIC PARTS | 6.89 |
| INCLUDED IN ESTIMATE OF NOZZLE LOSSES | 4.96 |
| REVISED WATER IMPACT LOADS | 17.35 |
| | 31.51 |
| CONVENTIONAL NOZZLE PLASTIC MATERIALS | 45.95 |
| TOTAL Δ COST | 77.46 |

* DELTA COST FOR PERFORMANCE.
COST OF INERT WEIGHT CONTINGENCY
NOT INCLUDED

TABLE XXVI

MASS PROPERTIES SUMMARY (WEIGHT-LB)

| COMPONENT | CONFIGURATION 0 | CONFIGURATION 1 | CONFIGURATION 2 |
|---|---|---|---|
| CASE | 90,548* | 98,460 | 106,950 |
| INSULATION, LINER, AND INHIBITOR | 13,281 | 13,630 | 13,940 |
| NOZZLE | 16,401 | 18,510 | 20,780 |
| IGNITER, RACEWAY, AND ATTACH HARDWARE | 958 | 1,070 | 1,100 |
| CONTINGENCY | 0 | 2,630 | 2,860 |
| TOTAL INERT WEIGHT | 121,188 | 134,300 | 145,630 |
| PROPELLANT WEIGHT | 1,035,860 | 1,072,300 | 1,128,700 |
| TOTAL MOTOR WEIGHT | 1,157,048 | 1,206,600 | 1,274,330 |

*INCLUDES 1,010 LB SRM/ET ATTACH RING

TABLE XXVII

CASE WEIGHT CHANGE DUE TO WATER IMPACT
AND REVISED SRM/ET ATTACHMENT

| | |
|---|---|
| GRIT BLAST | 1,740 |
| 1 ADDED JOINT | 760 |
| PENETRATION (2 AFT SEGMENTS) | 530 |
| CAVITY COLLAPSE (ONE STIFFENER) | 320 |
| INCREASE IN MEOP | 3,765 |
| WATER IMPACT (AFT DOME) | 885 |
| TOTAL WEIGHT INCREASE | 8,000 |

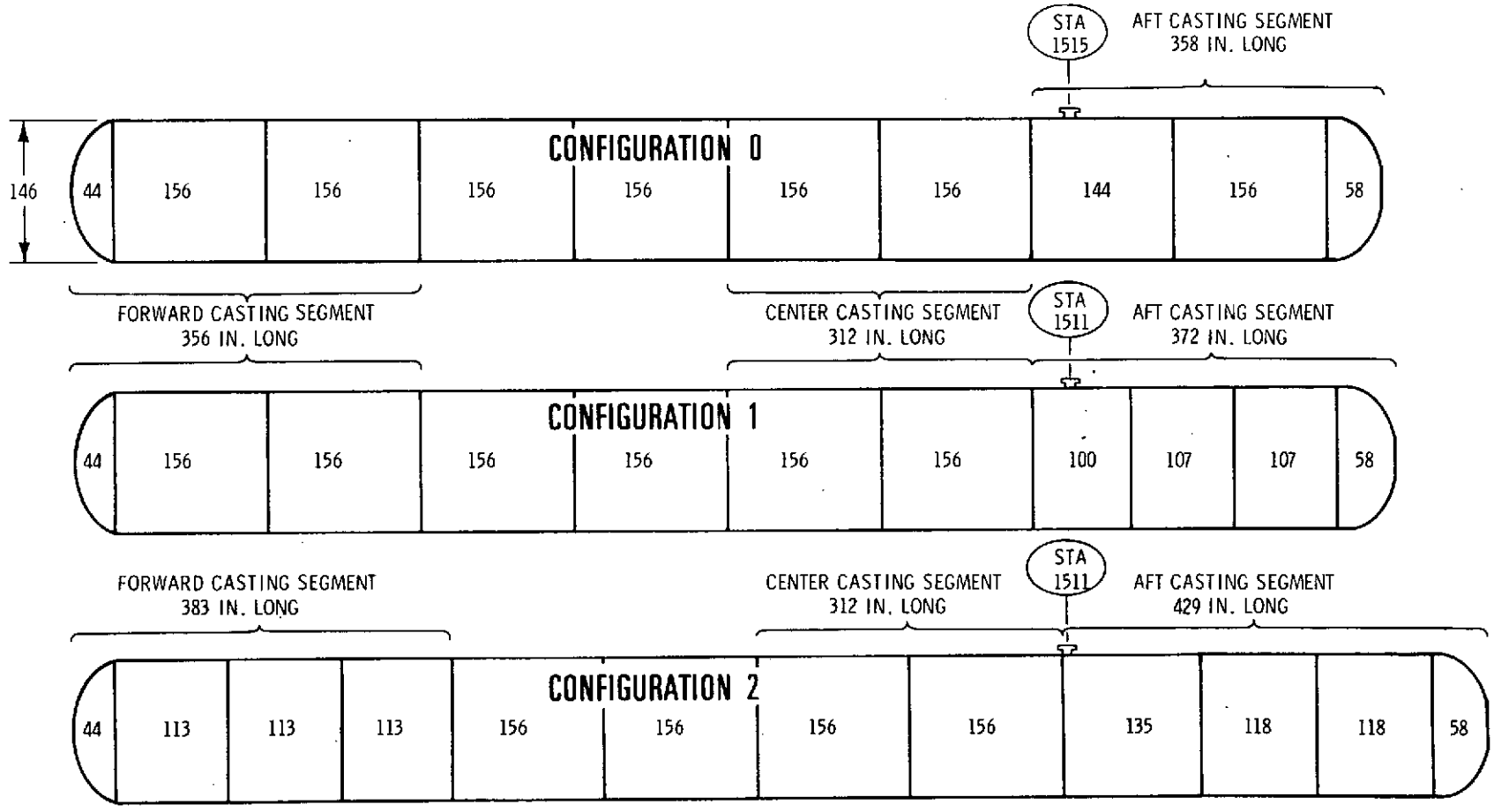


*DIMENSIONS IN INCHES

**Figure 3-57. Case Segment Configuration***

CYLINDRICAL SEGMENT
UP TO 0.581 THICKNESS

156 INCH PIN-TO-PIN

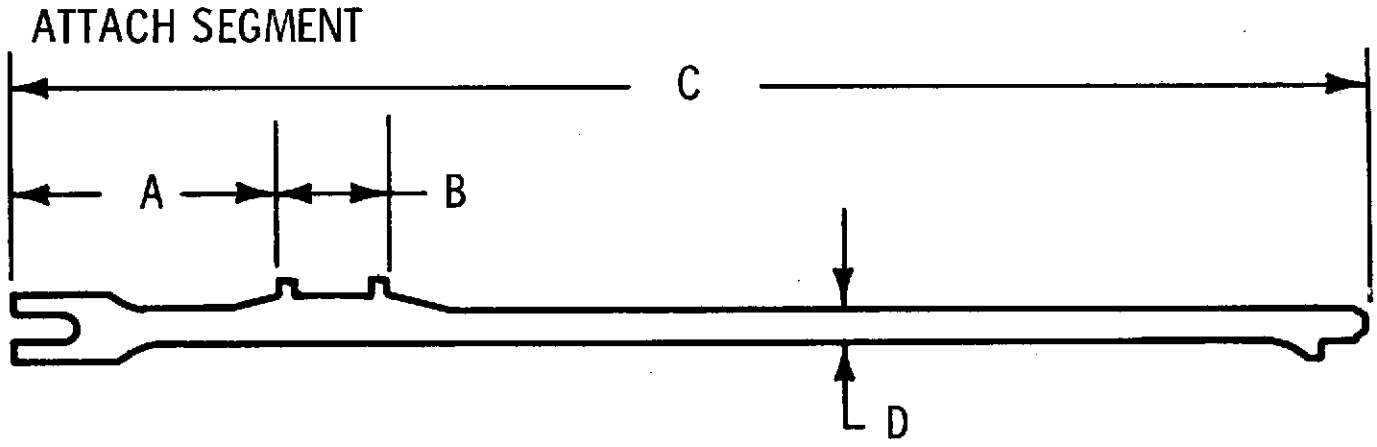


| A (IN.) | B (IN.) | C (IN.) | D (IN.) |
|---|---|---|---|
| 6 | 12 | 135 | 0.581 (MAX) |
| 13 | 12 | 112 | 0.581 (MAX) |
| 36 | 12 | 100 | 0.581 (MAX) |

Figure 3-58. Case Fabrication Constraints

Two alternated aft closure designs (2:1 ellipse and cone) are compared in figure 3-59 with the hemispherical closure design employed on all the configurations discussed in this presentation. The 2:1 ellipse permits an effective increase of about 210 pounds in propellant loading in the same overall length, while the conical design results in a 1,980 pound decrease in effective propellant weight due to the increased wall thickness.

The delivered specific impulse for SRM designs generated in this study was determined from the plot of $I_{sp}$ versus nozzle length-to-throat radius ratio for constant expansion ratios plotted on figure 3-60. The data required to plot these curves was developed by generating a family of nozzle contours and then performing a detailed analysis to determine the losses contributed by the following factors for each contour:

1. Divergence
2. Two-Phase Flow
3. Kinetics
4. Friction and Heat

The increase in propellant weight possible by increasing the maximum G* was determined for Configuration 1. The results of these calculations are plotted in figure 3-61. The plot shows that an additional 50,000 pounds of propellant could be cast in the motor if the maximum G* were increased from 3.1 to 4.0 lbm/in.$^2$-sec.

Some of the SRM designs generated by the ADP for the purpose of evaluating the effect of varying selected design parameters on motor performance, length, inert weight, and SRM program cost are presented on Tables XVIII and XXIX, the constraints listed below were held constant for all the designs except as noted to investigate the effect of selected design parameters on SRM weight and cost.

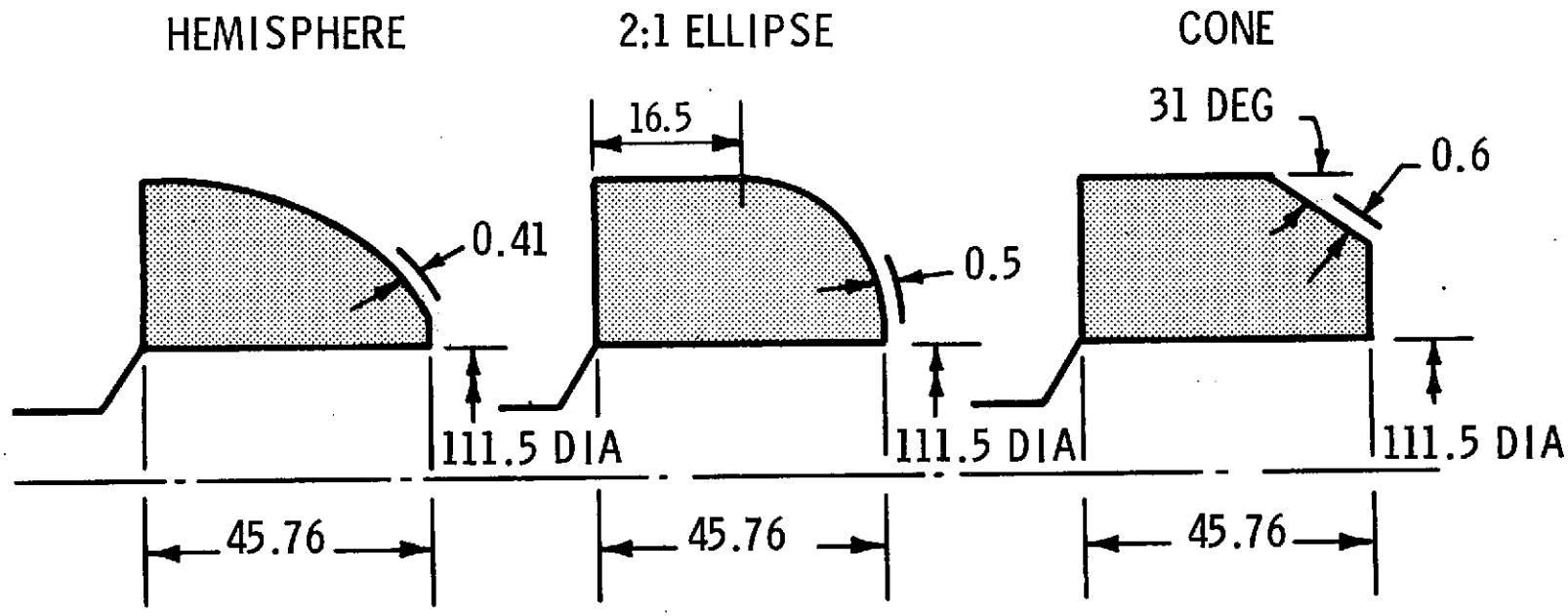


| | | | |
|---|---|---|---|
| PROPELLANT VOLUME ($IN.^3$) | 208,300 | 258,800 | 227,500 |
| PROPELLANT WEIGHT (LBM) | 13,220 | 16,430 | 14,440 |
| Δ PROPELLANT WEIGHT (LBM) | -0- | 3,210 | 1,220 |
| Δ INERT WEIGHT (LBM) | -0- | 1,500 | 1,600 |
| Δ EFFECTIVE PROPELLANT WEIGHT (LBM) | -0- | +210 | -1,980 |

Figure 3-59. Comparison of Propellant Loading in Three Aft Closure Designs for Configuration 1

CHAMBER PRESSURE = 600 PSIA

EXIT CONTOUR INITIAL ANGLE = 23.6 DEG

$R_2/R_t$ = 0.60 $R_t$ = 28.2

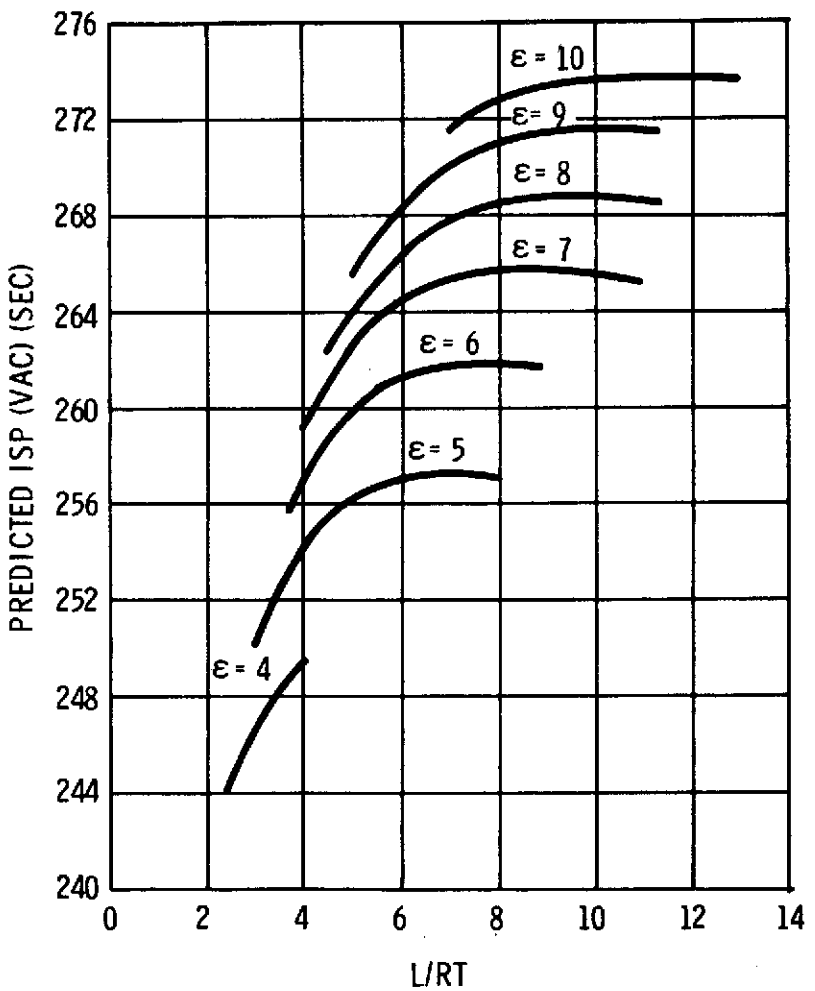


Figure 3-60. Delivered Specific Impulse Versus Nozzle Length-to-Throat Radius Ratio

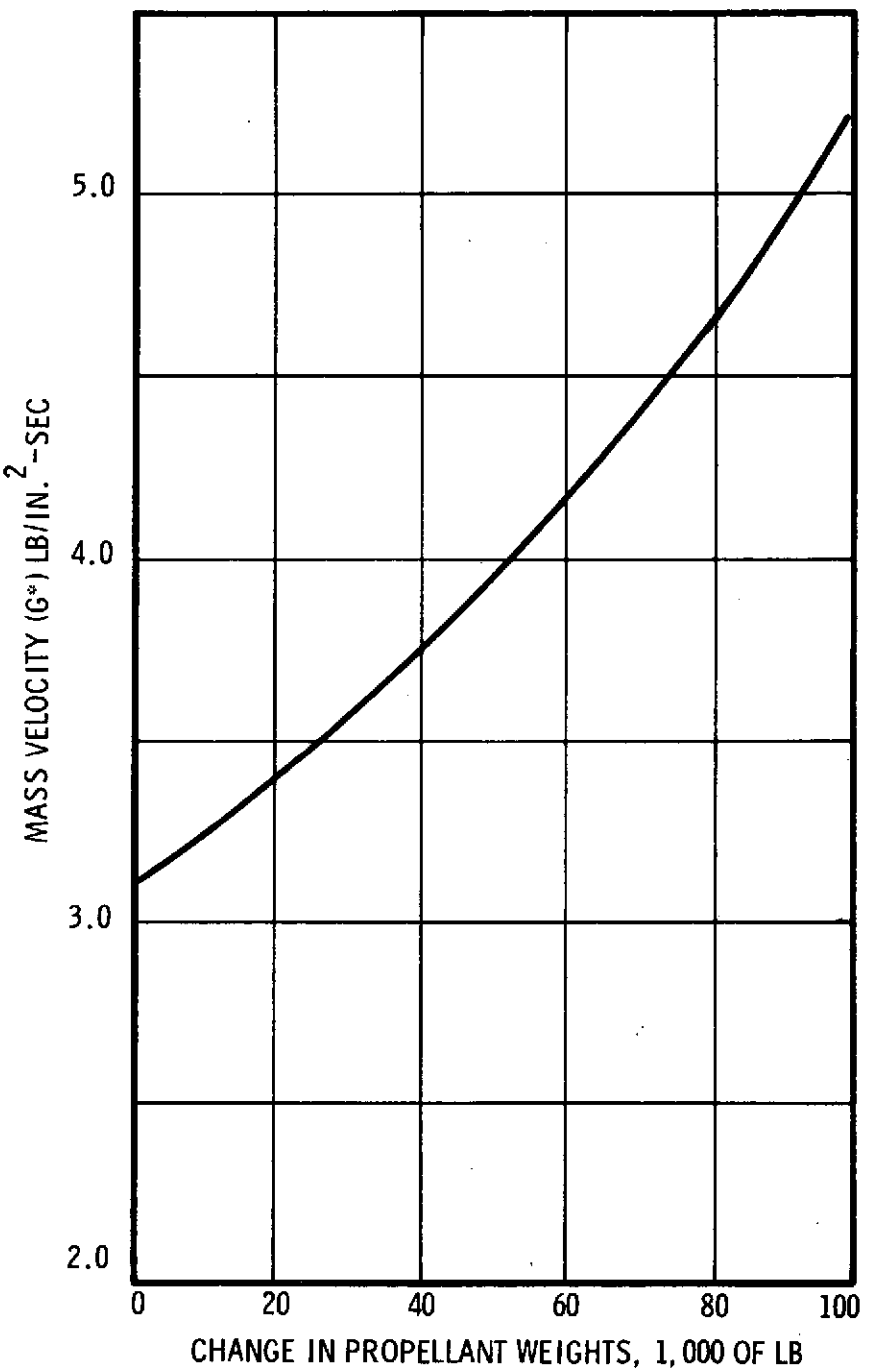


Figure 3-61. Maximum G* as a Function of Increased Propellant ($\Delta$Wp) Configuration 1

TABLE XXVIII

SRM CONFIGURATION COMPARISONS

| DESIGN NO. | 1 | 2 | 3 | 4 | 5 | 6 |
|---|---|---|---|---|---|---|
| | CONFIGURATION 1 | FREE G* $\varepsilon = 5.5$ | FIXED G* AND $\varepsilon = 6$ | FIXED G* AND $\varepsilon = 7$ | FIXED $D_C = 148$ $\varepsilon = 5.5$ | FREE $D_C$ $\varepsilon = 5.5$ |
| DIAMETER (IN.) | 146 | 146 | 146 | 146 | 148 | 149 |
| OVERALL LENGTH (IN.) | 1,454 | 1,479 | 1,458 | 1,461 | 1,432 | 1,422 |
| TOTAL DELIVERED IMPULSE (LBF-SEC X $10^6$) | 265.8 | 264.6 | 266.4 | 266.3 | 265.6 | 265.4 |
| G* (LBM/SEC-IN.$^2$) | 2.79 | 2.63 | 2.79 | 2.79 | 2.64 | 2.62 |
| PROPELLANT WEIGHT (LBM) | 1,072,300 | 1,070,990 | 1,068,100 | 1,063,440 | 1,074,650 | 1,068,600 |
| TOTAL INERT WEIGHT (LBM) | 134,300 | 131,600 | 137,100 | 137,100 | 133,900 | 133,400 |
| MEOP (PSIA) | 865 | 815 | 886 | 871 | 817 | 812 |
| EXPANSION RATIO (INITIAL) | 5.5 | 5.5 | 6 | 7 | 5.5 | 5.5 |
| NOZZLE LENGTH-TO-THROAT RADIUS RATIO | 4.45 | 4.25 | 4.86 | 4.99 | 4.37 | 4.92 |
| $I_{SP}$ (LBF-SEC/LBM) | 256.6 | 256.1 | 258.7 | 261.7 | 256.4 | 257.7 |
| MASS FRACTION | 0.889 | 0.891 | 0.886 | 0.886 | 0.889 | 0.889 |
| DELTA COST, SRM ($M) | -- | -0.9 | +1.5 | +2.7 | +1.6 | +2.0 |

TABLE XXIX

SRM CONFIGURATION COMPARISONS

| DESIGN | 1 | 7 | 8 | OFF-LOADED TO CONFIGURATION 1 REQUIREMENTS |
|---|---|---|---|---|
| | CONFIGURATION 1 | CONFIGURATION 2 | $\varepsilon = 7$ | |
| DIAMETER (IN.) | 146 | 146 | 146 | 146 |
| OVERALL LENGTH (IN.) | 1,454 | 1,496 | 1,496 | 1,496 |
| TOTAL DELIVERED IMPULSE (LBF-SEC X $10^6$) | 265.8 | 276.4 | 275.7 | 270.6 |
| G* (LBM-SEC/IN.$^2$) | 2.79 | 2.78 | 2.81 | 2.78 |
| PROPELLANT WEIGHT (LBM) | 1,072,300 | 1,128,700 | 1,108,950 | 1,105,700 |
| TOTAL INERT WEIGHT (LBM) | 134,300 | 145,600 | 146,250 | 145,600 |
| MEOP (PSIA) | 865 | 890 | 907 | 890 |
| EXPANSION RATIO (INITIAL) | 5.5 | 5.5 | 7 | 5.5 |
| NOZZLE LENGTH-TO-THROAT RADIUS RATIO | 4.45 | 3.44 | 4.24 | 3.44 |
| $I_{SP}$ (LBF-SEC/LBM) | 256.6 | 253.4 | 259.3 | 253.4 |
| MASS FRACTION | 0.889 | 0.886 | 0.884 | 0.884 |
| DELTA COST, SRM ($M) | -- | +23 | +24 | +18 |

| Parameter | Value | Reason for Constraint |
|---|---|---|
| Mass Velocity, G* (at 60° F) | $\leq 2.79 \frac{\text{lbm-sec}}{\text{in.}^2}$ | MSFC/TC agreed to limit based on Titan III data. |
| Overall SRM Length, $L_{SRM}$ (forward flange-to-exit) | ≤ 1,495.6 in. | MSFC change $X_B$ for exit plane from 1,951 in. to 1,989.6 in. permitting an increase of 38.6 in. in SRM length. |
| Minimum Case Wall Thickness | 0.466 + 0.010 = 0.476 in. | Minimum case wall required to survive slapdown loads + allowance for 19 grit blast cleanings. |
| Aft Case Segment Thickness | ≥ 0.51 in. | Minimum wall thickness required to react launch pad loads. |
| Stiffener Weight on Aft Case Segment | ~300 lb | Assumed weight of ring stiffener required on aft case segment to survive cavity collapse loads. |
| ET Attach Segment Length | ~100 in. | Requirement for double flange on attach segment reduced length from 142.7 to ~100 inches. |
| Number of Case Joints | 10 | Additional case segment had to be added in aft casting segment due to decrease in attach segment length. |
| Nozzle Expansion Ratio, $\epsilon$ | ≥5.5 | Lower limit specified as any cost/ weight variations are small below this value. |

The exceptions to these constraints are listed separately to identify the objective of each design.

Design No. 1 - (Configuration 1)

$G^* = 2.79$ lb-sec/in.$^2$

Design No. 2 - (Free G* and $\epsilon = 5.5$)

None

Design No. 3 - (Fixed G* and $\epsilon = 6$)

$G^* = 2.79$ lb-sec/in.$^2$

$\epsilon = 6$

Design No. 4 - Fixed G* and $\epsilon = 7$)

$G^* = 2.70$ lb-sec/in.$^2$

$\epsilon = 7$

Design No. 5 - (Fixed $D_c = 148$ and $\epsilon = 5.5$)

$D_c = 148$ in.

$\epsilon = 5.5$

Design No. 6 - (Free $D_c$ and $\epsilon = 5.5$)

$D_c$ = free variable

$\epsilon = 5.5$

Design No. 7 - (Configuration 2)

$L_{SRM} = 1,495.6$ in.

$I_{del}$ = maximum possible

$\epsilon = 5.5$

Number of Case Joints = 11 (additional case segment necessary to load increased propellant weight)

Design No. 8 - ($\epsilon = 7$)

$L_{SRM} = 1,495.6$ in.

$I_{del}$ = maximum possible

$\epsilon = 7$

Number of Case Joints = 11

Design No. 9 - (Off-loaded)

Design 7 off-loaded to meet Configuration 1 performance requirements.

The principal observation that can be made relative to the designs presented on Table XXVIII is the rather small difference in the SRM program cost. The delta cost for these designs range from -$0.9 M to +$2.7 M. This represents a variation of only $3.6 M which is a fraction of one percent of the total program cost.

## 4:0 VIBRATION AND ACOUSTIC DATA

A compilation of measured vibration and acoustic data on solid propellant rocket motors ranging in size from 52 in. to 156 in. in diameter is located in Appendix A.

A list of motors showing the type of data reported is presented below.

| Motor Designation | Diameter (in.) | Vibration Data | Acoustic Data |
|---|---|---|---|
| 156-1 (TU-412) | 156 | X | X |
| 156-7 (TU-393) | 156 | X | X |
| 156-8 (TU-312. L. 02) | 156 | X | -- |
| 156-2C-1 | 156 | X | X |
| 156-3 (LPC-L71) | 156 | X | X |
| UTC-DVXL5-1 | 120 | X | X |
| AGC 100 FW-1 | 100 | -- | X |
| Minuteman Stage I (TU-122) | 65 | X | X |
| Minuteman III Stage III | 52 | X | -- |
| Minuteman Missile (FTM 403) | 65 | -- | X |

A limited amount of vibration and acoustic data exists for solid propellant rocket motors. Combustion instability and its attendant vibrations is an area which was largely ignored until recently. The inclusion of aluminum early in the history of solid propellants eliminated most of the problems and until recently major emphasis was not directed at the problem.

Vibration and acoustic data measurement and analysis techniques have been improved significantly during the past few years. Also, engineers and technicians are currently more cognizant of combustion instability indications and are able to identify the modes. In the past, potential instability modes were often incorrectly

diagnosed as structural modes. Early solid motor program instrumentation was often not adequate to fully assess motor dynamic environment.

The data presented in Appendix A result from researching published reports, Thiokol engineering files, and, in some cases, reanalyzing the FM recorded motor firing data. Analysis of the limited data available indicates combustion instability was not present in any of the 156-in. motors fired at Thiokol. A detailed investigation of non-Thiokol fired motors is possible, but access to the original raw data is necessary.

## 5.0 LAUNCH SITE ASSEMBLY AND STACKUP TOLERANCE

The SRM assembly tolerance analysis was reviewed to determine the maximum possible displacement of the SRM centerline. Results indicate that the maximum lateral displacement could be as much as 0.625 in. for Configuration 1-1 if the case segment tolerances were stacked in the worst possible manner. A statistical treatment of the tolerances, assuming a random ordering of the tolerance combinations, indicated a more probable lateral displacement would be 0.177 in.

The maximum offset of the true centerline of Configuration 1-1, due to angular offset, diameter offset, and runout tolerances, is shown on figure 5-1. The simplifying assumption made in the calculations is that the case segments are rectangular in cross-section rather than circular. This reduces the analysis to a two-dimensional problem thus ignoring the complexity of including the location of the dimensional variations relative to the axis of the segments. The maximum centerline offset due to the maximum possible difference between segments is shown on figure 5-2. The dimensions used in these calculations are tabulated below:

| | |
|---|---|
| At O-ring Groove Area | |
| Tang ID | $144.613 \pm 0.004$ |
| Clevis OD | $144.603 \pm 0.004$ |
| Offset Calculation No. 1 | 144.617 max tang ID |
| | 144.599 min clevis OD |
| | $\frac{0.018}{2} = 0.009$ max diametral offset |
| Angularity Calculation No. 2: | Total runout of one horizontal locating surface to the one on the opposite end equals 0.010 total angular offset |
| Runout (Eccentricity): | O-ring surfaces at ends of each segment |
| | $\frac{0.010}{2} = 0.005$ per segment joint |

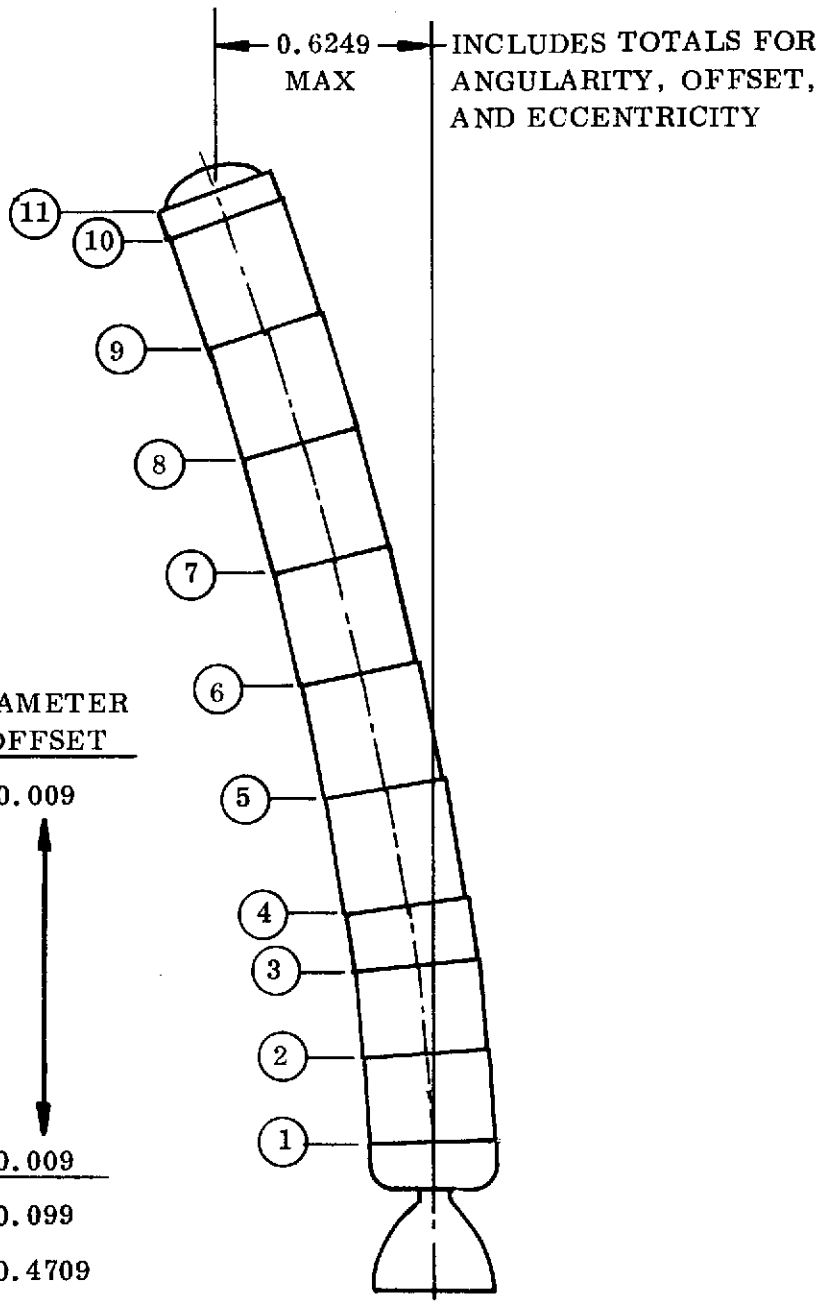


| INTERFACE NO. | ANGULAR OFFSET | DIAMETER OFFSET |
|---|---|---|
| 11 | 0.0104 | 0.009 |
| 10 | 0.0962 | |
| 9 | 0.0855 | |
| 8 | 0.0748 | |
| 7 | 0.0641 | |
| 6 | 0.0534 | |
| 5 | 0.0427 | |
| 4 | 0.0177 | |
| 3 | 0.0174 | |
| 2 | 0.0087 | |
| 1 | 0.0000 | 0.009 |
| TOTALS | 0.4709 | 0.099 |
| ANGULAR OFFSET = | | 0.4709 |
| DIAMETER OFFSET = | | 0.0990 |
| RUNOUT (ECCENTRICITY) 0.005 X 11 = | | 0.0550 |
| TOTAL | | 0.6249 |

Figure 5-1. Total Offset From True Centerline

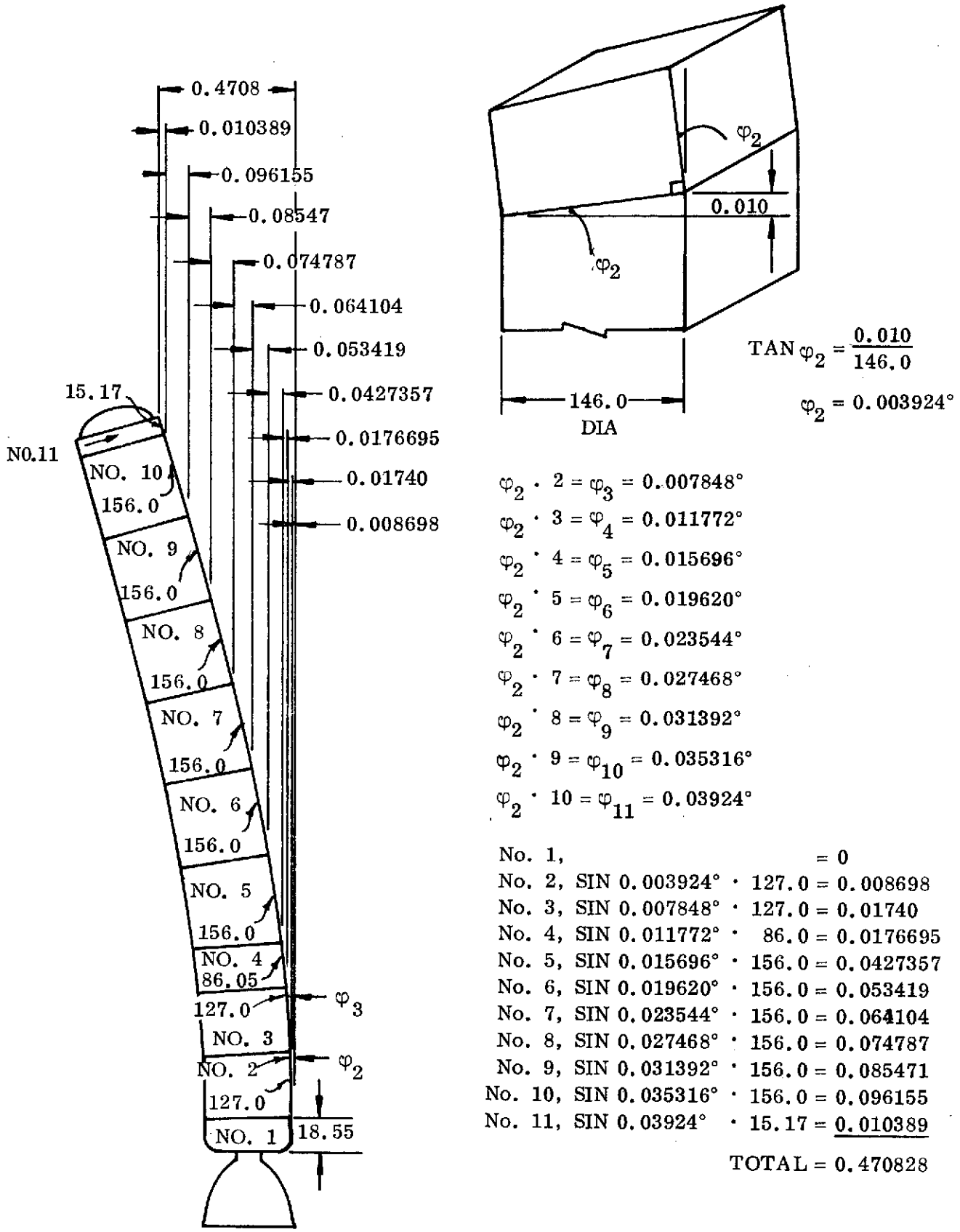


$$\text{TAN}\,\varphi_2 = \frac{0.010}{146.0}$$

$$\varphi_2 = 0.003924°$$

$\varphi_2 \cdot 2 = \varphi_3 = 0.007848°$
$\varphi_2 \cdot 3 = \varphi_4 = 0.011772°$
$\varphi_2 \cdot 4 = \varphi_5 = 0.015696°$
$\varphi_2 \cdot 5 = \varphi_6 = 0.019620°$
$\varphi_2 \cdot 6 = \varphi_7 = 0.023544°$
$\varphi_2 \cdot 7 = \varphi_8 = 0.027468°$
$\varphi_2 \cdot 8 = \varphi_9 = 0.031392°$
$\varphi_2 \cdot 9 = \varphi_{10} = 0.035316°$
$\varphi_2 \cdot 10 = \varphi_{11} = 0.03924°$

No. 1, = 0
No. 2, SIN 0.003924° · 127.0 = 0.008698
No. 3, SIN 0.007848° · 127.0 = 0.01740
No. 4, SIN 0.011772° · 86.0 = 0.0176695
No. 5, SIN 0.015696° · 156.0 = 0.0427357
No. 6, SIN 0.019620° · 156.0 = 0.053419
No. 7, SIN 0.023544° · 156.0 = 0.064104
No. 8, SIN 0.027468° · 156.0 = 0.074787
No. 9, SIN 0.031392° · 156.0 = 0.085471
No. 10, SIN 0.035316° · 156.0 = 0.096155
No. 11, SIN 0.03924° · 15.17 = 0.010389

TOTAL = 0.470828

Figure 5-2. Maximum Offset Due to Angularity Variation Between Segments

The maximum rotational displacement of the assembled SRM is shown in figure 5-3. The following calculation was used:

True Positional Tolerance of Rotational Index Slot or Skirt Index Holes to Index Pin.

For each segment: $\frac{0.010}{2} = 0.005$

The angular offset, diameter offset, and runout tolerances and maximum sum given in figure 5-1 are repeated below, along with the random or statistical combined sum in a parallel column.

| | Summed Tolerances (in.) | Combined Random Sum (in.) |
|---|---|---|
| Angular Offset | 0.4709 | 0.1735 |
| Diameter Offset | 0.0990 = 0.009 x 11 | $0.0299 = 0.0990 \div \sqrt{11}$ |
| Runout | 0.0550 = 0.005 x 11 | $0.0166 = 0.055 \div \sqrt{11}$ |
| Total | 0.6249 | 0.1768 |

Since the summed tolerances are linear sums, the random combinations are simply the square roots of the respective sum of squares, assuming each item is independent of all other items. The angular offsets, for each segment computed in figure 5-2, are based on the sum of the angles affecting all the preceding segments in the buildup. Identical angular offset values are obtained by considering separate angles affecting summed SRM segment lengths. However, the proper technique for computing the random combination of independent items is to consider the separate angles affecting the summed SRM segments. The results of these calculations, as shown on Table XXX, indicate the more probable angular offset for the stacked SRM case components is 0.1735 in. instead of 0.4709 in.

It is recognized that both treatments of the maximum offset question are quite cursory, and the results are only adequate for initial evaluation purposes. A much more detailed analysis, probably involving a Monte-Carlo simulation, will have to be conducted to determine the expected variation in offset during SRM assembly at the launch site.

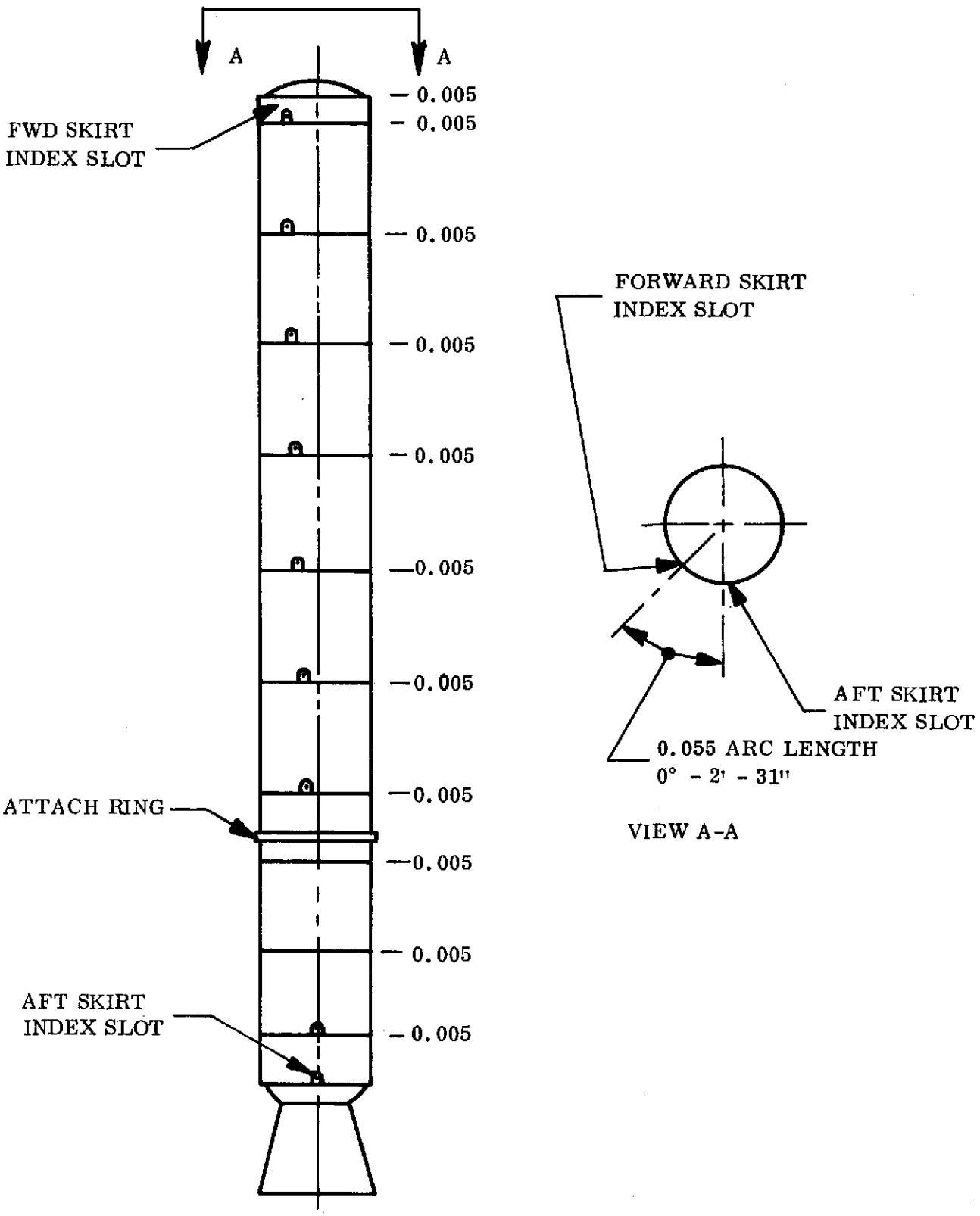


Figure 5-3. Rotational Maximum Misalignment

TABLE XXX

ANGULAR OFFSET
(IN.)

| Segment Number | Segment Length | Sum of Lengths | Sum of Lengths x (0.010/146) |
|---|---|---|---|
| 11 | 15.17 | 15.17 | 0.0010 |
| 10 | 156 | 171.17 | 0.0117 |
| 9 | 156 | 327.17 | 0.0224 |
| 8 | 156 | 483.17 | 0.0331 |
| 7 | 156 | 639.17 | 0.0438 |
| 6 | 156 | 795.17 | 0.0545 |
| 5 | 156 | 951.17 | 0.0651 |
| 4 | 86 | 1,037.17 | 0.0710 |
| 3 | 127 | 1,164.17 | 0.0797 |
| 2 | 127 | 1,291.17 | 0.0884 |
| Sum | | | 0.4709 |
| Square root of sum of squares | | | 0.1735 |

## 6.0 SRM DDT&E SCHEDULE

SRM project planning and development of DDT&E Schedules during this interim contract are based on MSFC supplied milestones, discussions with major component suppliers, and modifications to the RFP or the Thiokol proposal baseline schedule. The major changes which have occurred to influence the schedule include SRM ATP slip, PDR and CDR slip, FMOF slip, increase in the number of development and qualification motors, decrease in the number of ground test articles, and increase in component lead times.

The SRM case represents the most critical path, and case lead times paces the SRM project. Discussions with potential case suboontractor and forging suppliers have supplied current lead time outlook which is incorporated into the schedule shown in figure 6-1 . This schedule reflects case steel being placed on order in April 1974. The Ladish Company has placed D6AC steel billets on order with Latrobe and Republic Steel Companies. Commitment of dollars to support these orders is not required until September-October 1974 time period.

Nozzle steel material lead time is the second most critical path and lags the case by approximately one month.

During the interim contract period, NASA-MSFC and TC jointly agreed to incorporate conventional high-cost nozzle ablative materials in the first development motor static firing (DM-1). The newer low-cost materials, which will be thoroughly tested in laboratory and subscale motors (up to 38,000 pounds of propellant) over a 26-month period are scheduled for the second development motor test (DM-2).

Five development motors and four qualification motors are now planned with development motor testing being conducted from December 1976 to December 1977, and qualification motor testing accomplished from April 1977 through October 1978. The twelve DDT&E flight motors begin fabrication in October 1977, and the last motor is supplied in May 1979.

FOLDOUT FRAME 1

FOLDOUT FRAME 2

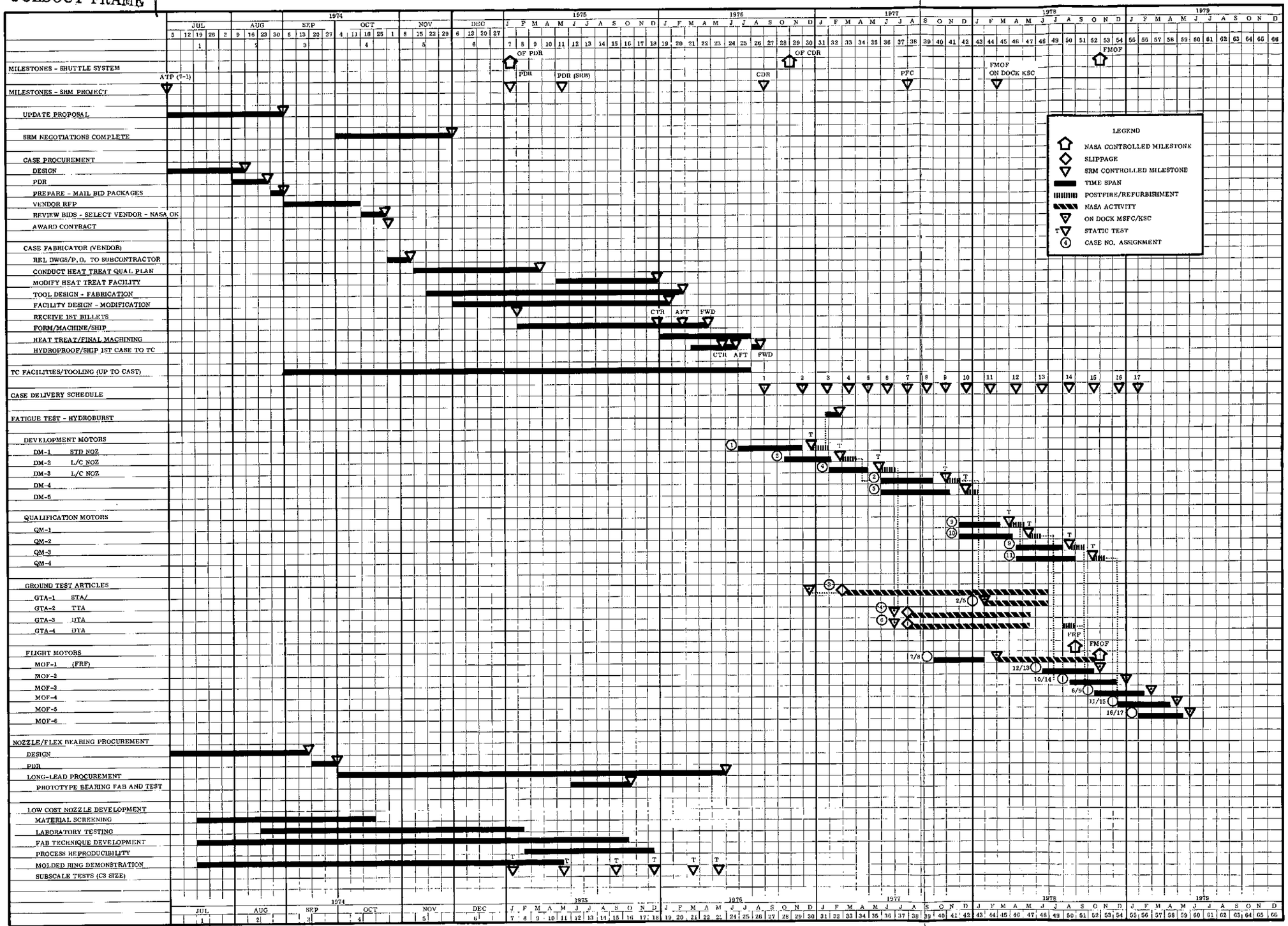


Figure 6-1. Preliminary Schedule E

Techniques used to develop the schedule include application of Industrial Engineering standard hour cycle times for tasks defined by SRM manufacturing plans. The following assumptions and ground rules were used:

1. Nozzle material data from DM-1 (standard materials) and DM-2 (low-cost materials) static testing to be reviewed and final material selection made prior to start of assembly of DM-3 nozzle
2. Demonstrate the refurbishment and reuse of cases, nozzles, bearings, and ignition system components during both development and qualification motor test series
3. Refurbish and reuse GTA hardware (post CDR) for flight motors
4. Demonstrate dual processing and dual motor loading in the development, and qualification motor series.

# APPENDIX A

## MEASURED VIBRATION AND ACOUSTIC DATA ON LARGE SOLID PROPELLANT ROCKET MOTORS

CONTENTS

## ILLUSTRATIONS

ILLUSTRATIONS (Cont)

## TABLES

# APPENDIX A
# MEASURED VIBRATION AND ACOUSTIC DATA ON LARGE SOLID PROPELLANT ROCKET MOTORS

## 1.0 INTRODUCTION

This report is a compilation of measured vibration and acoustic data obtained from static firings of large solid propellant rocket motors. Much of the data dates back five to ten years, particularly that of the 120- to 156-inch diameter motors. The test objectives of only a few of the motors included obtaining vibration and acoustic environment. In most cases, cost considerations limited the use of vibration transducers to a few locations on a motor nozzle or case as an aid in failure analysis.

The data in this report were gleaned from memoranda and final reports. The reports are referenced when only a summary of their data is presented in this report. A list of references, not received by Thiokol in time for this report, is included.

The motors included in this report vary in size from 52 inches in diameter to 156 inches in diameter. Aerojet-General Corporation fired 260-inch diameter solid propellant motors, but Thiokol has received no data from these tests.

Table I is a list of motors and the type of data reported. For some motors, data are limited to one channel.

Motor descriptive parameters are presented in Table II and individual sections when available to permit scaling of data. Classified data are excluded intentionally.

TABLE I

MOTORS REPORTED ON

| Motor Designation | Diameter (in.) | Vibration Data | Acoustic Data |
|---|---|---|---|
| 156-1 (TU-412) | 156 | X | X |
| 156-7 (TU-393) | 156 | X | X |
| 156-8 (TU-312. L. 02) | 156 | X | -- |
| 156-2C-1 | 156 | X | X |
| 156-3 (LPC-L71) | 156 | X | X |
| UTC-DVXL5-1 | 120 | X | X |
| AGC 100 FW-1 | 100 | -- | X |
| Minuteman Stage I (TU-122) | 65 | X | X |
| Minuteman III Stage III | 52 | X | -- |
| Minuteman Missile (FTM 403) | 65 | -- | X |

TABLE II

MOTOR PARAMETERS

| Motor | Port Dia (in.) | Port Length (in.) | Propellant Weight (lbm) | Mass Flow Rate (lbm/sec) | Avg Thrust Vac (lbf) |
|---|---|---|---|---|---|
| 156-1 (TU-412) | ~66 | ~784 | 690,500 | 5,311 | 1,408,000 |
| 156-7 (TU-393) | ~59 | ~155 | 128,800 | 1,124 | 331,900 |
| 156-8 (TU-312. L. 02) | ~76 | ~598 | 492,600 | 3,979 | 1,068,000 |
| 156-2C-1 | ~96 | ~988 | 798,100 | 10,953 | 3,279,000 |
| 156-3 (LPC-L71) | ~103 | ~737 | 423,600 | 3,800 | 975,200 |
| Stage I Minuteman | ~30 | ~245 | 45,800 | 747 | 221,200 |
| Stage III Minuteman | ~11 | ~72 | 7,300 | 121 | 34,600 |

## 2.0 VIBRATION AND ACOUSTIC DATA

### 2.1 156-1 (TU-412.01)

The Thiokol TU-412.01 (AF designation 156-1) was successfully static fired at Thiokol/Wasatch on 12 December 1964 in Test Bay T-24 in a horizontal, pin supported, multi-component test stand.

The motor consisted of three case segments of 18-percent nickel maraging steel; an omniaxes gimballed, thrust vector controlled nozzle; and a segmented, cylindrically perforated (CP) propellant grain. The rocket motor utilized an aft end ignition system. The motor configuration and descriptive parameters are shown in figure 1.

#### 2.1.1 156-1 (TU-412) Vibration Data

Five accelerometers were mounted on the motor system as follows:

| Accelerometer No. | Location |
|---|---|
| A201 | Nozzle Exit Cone, Vertical, Near Exhaust |
| A202 | Nozzle Exit Cone, Vertical, Near Mounting Flange |
| A001 | Motor Case Center, Radial |
| A002 | Aft Harness, Radial |
| A003 | Aft Harness, Vertical |

A summary of the composite peak acceleration values for these accelerometers follows:

Acceleration Peaks (G-Units)
(All Values Plus and Minus Values)

| | A001 | A002 | A003 | A201 | A202 |
|---|---|---|---|---|---|
| Average during ignition | 1 | 2 | 1 | 20-25 | 12-25 |
| Peak at ignition | 15 | 8.5 | 3.5 | 80 | 82 |
| Peak at 30 seconds | 2.5 | 3.2 | 1.8 | 70 | 43 |
| Peak at exit loss (loss of nozzle exit cone) | 3 | 10 | 6 | Lost at 37 sec | 40 |
| Peak at tailoff | 15 | 19 | 6 | ↓ | Lost at 99.6 sec |

**TU-412**
**126-KS-1,275,000**
**156-INCH BOOSTER**

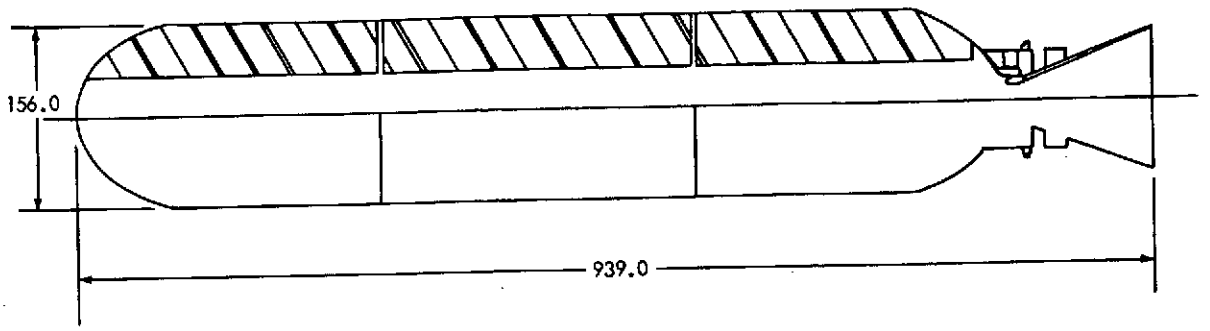


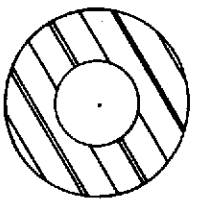

## CASE

| | |
|---|---|
| Material | 18% Nickel Maraged Steel |
| Minimum Ultimate Strength, psi | 240,000 |
| Minimum Yield Strength, psi | 230,000 |
| Hydrostatic Test Pressure, psi | 850 |
| Yield Pressure, psi | 1,260 |
| Hydrostatic Test Pressure/Maximum Pressure | 1.13 |
| Yield Pressure/Hydrostatic Test Pressure | 1.48 |
| Nominal Thickness, in. | 0.496 |

## NOZZLE

| | |
|---|---|
| Body Material | 4130 Steel |
| Throat Insert Material | Graphite Cloth Phenolic |
| Initial Throat Area, $in.^2$ | 1,134 |
| Exit Area, $in.^2$ | 9,070 |
| Expansion Ratio | 8.0 |
| Expansion Cone Half Angle, degrees | 17.5 |
| Type | Omniaxial Gimbaled |
| Number of Nozzles | 1 |

## LINER

| | |
|---|---|
| Type | HC Polymer-Asbestos |
| Density, $lbm/in.^3$ | 0.0357 |

## IGNITER

| | |
|---|---|
| Thiokol Drawing Designation | TU37067-01 |
| Type | Aft End Pyrogen with S&A |
| Minimum Firing Current, amperes | 4.5 |
| Circuit Resistance, ohms | 0.22 |
| No. of Squibs | 2 |

## PROPELLANT

| | |
|---|---|
| Propellant Designation and Formulation | TP-H-1011 |
| PBAA/AN - 14% | Type III |
| Al - 16% | |
| AP - 70% | |

## PROPELLANT CONFIGURATION

| | |
|---|---|
| Type | Segmented, Cylindrically Perforated |
| Web, in. | 44.0 |
| Web Fraction, % | 0.57 |
| Sliver Fraction, % | 1.31 |
| Propellant Volume, $in.^3$ | 10,790,000 |
| Volumetric Loading Density, % | 79 |
| Web Average Burning Surface Area, $in.^2$ | 242,000 |
| Initial Surface to Throat Area Ratio ($K_n$) | 194 |

## PROPELLANT CHARACTERISTICS

| | |
|---|---|
| Burn Rate @ 1000 psia ($r_b$), in./sec | 0.379 |
| Burn Rate Exponent (n) | 0.21 |
| Density, $lbm/in.^3$ | 0.064 |
| Temperature Coefficient of Pressure ($\pi_k$), %/°F | 0.102 |
| Characteristic Exhaust Velocity (C*), ft/sec | 5,173 |
| Adiabatic Flame Temperature, °F | 5,814 |
| Effective Ratio of Specific Heats (Chamber) | N.D. |
| (Nozzle Exit) | 1.18 |

## CURRENT STATUS

Feasibility Demonstration Complete

Figure 1. 156-1 (TU-412) Motor Description

The duration of the ignition transient was approximately 0.5 second. The g level decreased when the igniter left the nozzle. Instrument A201 was lost after 37 seconds, but examination of the other accelerometers shows no incident at this time.

Instrument A202 indicated that, after approximately 30 seconds of ignition, high transient spikes occur frequently throughout the remainder of firing. These spikes could result from material breaking away from or impacting against the nozzle exit cone. Instrument A202 indicated that the average magnitude of g values increases with ignition time. This could be attributed to a temperature rise of the accelerometer due to radiant heat exposure.

A high-speed runoff of the A201 trace shows that at T + 0.6 second a wave of 10 g's magnitude at 11-Hz is superimposed on the normal high frequency signal. This corresponds to a double amplitude motion of 1.5 inches at the exit plane of the divergent cone. These data are corroborated by an examination of the increased nozzle cyclic torque values. The 11-Hz wave is noted prior to T + 0.6 second, but it is obscured by the high ignition transient.

The 11-Hz frequency is thought to be the rigid body fundamental resonance of the nozzle and actuation system.

A spectral analysis of the accelerometer data acquisition tapes (FM type) has resulted in the following gravity root mean square (Grms) levels at the predominant frequencies and time periods noted.

| Accelerometer | Time | Filter | Frequency Range (Hz) | Grms |
|---|---|---|---|---|
| 002 | 2-7 | 50 | 600-1,200 | 0.61 |
| 002 | 2-7 | 50 | 2,000-2,300 | 0.33 |
| 201 | 2-7 | 50 | 400-1,200 | 2.77 |
| 201 | 26-35 | 50 | 400-1,400 | 3.64 |
| 001 | 105-111 | 50 | 2,000-2,600 | 0.84 |
| 002 | 105-111 | 50 | 600-1,200 | 1.22 |
| 002 | 105-111 | 50 | 1,600-2,200 | 1.0 |

| Accelerometer | Time | Filter | Frequency Range (Hz) | Grms |
|---|---|---|---|---|
| 002 | 105-111 | 50 | 2,400-3,000 | 1.0 |
| 201 | 26-35 | 50 | 2,400-3,000 | 2.24 |
| 202 | 2-7 | 50 | 400-1,800 | 2.87 |

FM tapes for the above data are located in Thiokol archives.

2.1.2 156-1 (TU-412) Acoustic Data

Air Force WADC personnel were to monitor the near and far field Sound Pressure Level (SPL), but their power supply malfunctioned. The acoustic Sound Pressure Level was measured at only one location, 8,900 feet from the motor at an angle of 104 degrees from the thrust centerline. The data are tabulated below.

| Reading No. | Frequency Pass Band (Hz) | SPL $\left(\text{dB ref } 0.0002 \frac{\text{dynes}}{\text{cm}^2}\right)$ |
|---|---|---|
| 1 | 20-37.5 | 103 |
| 2 | 37.5-53 | 106 |
| 3 | 53-75 | 102 |
| 4 | 75-106 | 106 |
| 5 | 106-150 | 106 |
| 6 | 150-212 | 108 |
| 7 | 212-300 | 104 |
| 8 | 300-425 | 104 |
| 9 | 425-600 | 102 |
| 10 | 600-850 | 103 |
| 11 | 850-1,200 | 100 |

2.2 156-7 (TU-393)

The Thiokol TU-393 (AF designation 156-7) motor was successfully static fired in a horizontal attitude at Thiokol/Wasatch on 13 May 1966 utilizing a 10-foot diameter by 82-foot long diffuser for altitude simulation. The motor was fabricated of a flightweight 156-inch diameter fiberglass reinforced plastic monolithic case, a submerged fixed nozzle, with a 34 to 1 expansion ratio, and an $N_2O_4$ Liquid

Injection Thrust Vector Control (LITVC) system. The motor configuration and descriptive parameters are shown in figure 2.

2.2.1 156-7 (TU-393) Vibration Data

Accelerometers were mounted on the $N_2$ tanks and the nozzle exit cone.

The following accelerations were experienced on the $N_2$ tanks (accelerometers A601 and A602):

80-to 100-gs peak at 50 Hz for 10 cycles

1.5 grms in 500-to 600-Hz range (predominant frequency)

Accelerometer A201, mounted vertically on the nozzle exit cone, experienced increased magnitudes as a function of fluid injection rate at the predominant frequency of 575 Hz as shown below.

| Fluid Injection Rate | Frequency (Hz) | Grms |
|---|---|---|
| 1 burst/second | 575 | 7 |
| 5 bursts/second | 575 | 22 |
| Sustained burst | 575 | 30 |
| No injection | 575 | 2.5 |

FM tapes of the above data are located in Thiokol's archives.

2.2.2 156-7 (TU-393) Acoustic Data

Two microphones were used to monitor the SPL. One, located 50 feet to the side and 25 feet aft of the diffuser exit plane, recorded the following:

160 to 170 dB in the 10-to 300-Hz range.

Less than 160 dB beyond the 300-Hz frequency range.

Greater than 180 dB at ignition and at diffuser burnthrough (occurring at 70 seconds), then dropped below 160 dB.

The recording system for the above instrument was limited to a 20-dB range from 160 to 180 dB.

The second microphone was located at 90 degrees to the thrust centerline, 9,000 feet from the motor. Results are shown in figure 3.

TU-393
110.0-KS-331,900
156-7
156-INCH BOOSTER

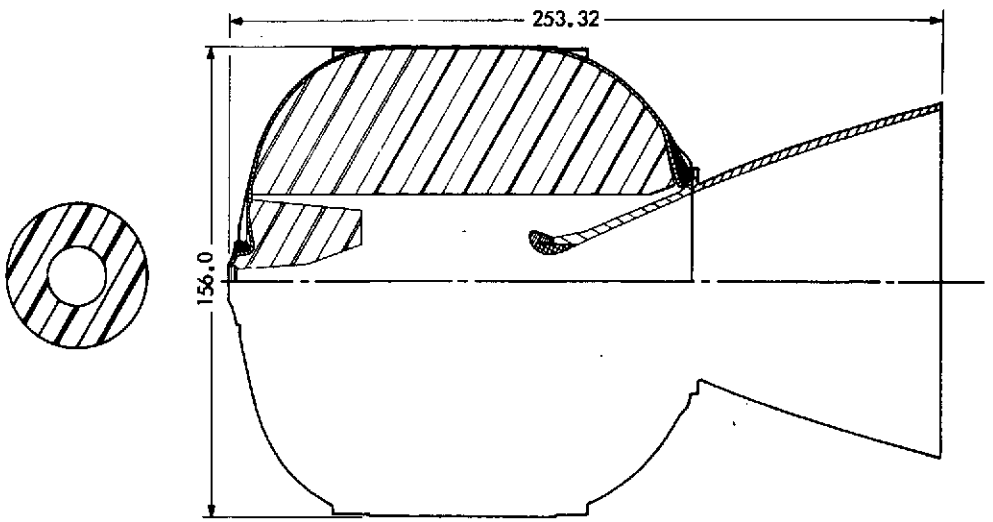


## CASE

| | |
|---|---|
| Material | (FRP) Fiberglass Reinforced Plastic |
| Minimum Ultimate Strength, psi | (Composite) 128,000 |
| Minimum Yield Strength, psi | Not Available |
| Hydrostatic Test Pressure, psi | 775 |
| Yield Pressure, psi | Not Available |
| Hydrostatic Test Pressure/Maximum Pressure | 1.1 |
| Yield Pressure/Hydrostatic Test Pressure | Not Available |
| Nominal Thickness, in. | 0.592 |

## NOZZLE

| | |
|---|---|
| Body Material | 18% Nickel Steel |
| Throat Insert Material | Graphite Cloth Phenolic |
| Initial Throat Area, $in.^2$ | 314.47 |
| Exit Area, $in.^2$ | 10,694.0 |
| Expansion Ratio | (Average) 32.53:1 |
| Expansion Cone Half Angle, degrees | 15 |
| Type | Fixed Semi-Submerged Contour |
| Number of Nozzles | 1 |

## LINER

| | |
|---|---|
| Type | HC Polymer-Asbestos |
| Density, $lbm/in.^3$ | 0.0357 |

## IGNITER

| | |
|---|---|
| Thiokol Drawing Designation | 7U-37635 |
| Type | Head-End, Four-Nozzle Pyrogen |
| Minimum Firing Current, amperes | 2 |
| Circuit Resistance, ohms | 39 |
| No. of Squibs | 2 |

## PROPELLANT

Propellant Designation and Formulation Type II TP-H-8163
AL - 16%
AP - 69%
Binder - 15%

## PROPELLANT CONFIGURATION

| | |
|---|---|
| Type | Cylindrical Perforate |
| Web, in. | 47.82 |
| Web Fraction, % | 62 |
| Sliver Fraction, % | 0 |
| Propellant Volume, $in.^3$ | 2,025,456 |
| Volumetric Loading Density, % | 91 |
| Web Average Burning Surface Area, $in.^2$ | 42,350 |
| Initial Surface to Throat Area Ratio ($K_n$) | 110.2 |

## PROPELLANT CHARACTERISTICS

| | |
|---|---|
| Burn Rate @ 1000 psia ($r_b$), in./sec | 0.428 |
| Burn Rate Exponent (n) | 0.38 |
| Density, $lbm/in.^3$ | 0.0636 |
| Temperature Coefficient of Pressure ($\pi_k$), %/°F | 0.12 |
| Characteristic Exhaust Velocity (C*), ft/sec | 5,164 |
| Adiabatic Flame Temperature, °F | 5,713 |
| Effective Ratio of Specific Heats (Chamber) | 1.14 |
| (Nozzle Exit) | 1.18 |

## CURRENT STATUS

Inactive

Figure 2. 156-7 (TU-393) Motor Description

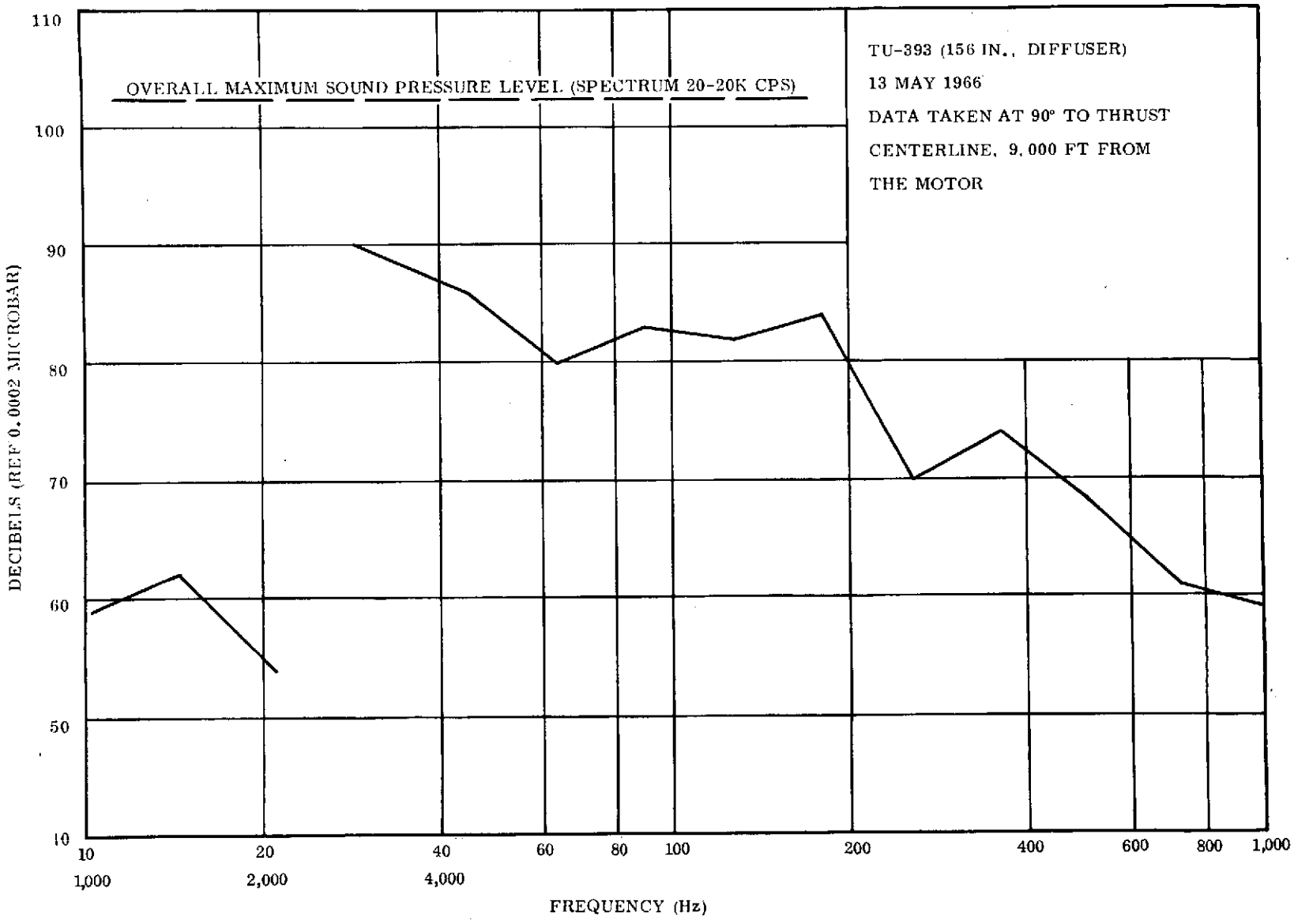


Figure 3. 156-7 (TU-393) Acoustic Sound Pressure Levels

## 2.3 156-8 (TU-312.L.02)

The Thiokol TU-312.L.02 (AF designation 156-8) was successfully static fired at Thiokol/Wasatch on 25 June 1968 under Contract AF 04(611)-11603. The motor was fired in a horizontal attitude.

The motor consisted of three fiberglass case segments (forward dome, center segment, and aft dome), cylindrically perforated propellant grain, and a fixed ablative nozzle. The motor descriptive parameters are classified confidential.

### 2.3.1 156-8 (TU-312.L.02) Vibration Data

Accelerometer data were taken to document the motor vibration characteristics during static test and to aid in analysis in case of failure. Data from three accelerometers are tabulated below. A spectral analysis was performed with a filter bandwidth of 10 to 50 Hz with the crossover frequency of 100 Hz.

## 2.4 156-2C-1

The Thiokol 156-2C-1 (Contract NAS3-6285) was successfully static fired at Thiokol Corporation, Brunswick, Georgia on 27 February 1965. The motor exhaust was directed vertically upward.

The motor consisted of four case segments of 18-percent nickel maraging steel, a fixed nozzle, and a continuous star perforated propellant grain. The motor configuration and descriptive parameters are shown in figure 4.

One of the objectives in this program was to measure acoustic and vibration data to verify theoretical predictions of rocket environment and/or to improve such predictions. The program was conducted with technical direction provided by NASA Vibration and Acoustic Branch, MSFC, Huntsville, Alabama.

A complete data analysis of the test results can be found in reference 1.

A summary of the instrumentation locations and test results is reported here.

TA-M-1
58.7-KS-2,970,000
156-2C-1
156-INCH BOOSTER

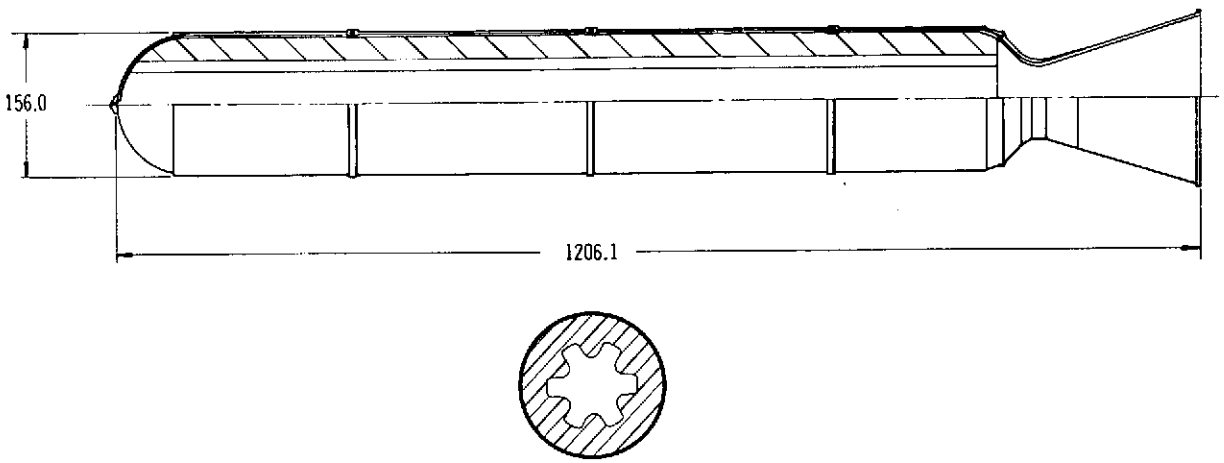


## CASE

| | |
|---|---|
| Material | 18% Nickel Maraging Steel |
| Minimum Ultimate Strength, psi | 240,000 |
| Minimum Yield Strength, psi | 230,000 |
| Hydrostatic Test Pressure, psi | 960 |
| Yield Pressure, psi | 1,260 |
| Hydrostatic Test Pressure/Maximum Pressure | 1.1 |
| Yield Pressure/Hydrostatic Test Pressure | 1.31 |
| Nominal Thickness, in. | 0.484 |

## NOZZLE

| | |
|---|---|
| Body Material | 18% Nickel Maraging Steel |
| Throat Insert Material | Graphite Cloth Phenolic |
| Initial Throat Area, $in.^2$ | 2,948 |
| Exit Area, $in.^2$ | 20,990 |
| Expansion Ratio | 7.12:1 |
| Expansion Cone Half Angle, degrees | 17.5 |
| Type | Fixed |
| Number of Nozzles | 1 |

## LINER

| | |
|---|---|
| Type | HC Polymer-Carbon Black |
| Density, $lbm/in.^3$ | 0.0399 |

## IGNITER

| | |
|---|---|
| Thiokol Model Designation | TX-359 |
| Type | Pyrogen - S&A |
| Minimum Firing Current, amperes | 4.5 per Squib |
| Circuit Resistance, ohms | 0.12 to 0.22 |
| No. of Squibs | 2 |

## PROPELLANT

| | |
|---|---|
| Propellant Designation and Formulation | TP-H-8163 |
| AP - 69% | $Fe_2O_3$ - 1% |
| AL - 16% | Binder - 14% |

## PROPELLANT CONFIGURATION

| | |
|---|---|
| Type | Six-Point Star |
| Web, in. | 28.62 |
| Web Fraction, % | 37.3 |
| Sliver Fraction, % | 7.86 |
| Propellant Volume, $in.^3$ | 12,489,000 |
| Volumetric Loading Density, % | 71.2 |
| Web Average Burning Surface Area, $in.^2$ | 402,100 |
| Initial Surface to Throat Area Ratio ($K_n$) | 128 |

## PROPELLANT CHARACTERISTICS

| | |
|---|---|
| Burn Rate @ 1000 psia ($r_b$), in./sec | 0.568 |
| Burn Rate Exponent (n) | 0.38 |
| Density, $lbm/in.^3$ | 0.0639 |
| Temperature Coefficient of Pressure ($\pi_k$), %/°F | 0.12 |
| Characteristic Exhaust Velocity (C*), ft/sec | 5,240 |
| Adiabatic Flame Temperature, °F | 5,734 |
| Effective Ratio of Specific Heats (Chamber) | - |
| (Nozzle Exit) | 1.18 |

## CURRENT STATUS

Feasibility Demonstration Complete

Figure 4. 156-2C-1 Motor Description

TABLE III

VIBRATION DATA SUMMARY

| Accelerometer Location | Direction | Predominant Frequency (Hz) | PSD ($G^2$/Hz) |
|---|---|---|---|
| Nozzle Exit Cone | Tangential | 40 | 0.00028 |
| | | 100 | 0.00014 |
| | | 200 | 0.00045 |
| | | 375 | 0.0002 |
| | | 470 | 0.00026 |
| | | 560 | 0.0004 |
| | | 700 | 0.0008 |
| Nozzle Exit Cone | Radial | 40 | 0.00048 |
| | | 100 | 0.0002 |
| | | 200 | 0.0018 |
| | | 375 | 0.0055 |
| | | 460 | 0.006 |
| On Case at Aft Attach Ring | Longitudinal | 250 | 0.0014 |
| | | 430 | 0.00028 |
| | | 600 | 0.0005 |

Above data tapes are located in Thiokol Archives.

2.4.1 156-2C-1 Vibration Data

Six channels of vibration data were recorded at select locations on the motor. The locations of the accelerometers are shown in figure 5. Results of the data are summarized below.

| Accelerometer No. | Initial Acceleration (g's) First Second | Steady Acceleration g's | Predominant Frequencies (Hz) |
|---|---|---|---|
| 19 | 43 | 13 to 7 | 20, 350, 3,500 |
| 20 | 46 | 13 | 20, 350, 3,500 |
| 21 | 5 | 5 (unsteady) | 20 |
| 22 | (No data, open circuit) | -- | -- |
| 23 | (No data, shorted circuit) | -- | -- |
| 24 | 35 | 6 | 20, 350, 3,500 |

2.4.2 156-2C-1 Acoustic Data

The microphone locations are shown in figure 6. Note that Balloon No. 2 was not used. The weather conditions for the firing (from Brunswick Flight Service Center) are shown below.

Clear with 15 miles visibility

Temperature: 60° to 60.3° F

Wet Bulb: 47%

Humidity: 33%

Wind Direction at Ground Level: 300°

Wind Velocity at Ground Level: 4 knots

Wind Velocity at 1,000 feet: 8 knots

Dew Point: 31° F

Barometer: 30.27 in. Hg

Results of the acoustic data are shown below.

The sound pressure spectral density profiles were nearly the same with time throughout the firing. The LPC firing at Redlands was similar.

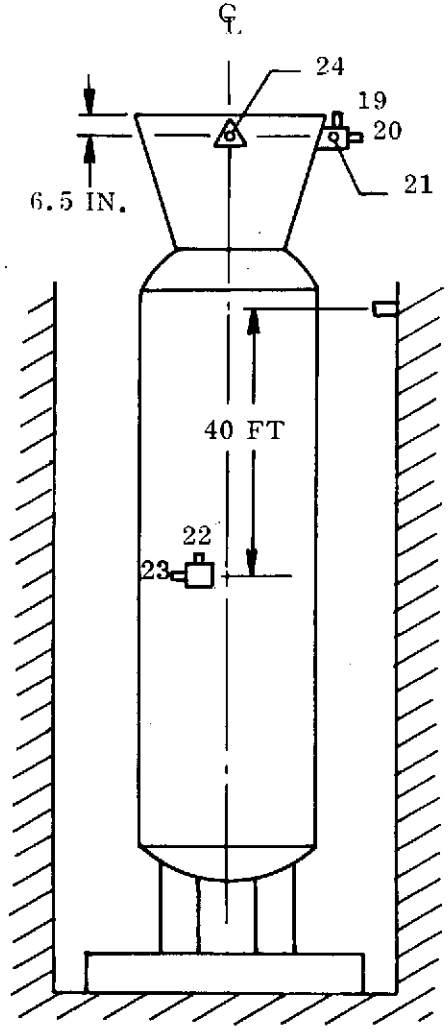


VIEW FROM 180° TRUE

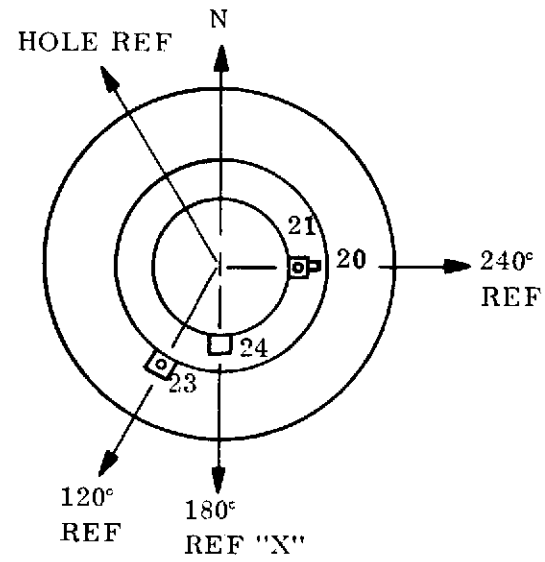


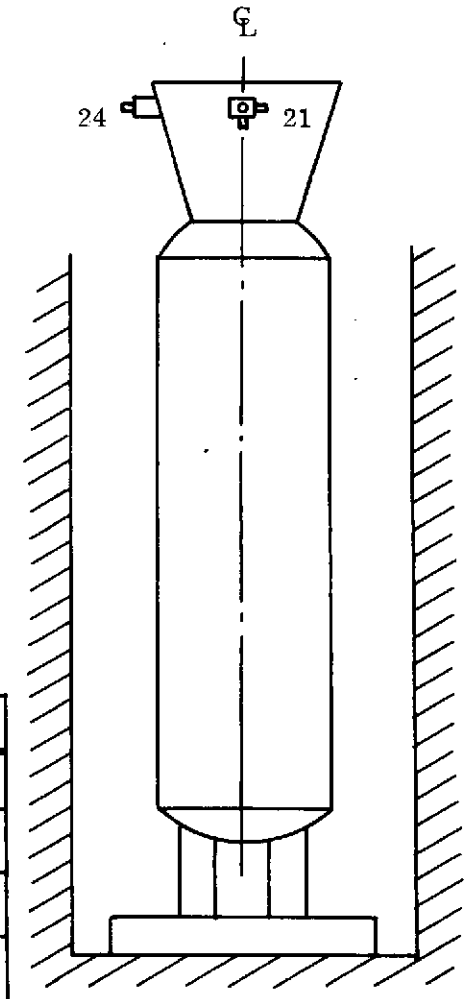


VIEW FROM 90° TRUE

| ACCEL NO. | ORIENTATION | LOCATION |
|---|---|---|
| 19 | LONGITUDINAL | NOZZLE |
| 20 | RADIAL | NOZZLE |
| 21 | TANGENTIAL | NOZZLE |
| 22 | LONGITUDINAL | C/L MOTOR |
| 23 | TANGENTIAL | C/L MOTOR |
| 24 | RADIAL | NOZZLE |

**Figure 5. 156-2C-1 Accelerometer Locations**

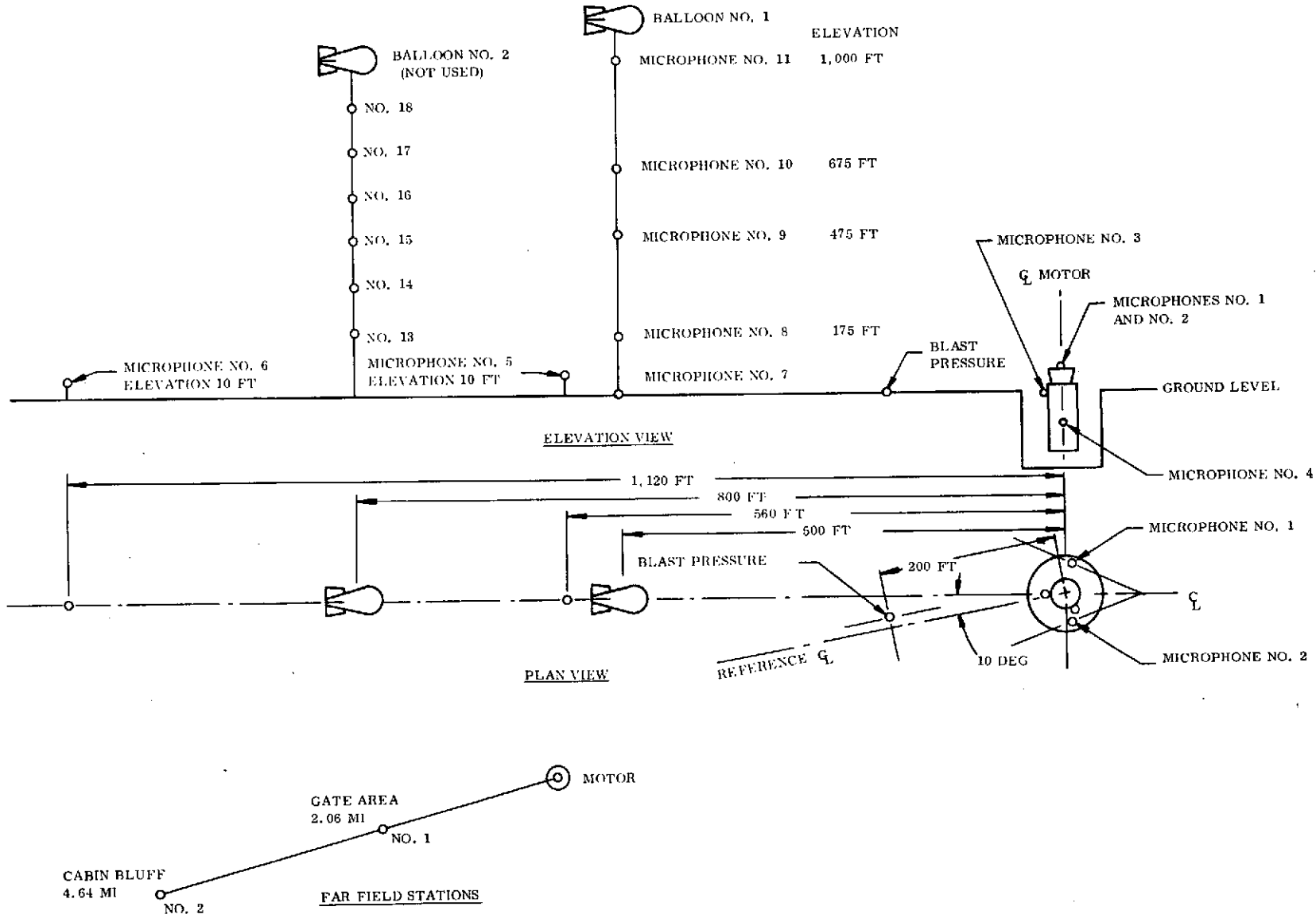


Figure 6. 156-2C-1 Acoustic Microphone Locations

156-2C-1 SOUND PRESSURE LEVELS AT MICROPHONE LOCATIONS
(dB re: 0.0002 Microbar)

| Microphone Number | Distance From Nozzle Center (ft) | Height Above (A) Below (B) Nozzle Exit (ft) | Sound Pressure Level (dB) |
|---|---|---|---|
| 1 | 15.17 | 0.58 (A) | No data |
| 2 | 15.17 | 0.58 (A) | No data |
| 3 | 6.99 | 18.93 (B) | 146 |
| 4 | 6.66 | 59.78 (B) | 148 |
| 5 | 560.0 | -- | 145 |
| 6 | 1,120.0 | -- | No data |
| 7 | 500.0 | 425.0 | No data |
| 8 | 500.0 | 600.0 | 144 |
| 9 | 500.0 | 900.0 | No data |
| 10 | 500.0 | 1,100.0 | No data |
| 11 | 500.0 | 1,425.0 | No data |
| Far Field | | | |
| 1 | 2.06 Miles | -- | 103-107 (greater decrease at frequencies beyond 700 Hz) |
| 2 | 4.64 Miles | -- | 100-104 (greater decrease at frequencies beyond 400 Hz) |

## 2.5 156-3 (LPC-L71)

The Lockheed Propulsion Company (LPC) 156-inch solid propellant rocket motor was successfully static fired on 28 May 1964 near Beaumont, California. The motor consisted of three segments with a fixed nozzle using jet tab TVC. The motor was fired with the exhaust directed vertically upward.

The Air Force Flight Dynamics Laboratory, Vehicle Dynamics Division, made a series of acoustic and vibration measurements during this test. The results are completely documented in reference 2.

A summary of the instrumentation locations and test results is reported here.

### 2.5.1 156-3 (LPC-L71) Vibration Data

Seventeen channels of vibration data were recorded. The transducer locations and measurement directions are shown in figure 7. A summary of the vibration data is shown below.

Vibration Data Summary

| Accelerometer No. | Location | Direction | Overall Grms | | Predominant Frequency (Hz) |
|---|---|---|---|---|---|
| | | | Ignition | Steady | |
| 1 | -- | -- | -- | -- | -- |
| 2 | -- | -- | -- | -- | -- |
| 3 | Aft Attach Ring | Tangential | 1.3 | 0.4 | -- |
| 4 | 2-3 Segment | Tangential | 2.4 | 0.24 | 376 |
| 5 | 2-3 Segment | Radial | 12.0 | 0.35 | 376 (12 g) |
| 6 | Center Midsegment | Thrust | 0.35 | 0.12 | 376 |
| 7 | 1-2 Segment | Tangential | 3.1 | 0.22 | 376 |
| 8 | 1-2 Segment | Radial | 12.0 | 0.31 | 376 (10 g) |
| 9 | Fwd Attach Ring | Tangential | 0.55 | 0.3 | -- |
| 10 | Fwd Attach Ring | Radial | 0.6 | 0.3 | -- |
| 11 | Fwd Attach Ring | Thrust | 0.98 | 0.4 | 376 |
| 12 | Exit Plane 0° | Tangential | 12.0 | (lost after few seconds) | |

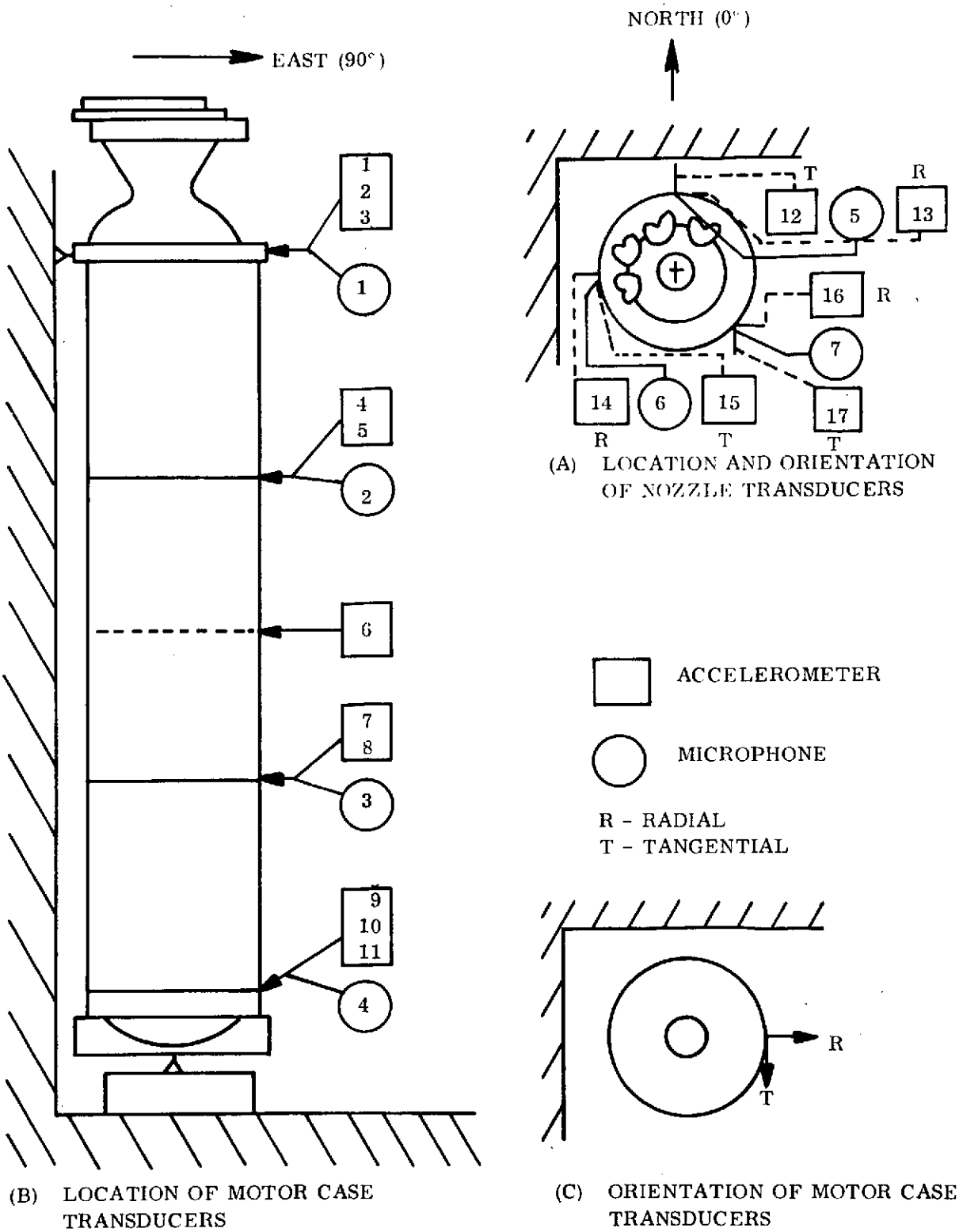


(A) LOCATION AND ORIENTATION OF NOZZLE TRANSDUCERS

(B) LOCATION OF MOTOR CASE TRANSDUCERS

(C) ORIENTATION OF MOTOR CASE TRANSDUCERS

Figure 7. 156-3 (LPC-L71) Transducer Locations

| Accelerometer No. | Location | Direction | Overall Grms Ignition | Overall Grms Steady | Predominant Frequency (Hz) |
|---|---|---|---|---|---|
| 13 | Exit Plane 0° | Radial | 12.0 | (lost after few seconds) | |
| 14 | -- | -- | -- | -- | -- |
| 15 | Exit Plane 270° | Tangential | 16.0 | (lost after few seconds) | |
| 16 | Exit Plane 135° | Radial | 8.0 | (lost after few seconds) | |
| 17 | Exit Plane 135° | Tangential | 11.0 | (lost after few seconds) | |

The peak loads occur within the first second after ignition with a periodic response at 376 Hz. The periodic response appeared on all unrestrained portions of the motor case, i.e., transducers located at the 1-2 segment joint, the center of the mid-segment, and the 2-3 segment joint. The most severe vibration appeared in the radial direction at the 2-3 segment joint at the 376 Hz predominant frequency. Accelerometers, numbers 12 through 17, were lost during the ignition transient, consequently, acceleration levels might have reached much higher levels than those tabulated.

### 2.5.2 156-3 (LPC-L71) Acoustic Data

Seventeen channels of acoustic data were recorded. Seven microphones were located on the motor as shown in figure 7. The locations of eight field microphones are shown in figure 8. The remaining two microphones were located in the recording van used by Air Force personnel. A summary of the acoustic data is shown in the following table.

The far field acoustic data resulted in sound power levels ranging from 204 to 207 dB.

TVC action increased the motor noise levels by about 8 to 9 dB.

## 2.6 RECENT SPECTRAL ANALYSIS OF 156-IN. DIAMETER MOTOR VIBRATION DATA

The longitudinal closed-closed acoustic mode of large solid propellant rocket motors could fall in the frequency range where POGO is experienced (5 to 25 Hz).

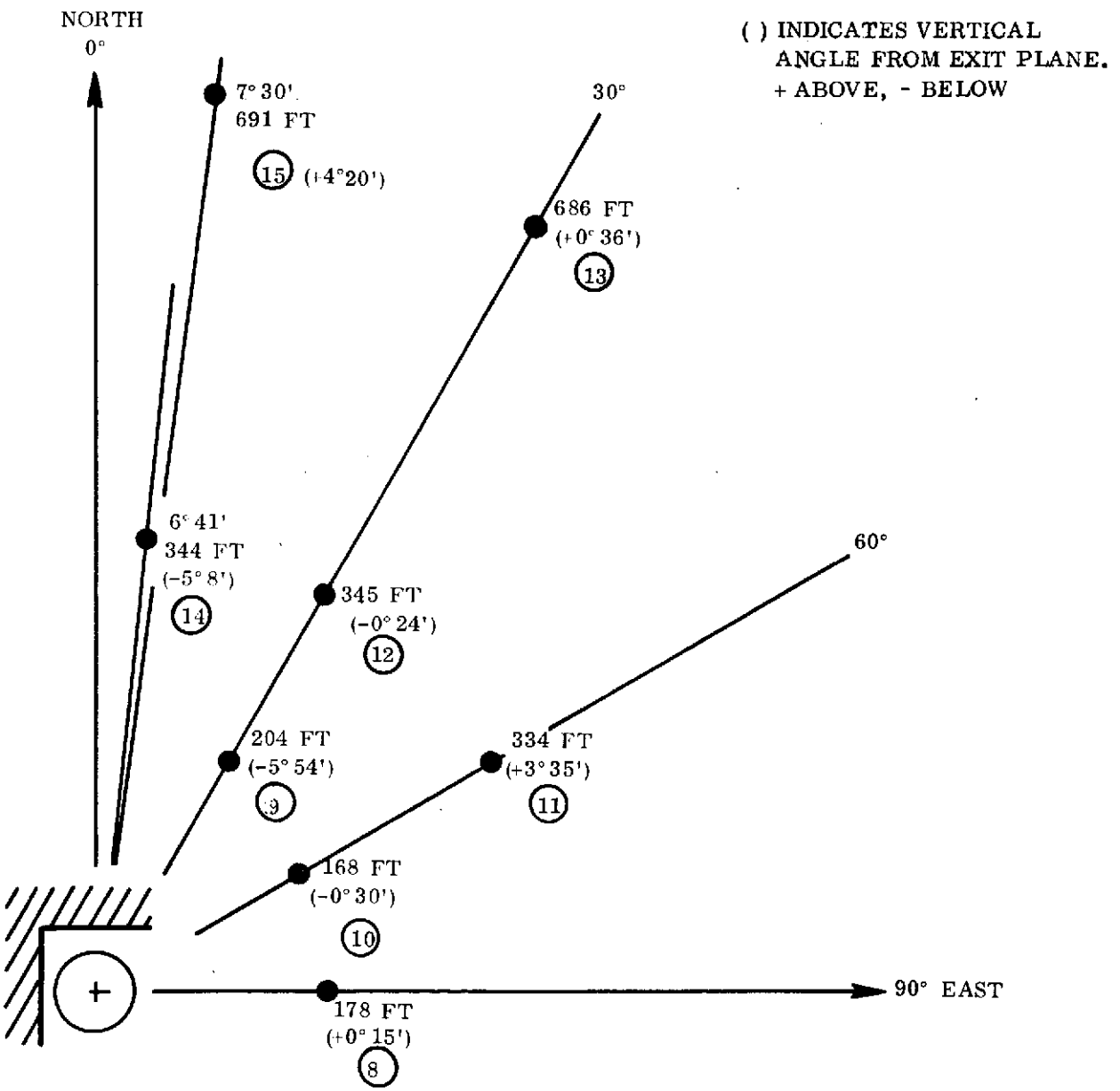


Figure 8. 156-3 (LPC-L71) Field Microphone Locations

## LPC-L71 ACOUSTIC DATA SUMMARY

| Acoustic Channel | Location | Vertical Angle | Overall 1/3 Octave Band Sound Pressure Level $\left(\text{dB ref } 0.0002 \frac{\text{dynes}}{\text{cm}^2}\right)$ | |
|---|---|---|---|---|
| | | | Peaks | Steady |
| 1 | Aft Attach Ring | | 150 | 142 |
| 2 | 2-3 Segment Joint | | 148 | 139 |
| 3 | 1-2 Segment Joint | | 149 | 142 |
| 4 | Fwd Attach Ring | | -- | -- |
| 5 | Exit Plane North | | 158 | -- |
| 6 | Exit Plane West | | 160 | -- |
| 7 | Exit Plane 135° | | -- | -- |
| 8 | 90° 178 ft | +0° 15' | 148 | 144 |
| 9 | 30° 204 ft | -5° 54' | 146 | 143 |
| 10 | 60° 168 ft | -0° 30' | 148 | 145 |
| 11 | 60° 334 ft | +3° 35' | 145 | 142 |
| 12 | 30° 345 ft | -0° 24' | 145 | 141 |
| 13 | 30° 686 ft | -0° 36' | 139 | 137 |
| 14 | 6° 41' 344 ft | -5° 8' | 141 | 140 |
| 15 | 7° 31' 690 ft | +4° 20' | 138 | 136 |
| 16 | Top of Van | | 139 | 135 |
| 17 | In Van | | 125 | 121 |

Preliminary analysis indicates that the longitudinal mode will be significantly damped (reference 3). To substantiate this conclusion, data from three large motor firings were reexamined recently for evidence of low-frequency response.

High-speed oscillograph traces were made on all thrust, pressure, and accelerometer channels on the 156-8 (TU-312), 156-1 (TU-412) and 156-7 (TU-393) motors. Strain channels on the TU-412 were also investigated.

Only two areas indicated any low-frequency data. At ignition of the TU-412 there were several cycles of data at about 6 Hz on the pressure trace. This data could not be correlated to a corresponding thrust nor was any indication given on the accelerometers during this same period. Both CEC traces and shock spectrum plots were made of the data with no indication of this frequency. It did, however, excite the accelerometers at the apparent natural frequency of the dome, at about 89 Hz. Due to the nature of the igniter on this motor it appears this pressure characteristic was caused by the ignition transients.

The only other area where low-frequency data could be deteced was on the TU-412, where a frequency of approximately 10 Hz was noted on the axial accelerometers between 1 and 2 seconds of firing. This frequency could not be detected on the pressure trace but correlated directly with test stand ring as indicated on the thrust channel. The amplitude of this data was in the order of 0.2 g's. It was concluded that the accelerometer data were a result of test stand ring and could not be related to motor performance.

On the TU-393 and TU-312 motors, there was no evidence of any low-frequency data on any channel. The pressure, accelerometer, and thrust channels were band passed, filtered, and amplified; but still no data were evident. It was concluded that the longitudinal acoustic mode was not excited on any of these three motors.

## 2.7 UTC DVXL5-1 (120-IN. DIAMETER MOTOR)

The DVXL5-1 solid fuel motor was static fired on 20 July 1963, by United Technology Center (UTC) in Morgan Hill, California. The motor exhausted upward, with the nozzle canted 6 degrees from vertical. TVC was accomplished by liquid injection.

Bolt Beranek and Newman Inc. made a series of acoustic and vibration measurements during the static firing. The results of their data analysis are completely documented in reference 4.

A summary of the instrumentation locations and test results is reported here.

2.7.1 UTC DVXL5-1 Vibration Data

Seven channels of vibration data were recorded. The transducer locations and measurement directions are shown in figure 9. A summary of the vibration data is shown below.

DVXL5-1 Vibration Data Summary

| Data Channel No. | Measurement and Location | Predominant Frequency (Hz) | Grms (maximum) No TVC | Grms (maximum) With TVC |
|---|---|---|---|---|
| 1 | Accelerometer-nozzle at motor-nozzle attachment flange - 220° (normal) | 600-800<br>5,000 | 0.6<br>0.6 | 0.7<br>0.9 |
| 2 | Accelerometer-nozzle 41 in. above motor-nozzle attachment flange (behind pitch and yaw control box) - 225° (normal) | 800<br>5,000 | 4.5<br>5.5 | 5.0<br>10.0 |
| 3 | Accelerometer-mounting frame of pitch and yaw control box near upper support ring - 220° (normal) | 400, 700<br>1,400 | 2.3<br>2.5 | 5.4<br>3.5 |
| 4 | Accelerometer-mounting frame of pitch and yaw control box near upper support ring - 220° (axial) | 250<br>500,<br>1,400<br>5,000 | 0.9<br>1.15<br>0.78<br>1.0 | 0.8<br>2.4<br>1.1<br>2.3 |
| 5 | Accelerometer-mounting frame of TVC junction box near lower support ring - 220° (normal) | 500<br>1,000<br>2,000 | 3.0<br>4.5<br>7.0 | --<br>--<br>-- |
| 6 | Accelerometer-nozzle-upper flange 81 in. above motor nozzle attachment flange - 225° (normal) | 250<br>800<br>5,000 | 0.7<br>1.25<br>2.2 | 1.0<br>4.5<br>6.3 |
| 7 | Accelerometer-motor case skirt near nozzle - 0° (normal) | 200<br>2,000-4,000 | 0.04<br>0.3 | 0.04<br>0.4 |

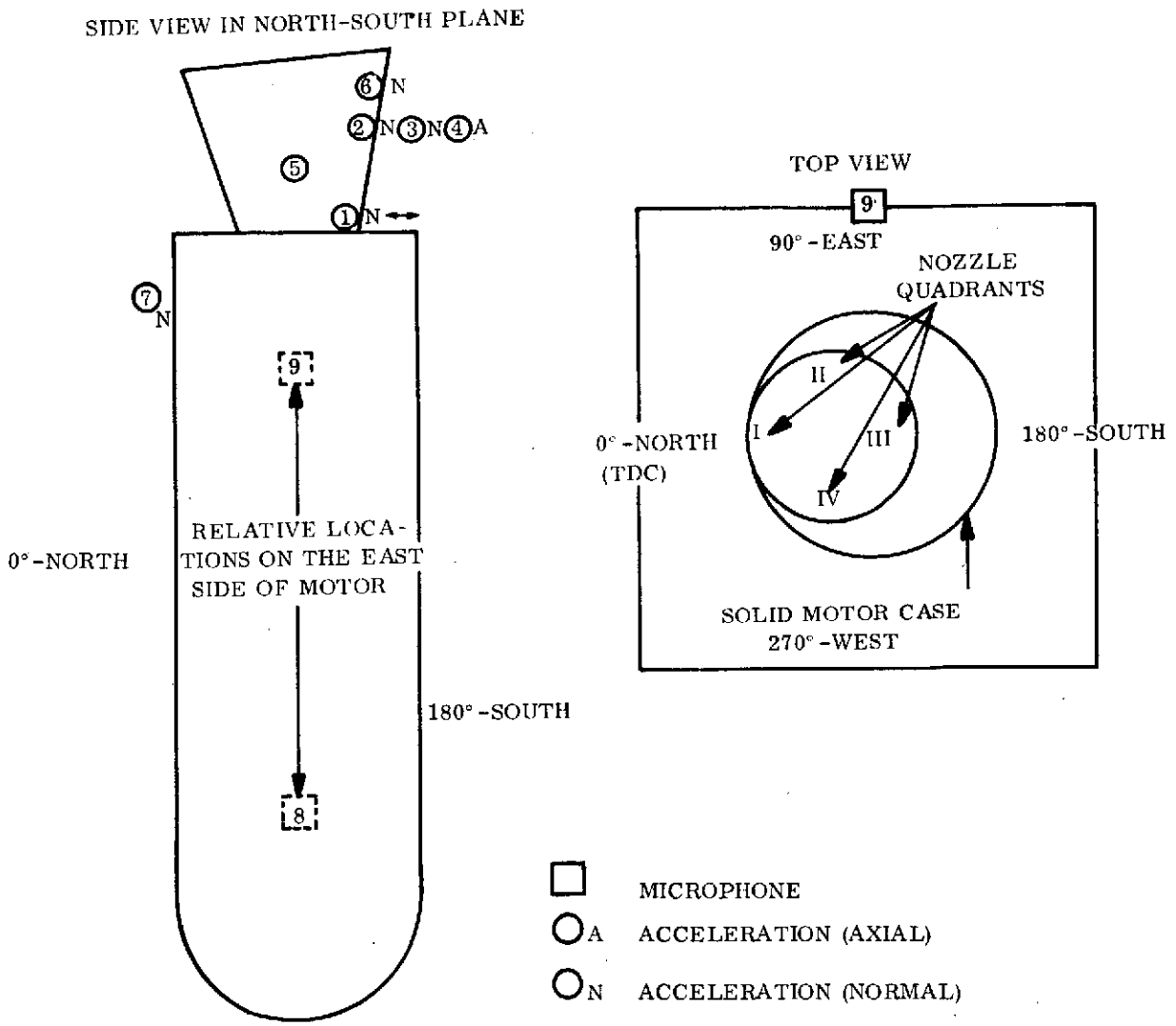


NOTES: CHANNEL NOS. ARE GIVEN IN CIRCLES AND SQUARES.
SKETCH NOT TO SCALE.

Figure 9. DVXL5-1 Near Field Acoustic and Vibration Measurement Positions

Vibration data show a definite increase in the measured vibration associated with TVC action. Since the near field acoustic levels are not affected by TVC, the vibration increases in the nozzle and equipment are primarily structure borne and not sound-induced.

### 2.7.2 UTV DVXL5-1 Acoustic Data

Five channels of acoustic data were recorded, one near field and four far field. The transducer locations are shown in figure 10. A summary of the acoustic data is shown below.

DVXL5-1 Acoustic Data Summary

| Data Channel No. | Measurement and Location | Sound Pressure Level In 1/3 Octave Band Decibels (re: 0.0002 Microbar) No TVC | With TVC |
|---|---|---|---|
| 8 | Microphone-test stand 2nd Platform - 90° | No data | -- |
| 9 | Microphone-test stand 6th Platform - 90° | 132 | 135 |
| 10 | Microphone - 470 ft - 109° (5°)* | 128 | 128 |
| 11 | Microphone - 700 ft - 157° (12°)* | 124.5 | 126.5 |
| 12 | Microphone - 650 ft - 21° (6°)* | 127 | 130 |
| 13 | Microphone - 406 ft - 56° (4°)* | 132 | 132 |

*Angles between horizontal plane and lines from microphones to nozzle exit are given in parentheses.

The sound power level in 1/3 octave band in Db re: $10^{-13}$ watts was 201 dB. This value corresponds to 1/4 of 1 percent of the mechanical power in the exhaust streams. For details, see reference 4.

The near and far field acoustics were not effected by TVC.

## 2.8 AGC 100 FW-1 (100-IN. DIAMETER MOTOR)

Acoustic data are presented on the Aerojet-General Corporation 100 FW-1 motor. The data are taken from an AGC Test Division sketch dated 7 September 1961. The near field acoustic data are shown in figure 11. The far field data are shown in figure 12.

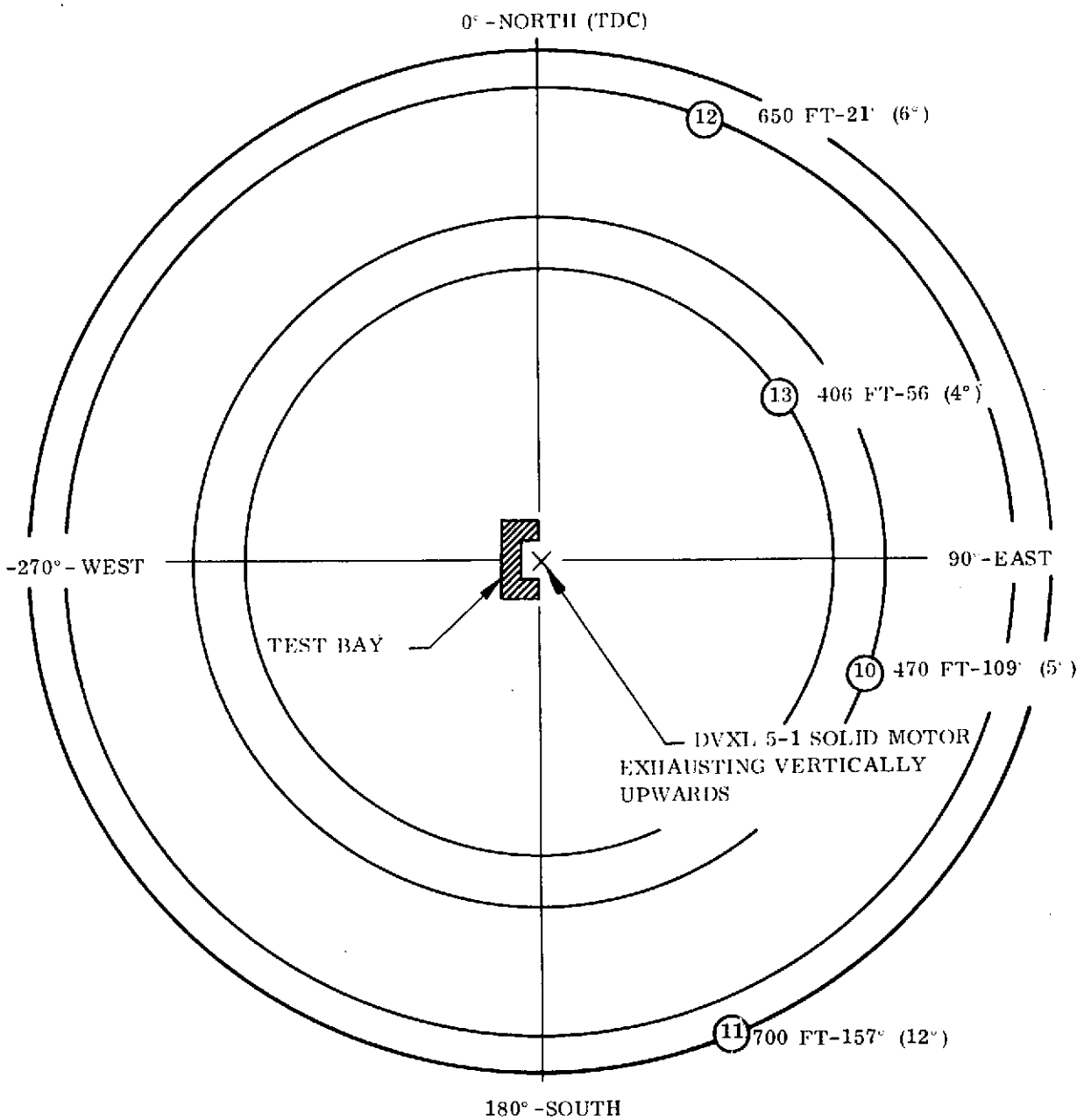


NOTES: CHANNEL NOS. ARE GIVEN IN CIRCLES.
ANGLES BETWEEN HORIZONTAL PLANE AND
LINES FROM MICROPHONES TO NOZZLE EXIT
ARE GIVEN IN PARENTHESES.

**Figure 10. DVXL5-1 Far Field Acoustic Measurement Positions**

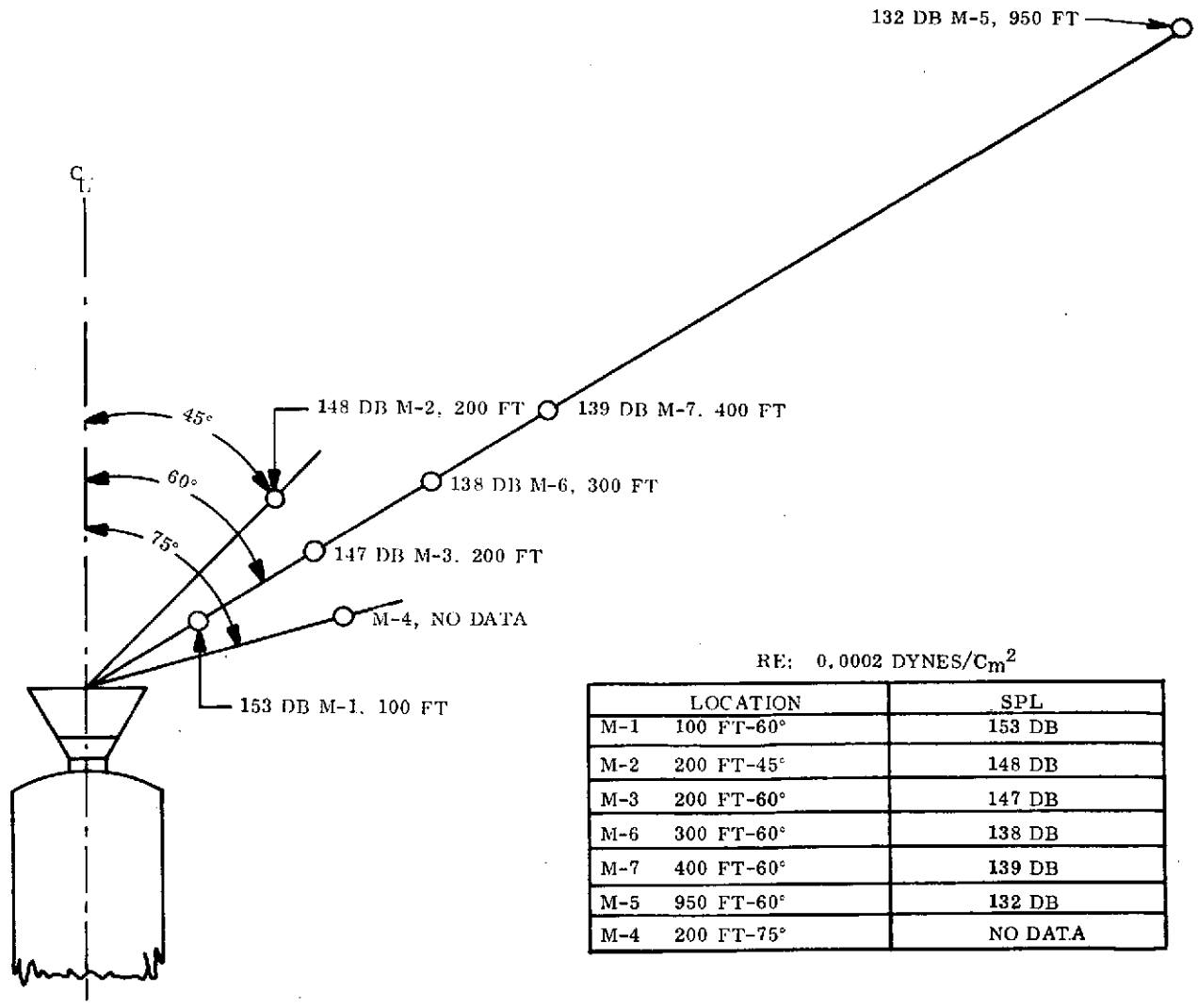


RE: 0.0002 DYNES/$Cm^2$

| LOCATION | SPL |
|---|---|
| M-1 100 FT-60° | 153 DB |
| M-2 200 FT-45° | 148 DB |
| M-3 200 FT-60° | 147 DB |
| M-6 300 FT-60° | 138 DB |
| M-7 400 FT-60° | 139 DB |
| M-5 950 FT-60° | 132 DB |
| M-4 200 FT-75° | NO DATA |

Figure 11. AGC-100 FW-1 Near Field Sound Pressure Level

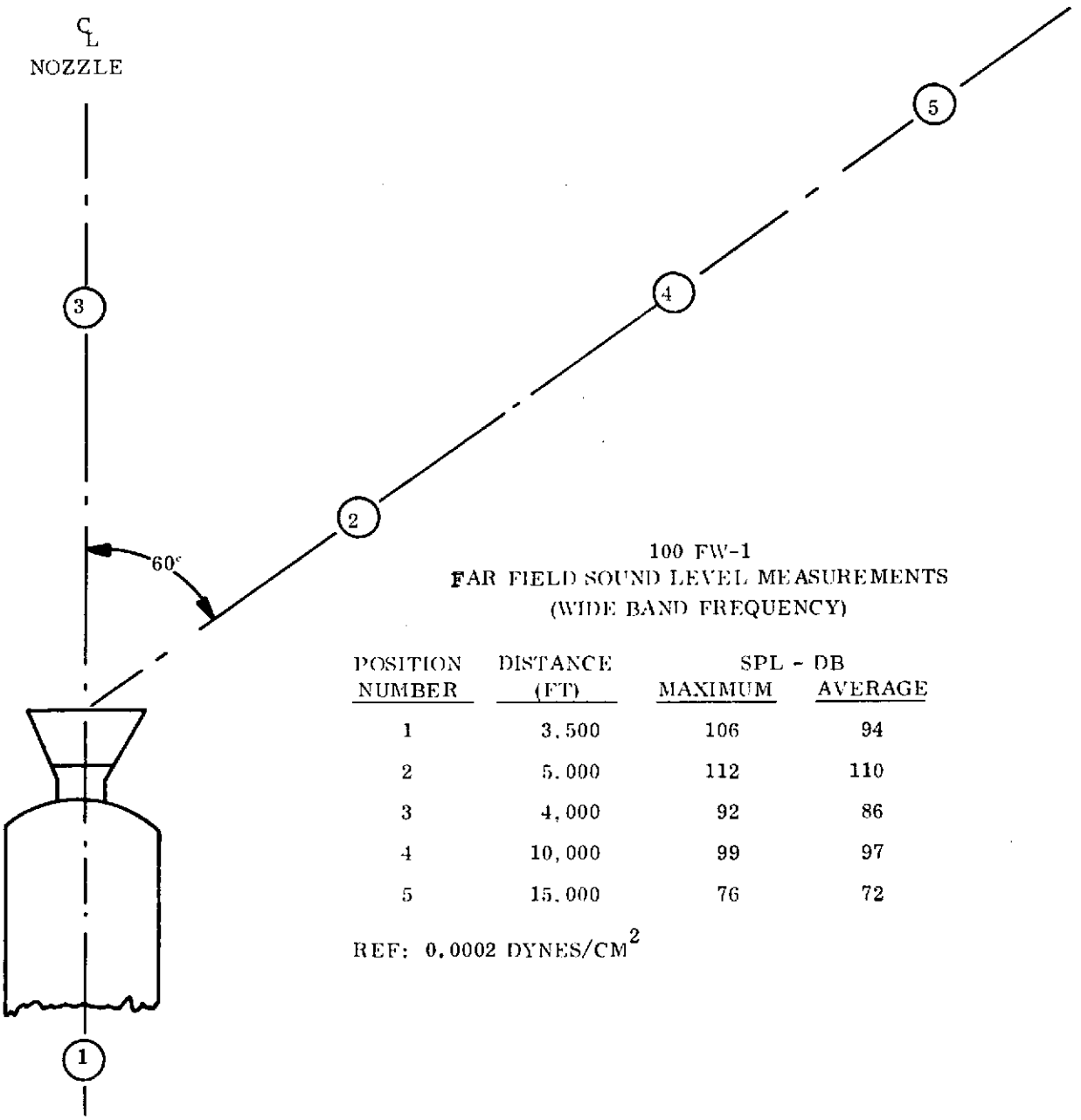


100 FW-1
FAR FIELD SOUND LEVEL MEASUREMENTS
(WIDE BAND FREQUENCY)

| POSITION NUMBER | DISTANCE (FT) | SPL - DB MAXIMUM | SPL - DB AVERAGE |
|---|---|---|---|
| 1 | 3.500 | 106 | 94 |
| 2 | 5.000 | 112 | 110 |
| 3 | 4,000 | 92 | 86 |
| 4 | 10,000 | 99 | 97 |
| 5 | 15.000 | 76 | 72 |

REF: 0.0002 DYNES/CM$^2$

Figure 12. AGC-100 FW-1 Far Field Sound Level Measurements

## 2.9 POSEIDON (C3) STAGE I

Approval to release Poseidon vibration data has been requested. Upon receipt of approval from the U.S. Navy, the C3 Stage I vibration data will be appended to this report.

## 2.10 TU-122 MINUTEMAN STAGE I MOTOR (65-IN. DIAMETER MOTOR)

The Thiokol TU-122 has a 65-inch diameter monolithic case of ladish D6AC steel, a star perforated propellant grain, and four movable nozzles (TVC). The motor descriptive parameters are shown in figure 13.

### 2.10.1 TU-122 Vibration Data

Typical measured vibration environment is tabulated below.

| Motor Component | Predominant Frequency (Hz) | Peak Acceleration Density ($G^2$/Hz) | Total Grms |
|---|---|---|---|
| Aft Closure | 550 to 700 | 0.001 to 0.004 | 2 to 3 |
| Case | 625 to 900 | 0.002 to 0.005 | 1.7 to 3.2 |
| Blast Tube | 6,800 to 10,000 | 0.007 to 0.016 | 5 to 7 |

Peak accelerations for the above locations range from 17 to 35 g during the ignition transient.

### 2.10.2 TU-122 Acoustic Data

Isoacoustic curves of dB versus field location are shown in figure 14 for a horizontal firing attitude. The plot is limited to a distance of 300 feet. Data for distances beyond 300 feet are tabulated below.

| Distance (Feet) | Overall Sound Pressure Level In Decibels (re: 0.0002 Microbar) |
|---|---|
| 500 | 137 |
| 800 | 132 |
| 1,000 | 130 |
| 1,500 | 125 |
| 2,000 | 122 |

TU-122
52.6-KS-194,600
M55E1 MINUTEMAN
STAGE I, WING II

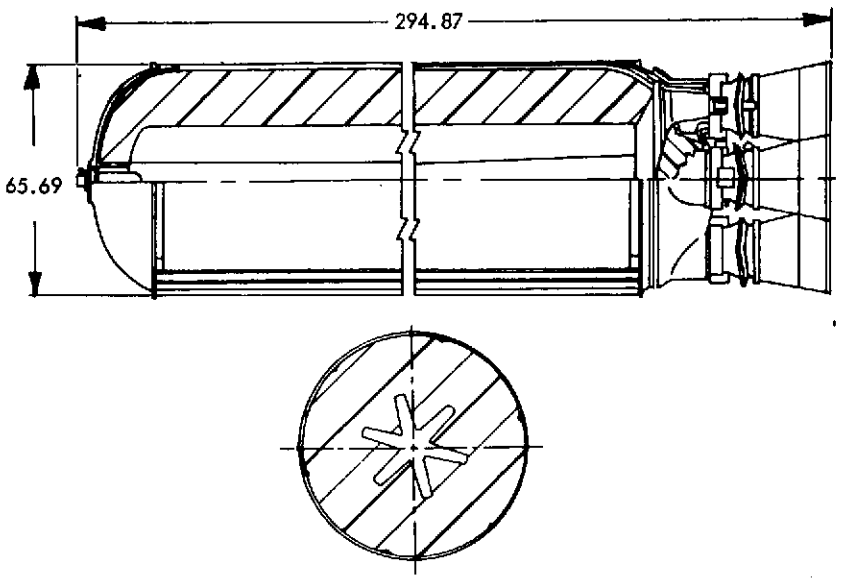


## CASE

| | |
|---|---|
| Material | Ladish D6AC Steel |
| Minimum Ultimate Strength, psi | 225,000 |
| Minimum Yield Strength, psi | 195,000 |
| Hydrostatic Test Pressure, psi | 940 |
| Yield Pressure, psi | 985 |
| Hydrostatic Test Pressure/Maximum Pressure | 1.1 |
| Yield Pressure/Hydrostatic Test Pressure | 1.05 |
| Nominal Thickness, in. | 0.148 |

## NOZZLE

| | |
|---|---|
| Body Material | AISI 4130 Steel |
| Throat Insert Material | Forged Tungsten |
| Initial Throat Area, $in.^2$ | 164.2 |
| Exit Area, $in.^2$ | 1642 |
| Expansion Ratio | 10:1 |
| Expansion Cone Half Angle, degrees | 11.4 |
| Type | Movable |
| Number of Nozzles | 4 |

## LINER

| | |
|---|---|
| Type | HC Polymer-Asbestos |
| Density, $lbm/in.^3$ | 0.0394 |

## IGNITER

| | |
|---|---|
| Thiokol Model Designation | TU-P-122 |
| Type | Pyrogen - S&A |
| Minimum Firing Current, amperes | 4.9 |
| Circuit Resistance, ohms | 0.22 ± 0.10 |
| No. of Squibs | 2 |

## PROPELLANT

| | |
|---|---|
| Propellant Designation and Formulation | TP-H-1011 |
| HB/ECA - 14% | |
| Al - 16% | |
| $NH_4ClO_4$ - 70% | |

## PROPELLANT CONFIGURATION

| | |
|---|---|
| Type | (Cylindro-Conical) Six-Point Star |
| Web, in. | 17.357 |
| Web Fraction, % | 53.3 |
| Sliver Fraction, %** | 5.93 |
| Propellant Volume, $in.^3$** | 709,400 |
| Volumetric Loading Density, % | 88.7 |
| Web Average Burning Surface Area, $in.^2$** | 38,500 |
| Initial Surface to Throat Area Ratio ($K_n$) | 217 |

## PROPELLANT CHARACTERISTICS

| | |
|---|---|
| Burn Rate @ 1000 psia ($r_b$), in./sec | 0.349 |
| Burn Rate Exponent (n) | 0.21 |
| Density, $lbm/in.^3$ | 0.0636 |
| Temperature Coefficient of Pressure ($\pi_K$), %/°F | 0.102 |
| Characteristic Exhaust Velocity (C*), ft/sec | 5,180 |
| Adiabatic Flame Temperature, °F | 5,790 |
| Effective Ratio of Specific Heats (Chamber) | N.D. |
| (Nozzle Exit) | 1.18 |

## CURRENT STATUS

Production

**Case Propellant Only.

Figure 13. TU-122 Motor Description

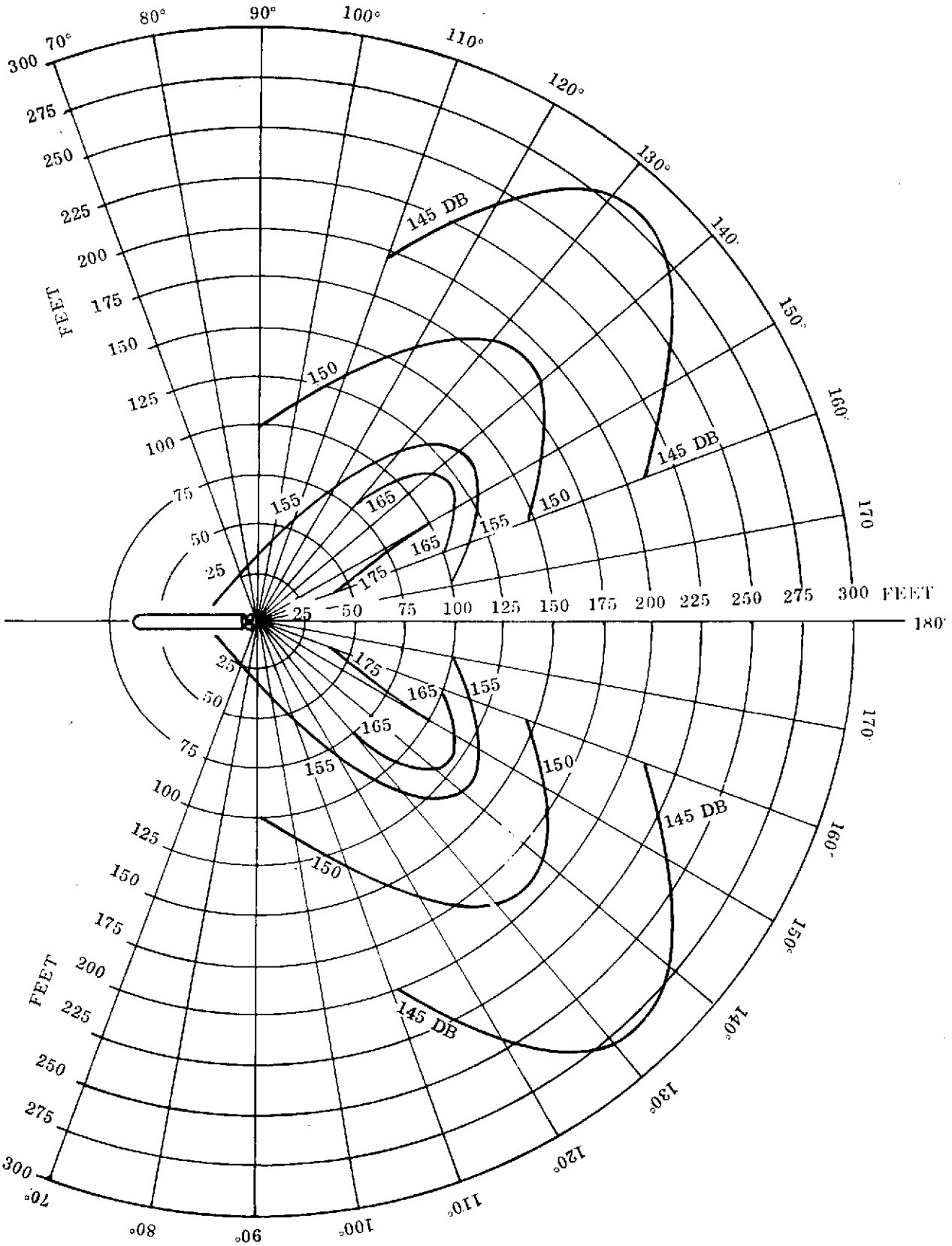


Figure 14. TU-122 Isoacoustic Curves of Decibels Versus Field Locations

| Distance (Feet) | Overall Sound Pressure Level In Decibels (re: 0.0002 Microbar) |
|---|---|
| 2,500 | 119 |
| 3,000 | 117 |
| 3,500 | 114 |
| 4,000 | 113 |
| 5,000 | 109 |
| 6,000 | 106 |
| 7,000 | 104 |
| 8,000 | 101 |
| 9,000 | 99 |
| 10,000 | 97 |
| 15,000 | 89 |
| 20,000 | 83 |

## 2.11 MINUTEMAN III STAGE III MOTOR

The Minuteman III Stage III Motor was originally developed and produced by Aerojet Solid Propulsion Company (ASPC). It is now being produced by Thiokol Corporation (TC). The grain configuration is a center perforate with six forward end fins. The motor utilizes an 88-percent solids, 15-percent aluminum carboxyl-terminated polybutadiene (PBAN) propellant. Pertinent motor information is presented in figure 15. The motor exhibited acoustic instability and has been evaluated extensively both analytically and experimentally. ASPC was funded to investigate and characterize the oscillatory burning characteristics of the motor, to identify the influence of propellant raw materials and processing variables on the stability of the motor (reference 5).

### 2.11.1 Minuteman III Stage III Motor Vibration Data

The motor exhibits two distinct acoustic instability modes. During the first 4 seconds of burning a tangential mode associated with the forward fins is present (~800 Hz). During the time period from 4 to 16 seconds the first longitudinal

60.1-KS-34,560
STAGE III MINUTEMAN

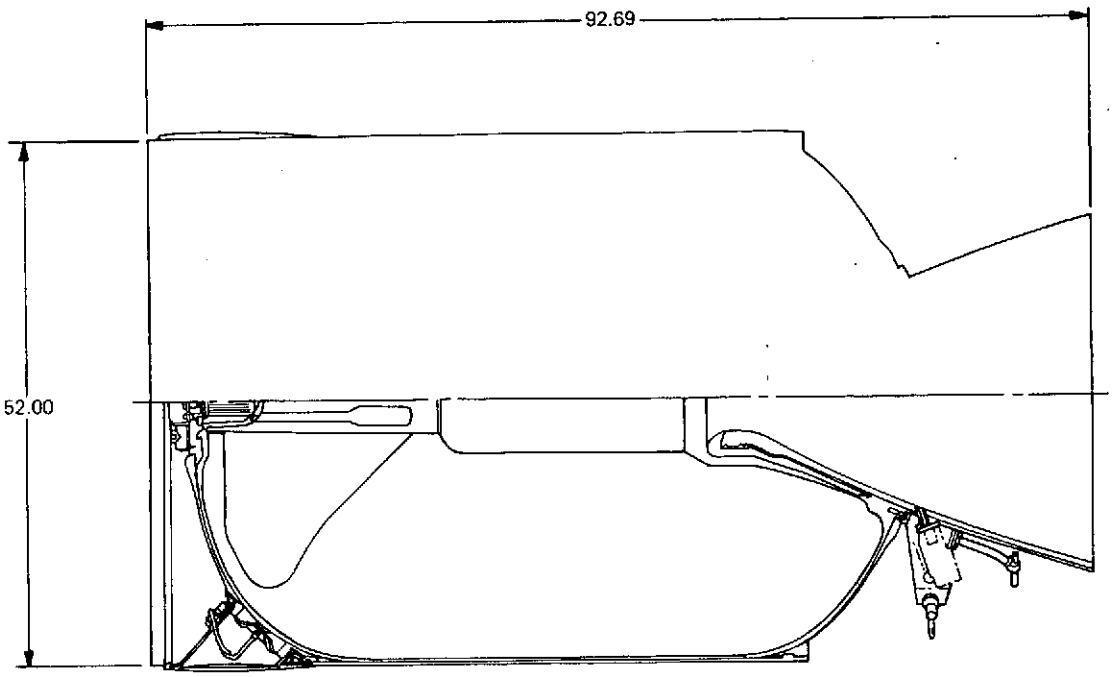


## CASE

| | |
|---|---|
| Material | S901 Fiberglass, EF-2 Resin System |
| Minimum Ultimate Glass Strength, psi | 440,000 |
| Minimum Yield Strength, psi | - |
| Hydrostatic Test Pressure, psi | 715.0 |
| Yield Pressure, psi | - |
| Hydrostatic Test Pressure/Maximum Pressure | 1.42 |
| Yield Pressure/Hydrostatic Test Pressure | - |
| Nominal Thickness, in. | 0.160 |

## NOZZLE

| | |
|---|---|
| Body Material | 7075-T73 Aluminum |
| Throat Insert Material | Forged Tungsten |
| Initial Throat Area, $in.^2$ | 37.122 |
| Exit Area, $in.^2$ | 874.587 |
| Expansion Ratio | 23.55 |
| Expansion Cone Half Angle, degrees | (Contoured) 16.5 |
| Type | Fixed Submerged-LITVC |
| Number of Nozzles | 1 |

## LINER

| | |
|---|---|
| Type | Asbestos-Filled CTPB SD851-2 |
| Density, $lbm/in.^3$ | 0.034 |

## IGNITER

| | |
|---|---|
| Thiokol Model Designation | 1128361-149 |
| Type | Head End Pyrogen with S&A |
| Minimum Firing Current, amperes | 4.5 |
| Circuit Resistance, ohms | 0.22 |
| No. of Squibs | 2 |

## PROPELLANT

Propellant Designation and Formulation: ANB-3066

CTPB/BITA - 9%  Al - 15%
Polybutene - 3%  AP - 73%

## PROPELLANT CONFIGURATION

| | |
|---|---|
| Type | Head End Fins (6)-Stepped CP |
| Web, in. | 20.43 |
| Web Fraction, % | 0.79 |
| Sliver Fraction, % | 0.11 |
| Propellant Volume, $in.^3$ | 115,193 |
| Volumetric Loading Density, % | 94.0 |
| Web Average Burning Surface Area, $in.^2$ | 5,638.0 |
| Initial Surface to Throat Area Ratio ($K_n$) | 104.0 |

## PROPELLANT CHARACTERISTICS

| | | |
|---|---|---|
| Burn Rate @ 1000 psia ($r_b$), in./sec | | 0.417 |
| Burn Rate Exponent (n) | | 0.30 |
| Density, $lbm/in.^3$ | | 0.064 |
| Temperature Coefficient of Pressure ($\pi_K$), %/°F | | 0.120 |
| Characteristic Exhaust Velocity (C*), ft/sec | | 5,200 |
| Adiabatic Flame Temperature, °F | | 5,730 |
| Effective Ratio of Specific Heats | (Chamber) | 1.14 |
| | (Nozzle Exit) | 1.18 |

## CURRENT STATUS

Production

Figure 15. Minuteman III Stage III Motor Description

mode is present in the motor (~200 to 350 Hz). Difficulties were encountered in measuring the pressure vibrations during the transverse mode operation:

1. The transducer had to be installed near the igniter at the forward polar boss, thus it is near the pressure nodal point for the transverse mode.
2. The split flap forms a separate cavity which is monitored by the standard transducer mounting.
3. The standard operational pressure transducer (OPT) has poor signal-to-noise ratio, and the interconnecting channel between the chamber and the transducer modifies the frequency response of the measurement system.

A dynamically calibrated helium-bleed transducer system was designed and installed on two static firings. The system included a tube to provide direct measurement in the main motor cavity. This indicated a peak amplitude of 10.1 psi which when corrected to the maximum amplitude position at the fin extremities amounts to an amplitude of 100 psi (0 to peak).

Numerous accelerometers have been mounted on the forward and aft domes. These accelerometers display a wide variation in amplitudes from motor to motor and between locations. Standardized accelerometer locations were established and used to monitor and compare individual motor vibrational characteristics. The standard headend accelerometer (AIGN 30Y) is mounted on the igniter boss at the 30-degree location. This location was chosen for the following reasons:

1. The forward dome sinusoidal vibrations were more consistent than the aft dome with much lower random vibration.
2. The igniter boss provided a rigid mechanical attachment surface.

The FM tape recorded data are processed through an MB Electronics Model N982 Shock Spectrum Analyzer to determine maximum amplitudes at various center band frequencies. The analyzer is set at an amplification factor (Q) of ten.

MINUTEMAN III STAGE III MOTOR VIBRATION
AMPLITUDE AND FREQUENCY SUMMARY
HEADEND ACCELEROMETER (AIGN-30Y)

| Frequency | Amplitudes (g) Q = 10 PQA Average | PQA Average +3σ |
|---|---|---|
| Time 0.100 to 4 seconds | | |
| 555 | 37 | 80 |
| 629 | 40 | 71 |
| 710 | 56 | 85 |
| 806 | 161 | 276 |
| 888 | 140 | 278 |
| 987 | 73 | 136 |
| 1,116 | 50 | 87 |
| 1,246 | 47 | 75 |
| 1,408 | 51 | 87 |
| 1,594 | 77 | 154 |
| 1,825 | 60 | 120 |
| 2,020 | 48 | 89 |
| Time 4 to 16.1 seconds | | |
| 139 | 33 | 60 |
| 159 | 79 | 159 |
| 181 | 131 | 252 |
| 199 | 70 | 110 |
| 219 | 44 | 70 |
| 248 | 36 | 54 |
| 278 | 48 | 65 |
| 321 | 105 | 161 |
| 349 | 85 | 120 |
| 398 | 53 | 74 |
| 448 | 43 | 65 |
| 496 | 40 | 69 |

The center band frequencies, nominal amplitudes and upper three sigma amplitudes from 16 PQA motors are presented below. The quality of the data is such that the values can be divided by 10 to arrive at 0 to peak values.

## 2.12 MINUTEMAN MISSILE PAD LAUNCH

Acoustic field data were measured by The Boeing Company during a pad launch of Minuteman Flight Test Motor (FTM) 403. The data cover ignition and flight.

The data were extracted from reference 6.

The field microphone locations are shown in figure 16. The sound pressure levels at the various field location are shown in figures 17 through 21. The SPLs shown in figure 17 are the average of two axes for each distance.

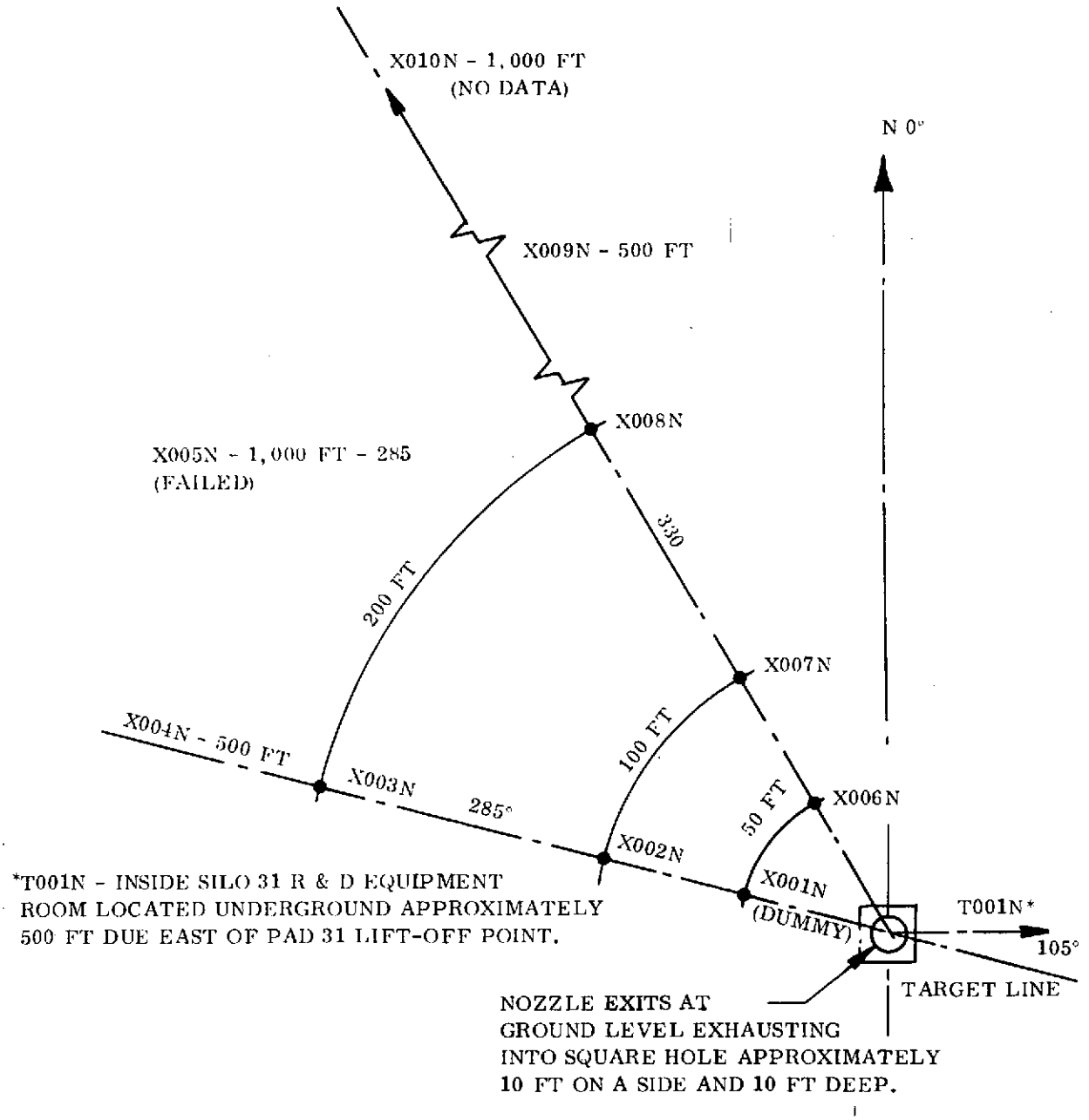


Figure 16. Minuteman Pad Launch Measurement Locations

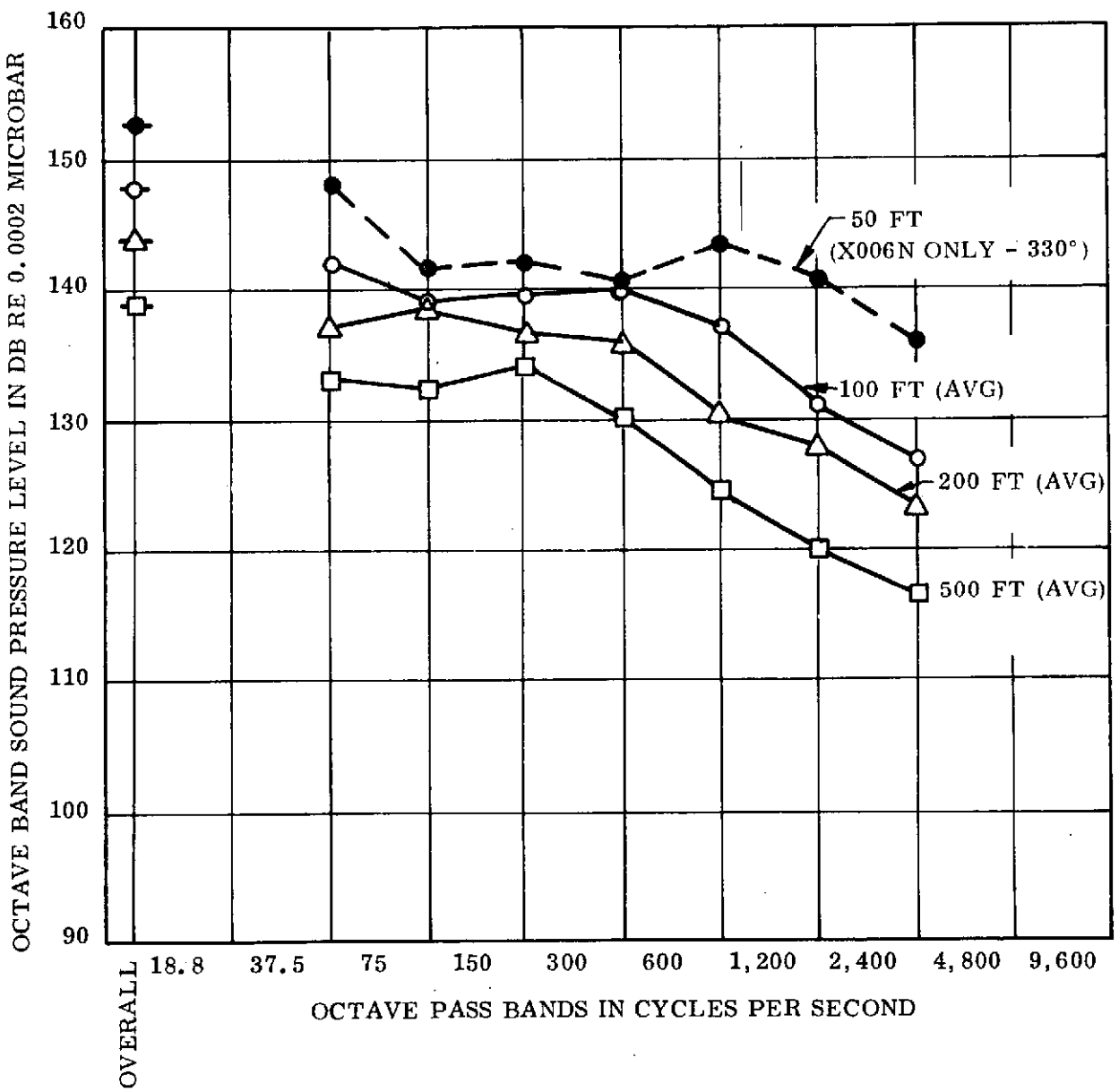


Figure 17. Minuteman Pad Launch Maximum Octave Band Levels Measured During Launch

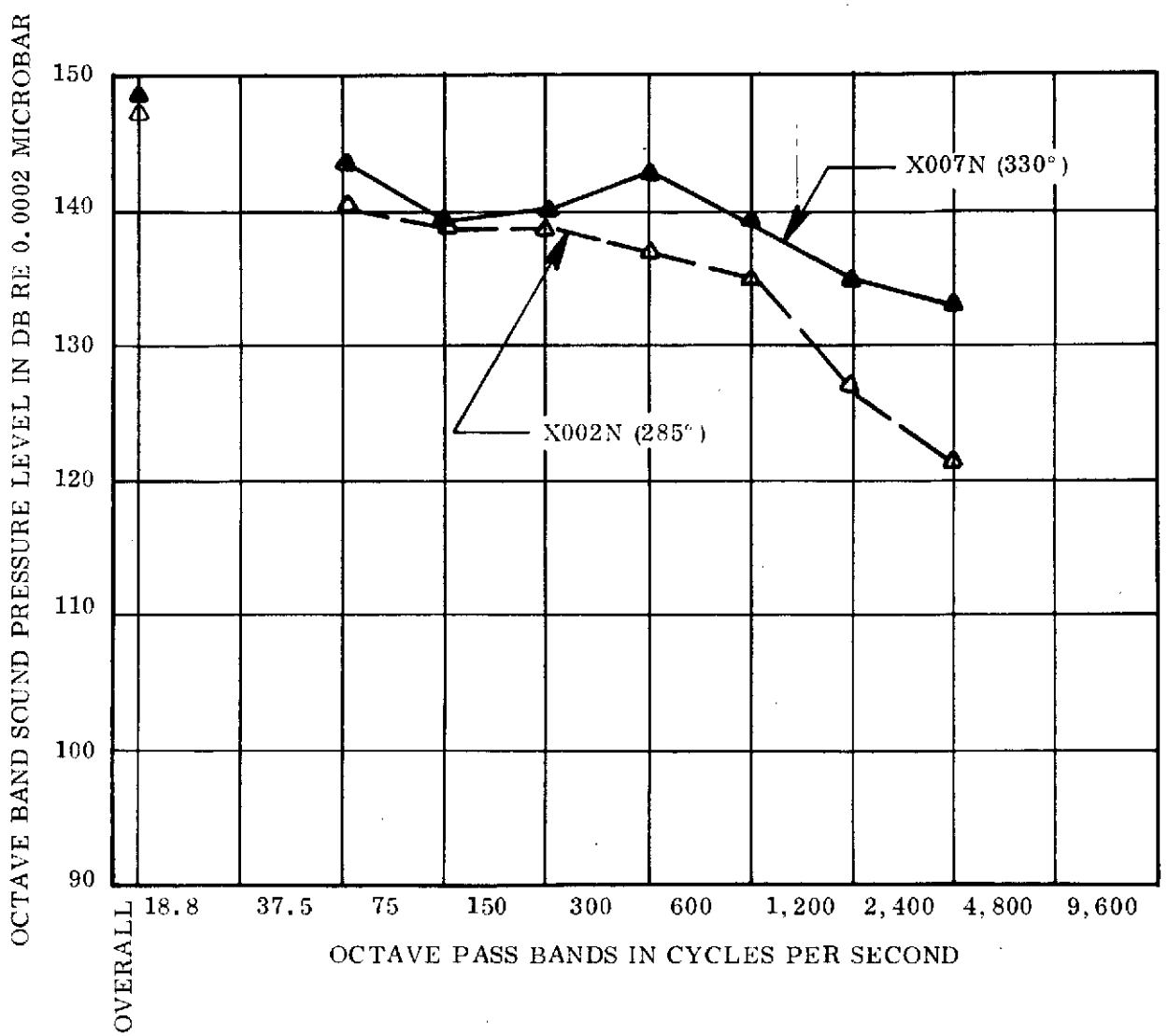


Figure 18. Minuteman Pad Launch Maximum Octave Band Levels (100 Feet)

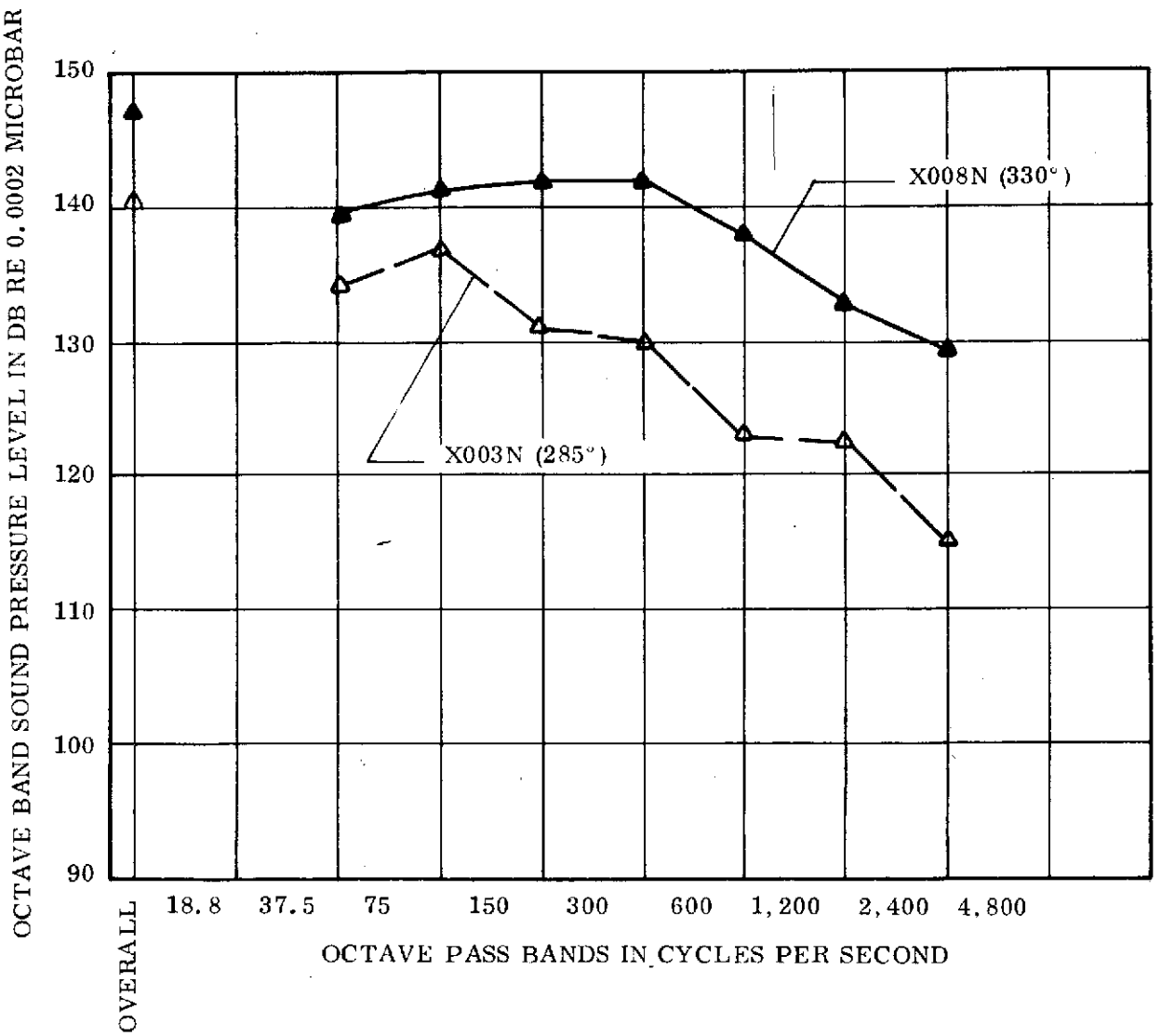


Figure 19. Minuteman Pad Launch Maximum Octave Band Levels (200 Feet)

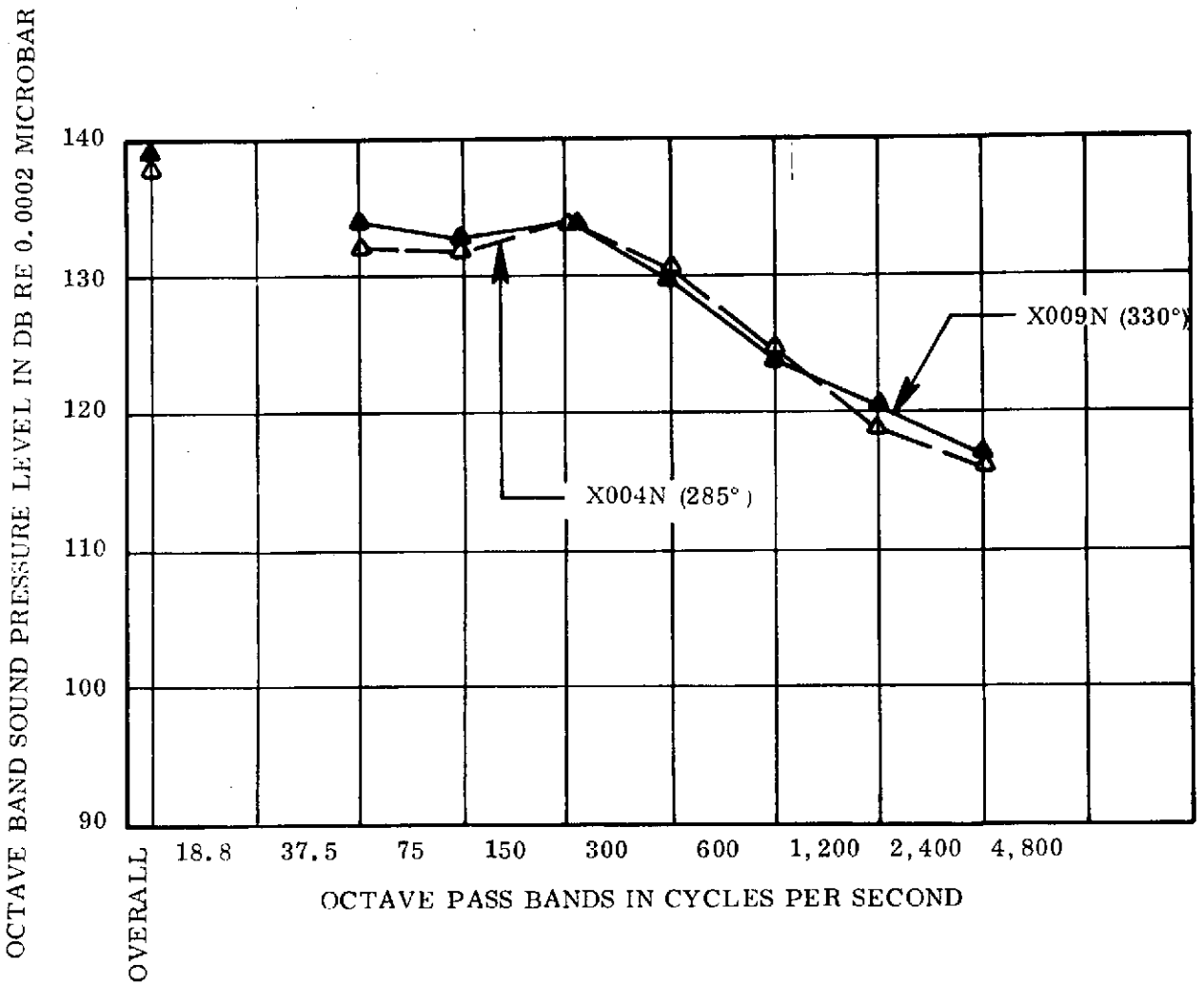


Figure 20. Minuteman Pad Launch Maximum Octave Band Levels (500 Feet)

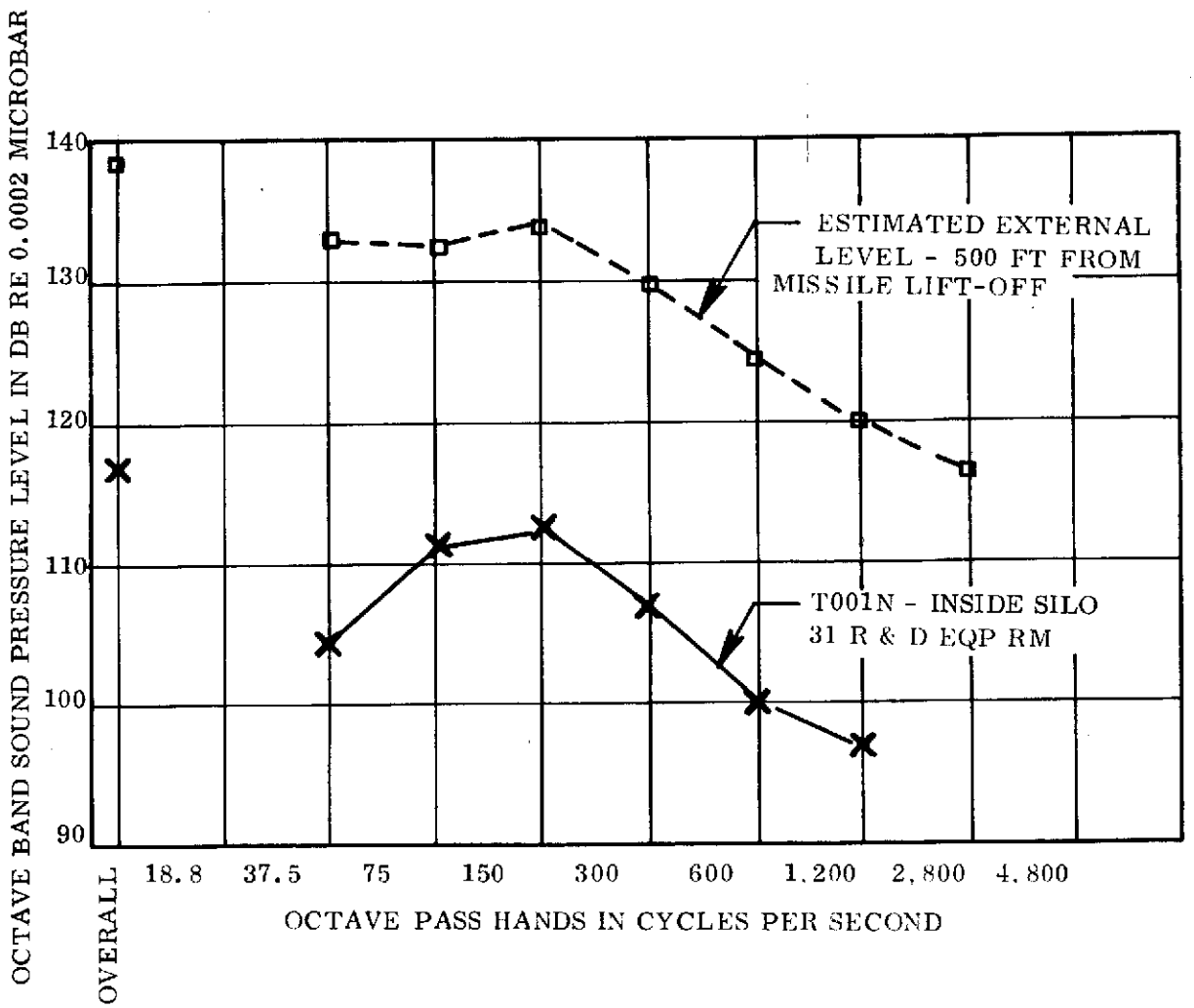


Figure 21. Minuteman Pad Launch Maximum Octave Band Levels (Inside Levels--R & D Equipment Room)

## APPENDIX A

## REFERENCES CITED


1. Anon: Final Test Results of the 156-2C-1 Motor Firing. Thiokol Chemical Corporation, Rpt No. SBR-84.565, Appendix B, 1965 or

   Anon: Data Acquisition Report for Solid Propellant Rocket Motor Static Firings. Datacraft, Inc., Test Rpt No. 3-1103-2, 1965. (For comparison purposes, this report covers the 156-in. solid propellant static rocket motor firing performed at LPC, Beaumont, Calif. on 30 Sep 1964.)

2. Plzak, G. A.; Smith, D. L., and Holtz: 156 Inch Solid Fuel Motor Firing Acoustic and Vibration Spectra. AF Flight Dynamics Library Tech. Memorandum No. FDD-TM-64-62.

3. Anon: Proposal for Solid Rocket Motor Project for the Space Shuttle Program. Thiokol Corporation, Vol. III, 1973.

4. Anon: DVXL5-1 Solid Fuel Motor Static Firing, Acoustic and Vibration Spectra. Bolt Beranek and Newman, Inc., Rpt No. 1035 (submitted to Aerospace Corp., 1963).

5. Anon: ASPC Rpt No. 1387-01F, 1971.

6. Anon: Acoustic Data Summary - AMR Test Series: FTM 401 through 411. Boeing Co., Rpt No. DL-2-265, 1962.


## REFERENCES NOT CITED


1. Anon: P-1-2 Solid Fuel Motor Static Firing--Acoustic and Vibration Spectra. Bolt Beranek and Newman, Inc., Rpt No. 823, 1962.

2. Anon: 100 FW3 Solid Fuel Motor Static Firing--Acoustic and Vibration Spectra. Bolt Beranek and Newman, Inc., Rpt No. 822, 1962.

## REFERENCES NOT CITED (Cont)


3. Cole, J. N., et al.: Noise Radiation from Fourteen Types of AF Rockets in the 1,000 to 130,000 Pound Thrust Range. Wright Air Development Center, NAOC TR 57-354, 1957.

4. Anon: Solid Fuel Motor Static Firing. Bolt Beranek and Newman, Inc., Rpt No. 1088, 1962 (UA 1205-2, 120-in. diameter).

5. Anon: Solid Fuel Motor Static Firing. Bolt Beranek and Newman, Inc., Rpt No. 1090, 1964 (UA 1205-3, 120-in. diameter).

6. Crane, K. L.: Evaluation of Acoustic Data from Reports of Large Solid Propellant Rocket Engines. Datacraft, Inc. (NASA Literature Search No. 70X73015).

7. Anon: Data Acquisition Report for Solid Propellant Rocket Motor Static Firing--260-In. Aerojet Rocket Firing, Homestead, Fla., 25 Sep 1965. Datacraft, Inc., ITS Test Rpt No. 208 (NASA Literature Search No. 68X86561).

8. Johnson, D. G., Kennedy, B.: Acoustic Environment of Very Large Solid Propellant Motors Final Report. Datacraft, Inc. (NASA Literature Search No. 68X11717).